Università degli Studi di Napoli Federico II

Ph.D. Program in

Computational and Quantitative Biology

XXXVII Cycle

Thesis for the Degree of Doctor of Philosophy

Harnessing Deep Learning for Antimicrobial Peptide Design: A Journey from Computational Models to Functionalized Membranes

by

Silvia Arino

Advisors: Prof. Flavia Nastri and Prof. Alfonso De Simone

Scuola Politecnica e delle Scienze di Base
Dipartimento di Ingegneria Elettrica e delle Tecnologie dell'Informazione

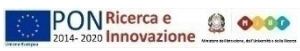

Ph.D Thesis presented

for the fulfilment of the Degree of Doctor of Philosophy in Computational and Quantitative Biology

Harnessing Deep Learning for Antimicrobial Peptide Design: A Journey from Computational Models to Functionalized Membranes

by

Silvia Arino

December 2024

Approved as to style and content by

Prof. Flavia Nastri

Prof. Alfonso De Simone

Università degli Studi di Napoli Federico II

Ph.D Program in Computational and Quantitative Biology

XXXVII cycle – Chairman; Prof. Michele Ceccarelli

Candidate's declaration

I hereby declare that this thesis submitted to obtain the academic degree of Philosophiæ Doctor (Ph.D.) in Computational and Quantitative Biology is my own unaided work, that I have not used other than the sources indicated, and that all direct and indirect sources are acknowledged as references.

Part of this dissertation is currently being published in international journals and/or conference articles.

Napoli, December 2024

Silvia Arino

Table of Contents

List of Acronyms and Abbreviations

The following acronyms and abbreviations are used throughout the thesis.

aa	Amino Acids
ACN	Acetonitrile
Ahx	6-Aminohexanoic Acid
AI	Artificial Intelligence
AMPs	Antimicrobial Peptides
Arg	Arginine
Bi-LSTM	Bidirectional Long Short-Term Memory
Boc	tert-Butyloxycarbonyl
CD	Circular Dichroism
CNNs	Convolutional Neural Networks
Cys	Cysteine
DCM	Dichloromethane
DIPS	Diffusion-Induced Phase Separation
DL	Deep Learning
DNA	Deoxyribonucleic Acid
DPH	1,6-Diphenyl-1,3,5-Hexatriene
DSC	Differential Scanning Calorimetry
E. coli	*Escherichia coli*
ESI-IT-TOF	Electrospray Ionization Ion Trap Time-of-Flight
e-spin	Electrospinning
Fmoc	Fluorenylmethyloxycarbonyl
GAN	Generative Adversarial Network

Gln	Glutamine
Gly	Glycine
GP	Generalized Polarization
GPLs	Glycopeptidolipids
HCl	Hydrochloric Acid
His	Histidine
Ile	Isoleucine
IP	Phase Inversion
K	Lysine
LC-MS	Liquid Chromatography - Mass Spectrometry
Leu	Leucine
LP	Lipid-to-Peptide Ratio
LSTM	Long Short-Term Memory
LUVs	Large Unilamellar Vesicles
Lys	Lysine
M. abscessus	*Mycobacterium abscessus*
M. avium	*Mycobacterium avium*
M. chelonae	*Mycobacterium chelonae*
M. smegmatis	*Mycobacterium smegmatis*
Met	Methionine
MHB	Mueller-Hinton Broth
MIC	Minimum Inhibitory Concentration
ML	Machine Learning
MLVs	Multilamellar Vesicles
NaOH	Sodium Hydroxide

NIPS	Non-Solvent Induced Phase Separation
NLP	Natural Language Processing
NMR	Nuclear Magnetic Resonance
P. aeruginosa	*Pseudomonas aeruginosa*
PA	Polyamide
PA 6,10	Polyamide 6,10
PA 6,6	Polyamide 66
Phe	Phenylalanine
POPE	Phosphatidylethanolamine
POPG	Phosphatidylglycerol
Pro	Proline
Q	Glutamine
R	Arginine
RH-HPLC	Reversed-Phase High-Performance Liquid Chromatography
RNN	Recurrent Neural Network
S. aureus	*Staphylococcus aureus*
SEM	Scanning Electron Microscope
SPPS	Solid Phase Peptide Synthesis
T*c*	Cooling Temperature
TFA	Trifluoroacetic Acid
TGA	Thermogravimetric Analysis
TIPS	Thermally Induced Phase Separation
TIS	Triisopropylsilane
T*m*	Melting Temperature
Trp	Tryptophane

TSA	Tryptic Soy Agar
UV-Vis	Ultraviolet-Visible Spectroscopy
VAE	Variational Autoencoder
VIPS	Vapor-Induced Phase Separation
W	Tryptophan
WAXS	Wide-Angle X-ray Scattering
Δ*H*$_m$	Change in Enthalpy
µM	Micromolar

Abstract

Advances in tools and methods from Artificial Intelligence (AI) applied to peptide and protein design has strongly propelled the design of novel biomolecules with new shapes and desired molecular functions, with applications ranging from diagnostics, medicine, catalysis and material science. Within the area of AI, Deep Learning (DL) is a core technology thanks to its ability to independently learn and extract meaningful patterns from complex data. For these features, DL algorithms represent useful tools in the context of computing and are now widely applied in a variety of research fields. In particular, they offer several advantages over conventional methods in the field of peptide design.

Driven by the fascinating application of AI tools in guiding future discoveries in life science, this Ph.D. thesis has been focused on the use of DL approaches for the development of novel peptide sequences with antimicrobial activity to be used in real world applications. This goal was pursued by addressing two main aspects: the application of DL algorithms to design antimicrobial peptide sequences and subsequent validation by wet-lab experiments (described in *Section 1*) and immobilization of the most active peptide sequence on Nylon membranes for the development of new materials with antimicrobial behaviors (described in *Section 2*).

Section 1

The application of two DL algorithms, HydrAMP and Amplify, allowed the design and selection of three peptide sequences, namely

AMP1, AMP and AMP3 with in silico predicted antimicrobial activity. A comprehensive validation of the computational design results was performed by wet lab experiments, with a first focus on the determination of the peptide antimicrobial activity on different bacterial strains. In details, the Minimum Inhibitory Concentrations (MIC) against various bacterial strains (e.g., *E. coli*, *S. aureus*), was determined by using the two-fold broth microdilution method. AMP3 emerged as the most active among the three sequences, both against *E. coli* and *P. aeruginosa*, which is notorious for its antimicrobial resistance, exhibiting MIC values of 15 μM and 125 μM, respectively. A detailed biophysical characterization on model membranes, by combining differential scanning calorimetry, circular dichroism, and fluorescence spectroscopy, was carried out on AMP3. This revealed that the efficacy of AMP3 peptide relies on its ability to efficiently integrate into the lipid bilayers, as highlighted by the very high mole fraction partition constant value (Kx).

Section 2

The peptide sequences developed were assayed for real-world applications by investigating their behaviors upon immobilization on Nylon membranes. To this end, peptide sequences were incorporated into the polymer matrix by a grafting through strategy. A detailed physico-chemical analysis, by DSC, WAXS and UV-Vis spectroscopy, confirmed the effective incorporation of the peptide without compromising the semi-crystalline structure of Nylon 6,6. Next, Peptide-Nylon membranes were produced by electrospinning and phase inversion approaches. The membranes produced by

electrospinning showed a nanofiber like structure, high porosity and improved hydrophilic properties, making them particularly suitable for antimicrobial applications. Interestingly, these peptide-membrane composite assayed for their activity against *E. coli,* caused a significant reduction of bacterial viability.

In conclusion, the research activities carried out and the results obtained in this PhD project demonstrate the useful application of DL algorithms to design novel and active AMPs. Further, the combined approach of computational predictions and experimental implementation allowed the construction of multifunctional materials with potential applications in different fields.

Keywords: Artificial Intelligence (AI), Deep Learning (DL), Antimicrobial Peptides (AMPs), Antimicrobial Membrane.

Section 1

Algorithms and Amino Acids: From Computational Design to Biological Validation

Chapter 1

Introduction

1.1 Machine Learning applied to de novo design of proteins and peptides

Artificial Intelligence (AI) and Machine Learning (ML) emerged as important innovations in many fields ranging from industry to agriculture and scientific research, bringing novelty and new possibilities for data analysis.[1,2] In science, advanced tools for complex dataset analysis and computational simulations are transforming the research landscape, especially in fields such as physics, biology and chemistry.[3] Among the emerging applications, peptide and protein design is attracting increasing attention.[4,5] Why are these molecules so important? Peptides, short chains of amino acids, are often used as drugs or signal molecules, while proteins - macromolecules essential for life - perform a multitude of biological functions.[6] However, designing these structures with specific properties has always been an extremely complex task. Until a few years ago, the design of proteins was based on traditional computational approaches and experimental methods that included molecular models such as dynamic simulation and molecular docking techniques to predict protein-ligand interactions and energetically favorable conformations;[7] exploiting rational design, which used NMR studies and crystallographic structure analysis to identify active sites and driving mutations aimed at improving stability or activity. Directed evolution, based on site-specific mutagenesis and high-capacity screening of mutant libraries, appear a key method for obtaining protein variants with desired properties, while biophysical and energy models combined with statistical analysis sought to predict and optimize protein behaviour.[8,9] The

introduction of DL has revolutionized this field.[10] Indeed, whereas AI generally seeks to replicate human cognitive functions, ML focuses on data analysis and interpretation, whereas DL elevates this analysis, enabling the identification of patterns and independent learning from extensive datasets (Figure 1.1).[11,12] These technologies enable the development of advanced applications, including computer vision and natural language comprehension, facilitating new solutions across diverse domains.

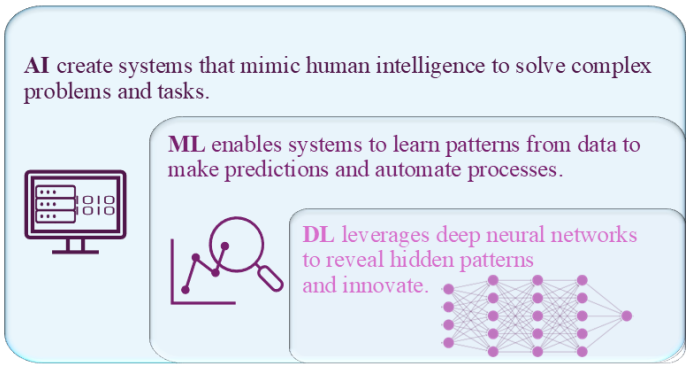

Fig. 1.1 Visual representation of AI, ML, and DL: AI encompasses intelligent systems and automation, ML focuses on data analysis and pattern recognition, and DL leverages neural networks to uncover complex relationships and drive innovation.

DL-based workflows automate the design process, integrating structural and functional data with advanced algorithms to discover innovative sequences and functions[13,14]. The comparison of the two approaches reveals fundamental differences (Figure 1.2). In traditional methods, design was based on a combination of energy models and pre-existing knowledge, with particular emphasis on the optimization of already known proteins or incremental modifications. These methods excel at improving properties such as

thermodynamic stability and enzyme activity but have been ineffective in creating new functions or protein replications. DL, on the other hand, allows exploring in a systematic and scalable way the space of protein sequences, overcoming the dependence on manual heuristics and static models. Another point of difference concerns the generalization capability. Traditional methods excelled in optimizing known proteins but struggled with novel designs. In contrast, DL models leverage large datasets to generate innovative sequences with unprecedented functions.[15]

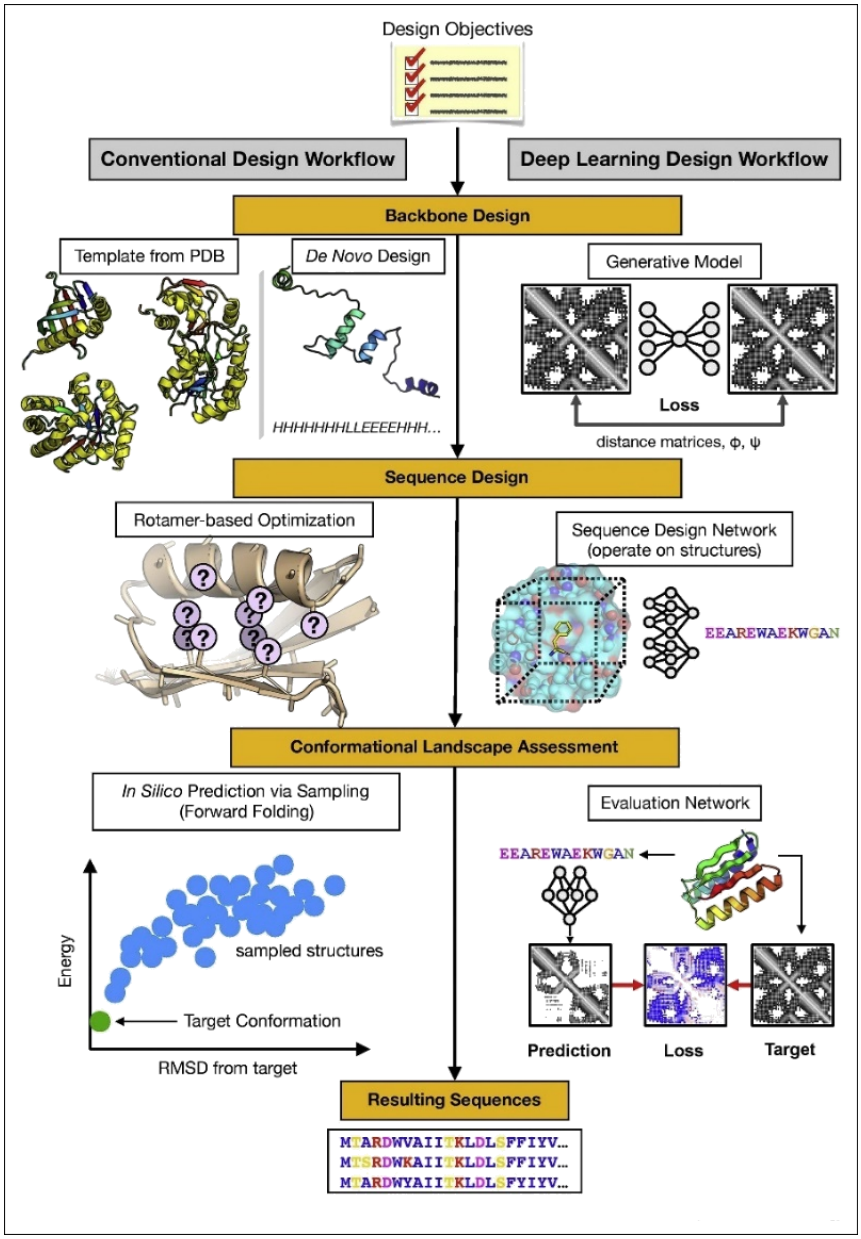

Fig. 1.2 Comparison between traditional and DL based workflows for protein design. Traditional methods are based on pre-existing models and energy simulations, while DL automates the generation of innovative sequences and structures by integrating multidimensional data. Taken with permission from a reference "Structure-based protein design with deep learning" (Current Opinion in Chemical Biology, 2021).

The combination of traditional methods, which provide in-depth physico-chemical validation, with the efficiency, scalability and automation of DL methods is a highly promising strategy for the future of protein design.

This synergistic approach integrates experiments, simulations and bioinformatics with machine learning techniques, creating an iterative cycle in which experimental data feeds predictive models that, in turn, drive new experiments (Figure 1.3).[16,17]

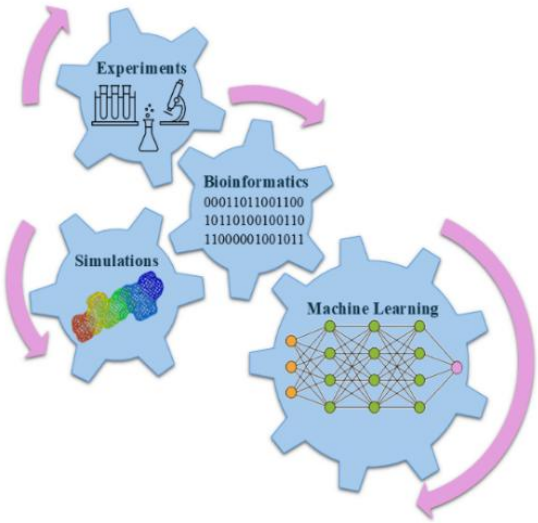

Fig. 1.3 Integrating experiments, bioinformatics, simulations, and machine learning requires synergy to drive advancements in modern research.

This transformative change in protein design culminated in 2024 with the Nobel Prize for chemistry, awarded to David Baker, Demis Hassabis and John M. Jumper for their pioneering work in the prediction and design of proteins by AI. Their achievements underline the profound impact of these advances on science and

technology. David Baker's work focuses on the development of computational tools for designing proteins that do not exist in nature. His laboratory has created Rosetta, a platform for the simulation and design of protein structures, both de novo and by modifications to existing proteins.[18,19] Hassabis and Jumper have developed AlphaFold, a DL model that solves the "protein folding problem" by predicting 3D structure of proteins with great precision.[20] This discovery has accelerated drug development and improved our understanding of genetic diseases. Baker's tools have also opened up new possibilities in biotechnology, including the treatment of diseases and cleaning up pollutants. Custom-designed proteins are already being used for environmental solutions such as plastic degradation and gene therapy.[21]

DL-based approaches are central to this transformation, enabling revolutionary applications in protein design. Techniques such as the variational autoencoders (VAE) and generative adversarial networks (GAN) allow proteins to be created with completely new functions and folds.[22,23] One of the most important applications has been the design of enzymes such as PETase, which can degrade synthetic materials such as polyethylene terephthalate with increased stability and activity.[15] In the biomedical field, DL has helped to optimize antibodies to improve their affinity and specificity. Models such as the Regression Transformer and ProteinMPNN have been used to design sequences that bind therapeutic targets such as PD-L1 and SARS-CoV-2, achieving improvements of up to 160 times in terms of affinity compared to original antibodies. [24]

In addition to the healthcare sector, DL is transforming industrial sustainability by enabling the design of enzymes optimized for extreme conditions such as pH or temperature.

1.2 Deep Learning Tools applied to AMPs

Among the most promising applications of AI tools is in the study of antimicrobial peptides (AMPs), which play a crucial role in facing the growing challenge of antimicrobial resistance.[25,26] The development and success of a variety of DL algorithms in this field is the availability of extensive, rich data sets of AMPs information. These data sets include structure-activity relationships (SAR), physico-chemical properties, sequence patterns and experimental data on antimicrobial activity, toxicity and stability.[27] For example, SAR data can reveal how specific sequence changes impact activity against different pathogens, providing a solid basis for DL models to learn and predict results. These data sets allow DL models to extract important information and identify patterns that were previously obscured by the complexity of the data.[28,29] Moreover, DL can recognize sequence patterns associated with specific biological functions and understand the structural requirements to bind to bacterial membranes. For instance, one of these algorithms named HydrAMP successfully identified a peptide sequence that exhibited strong activity against *E. coli* by targeting its membrane integrity, a result later confirmed through Minimum Inhibitory Concentration (MIC) assays. As numerous peptide libraries are available to make such analysis easier, this not only expedites venturing for more AMPs, but also empowers modification of already available

candidates by forecasting enhancements on its stability or selectivity.[30]

In addition, DL models are continuously improved as they are built on next-generation experimental data, creating an iterative cycle of refinement.[31,32] This adaptability ensures that forecasts become more and more reliable over time, driving progress in AMP design. Utilizing the available database more fully, DL offers a new way of approaching peptide discovery, allowing scientists to construct potent and selective antimicrobial agents to respond timely to the problem of resistance.[33,34]

1.2.1 Understanding Antimicrobial Peptides: structure and function

Antimicrobial peptides (AMPs) are a heterogeneous class of small peptides that play a central role in the innate immune response of many organisms, including animals, plants and bacteria. Their scientific importance has grown over time. This is due to their mechanisms of action and their effectiveness against resistant pathogens. [35] The structural diversity of AMPs is one of their main features. It enables them to act against a wide range of targets: viruses, bacteria, fungi and other species harmful to humans. AMPs are short peptide sequences, typically ranging from 12 to 60 amino acid residues, and can have various secondary structures, including α-helices and β-sheets (Figure 1.4).[36]

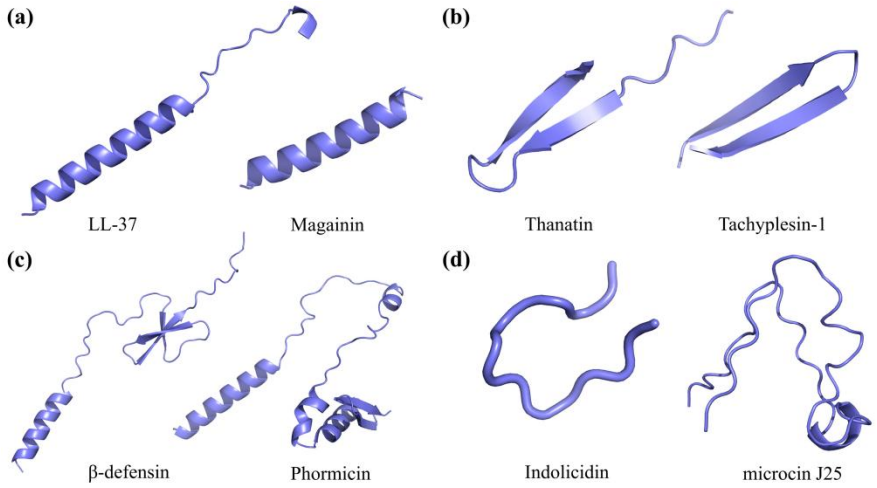

Fig. 1.4 Secondary structures of several representative AMPs. (**a**) α-helix antimicrobial peptide; (**b**) β-sheet AMPs; (**c**) αβ antibacterial peptides; (**d**) non-αβ antibacterial peptides. Taken with permission from reference "A Review of Antimicrobial Peptides: Structure, Mechanism of Action, and Molecular Optimization Strategies" (Fermentation, 2024).

The amphipathic nature of many AMPs, characterized by both hydrophilic and hydrophobic regions, and their positive charge, enables them to interact directly with microbial membranes, leading to disruption of membrane integrity through physical mechanisms.[37,38,39]

It is widely accepted that the final target of AMPs is the lipid matrix of the membrane. This interaction is non-specific and does not engage receptors, as evidenced by the observation that antimicrobial activity remains unaltered despite the complete substitution of all L-amino acids in their sequence with D-enantiomers. At physiological pH, antimicrobial peptides (AMPs) possess a positive charge and adhere to negatively charged lipids on bacterial membranes. They subsequently penetrate the outer membrane and cell wall of Gram-

negative bacteria or the cell wall of Gram-positive bacteria to access the cytoplasmic membrane. In Gram-negative bacteria, peptides seem to replace divalent ions linked to lipopolysaccharides, thereby weakening the membrane and enabling access to the inner membrane. In Gram-positive bacteria, teichoic acids may obstruct peptide transport, whereas peptidoglycan appears to exert no considerable influence on membrane permeability. Upon reaching the cytoplasmic membrane, AMPs adsorb to its surface and undergo a conformational transformation, frequently shifting from a random-coil structure to an α-helix, especially in the case of linear AMPs. The three stages—attraction, penetration, and adsorption—represent the binding phases that are universal to all AMPs. The mechanism by which a peptide interferes with a membrane is influenced by various factors, including lipid composition and the physicochemical characteristics of both the membrane and the peptide. Indeed, the mechanisms of action for the antimicrobial activity of AMPs has been interpreted trough several models. The most widely applied are the **barrel-stave**, **carpet**, and **toroidal-pore** model mechanisms (Figure 1.5). [40 41]

The carpet model describes how AMPs are distributed on the membrane surface, forming a layer similar to a carpet. With increasing local concentration, this process leads to cellular damage through mechanisms such as phase separation, in which anionic and zwitterionic lipids are secreted, progressive thinning, destabilization, and finally membrane lysis.

In the barrel-stave model, AMPs align perpendicular to the membrane surface. These form stable pores consisting exclusively of peptide molecules, with the apolar residues directed towards the hydrophobic core of the membrane and the polar ones towards the hydrated centre of the pore. Initially, the peptides bind in monomer form to the polar head groups of lipids, causing a local thinning of the membrane. When a threshold concentration is reached, the monomers self-assemble and insert themselves deeply into the membrane, forming pores.

The toroidal pore model is similar to the barrel-stave but it is distinguished by the strong interaction of peptides with the head groups of phospholipids. This interaction causes a curvature in the double lipid layers, which connect, forming pores coated by both peptide and head groups. Unlike the barrel-stave, the toroidal pores do not require direct contact between peptides, and their stability can be achieved even with a single peptide molecule.[36]

These models, called membranolytic mechanisms, involve the direct destruction of the membrane by stable pores or detergent-like effects. However, non-destructive mechanisms have also been proposed, involving different modes of interaction with the membrane. For example, the mechanism of the aggregate channel describes a non-membranolitic action. The peptides fit into the membrane, forming unstructured and transient aggregates, allowing them to cross it without causing significant disruption. Once inside, the peptides can interact with intracellular targets such as DNA, RNA, or proteins. Another hypothesized mechanism of action is the model of molecular

electroporation, where peptides, due to their high charge density, generate an electric field that promotes the formation of temporary pores, increasing permeability without permanent damage.

Finally, some AMPs can destabilize the membrane by promoting lipid domain formation. Preferentially interacting with negatively charged lipids, such as phosphatidyl glycerols or cardiolipins, they induce a lateral segregation between anionic and zwitterionic lipids. This leads to the formation of defects at the domain boundaries, which increase the permeability of the membrane without destroying it.[42]

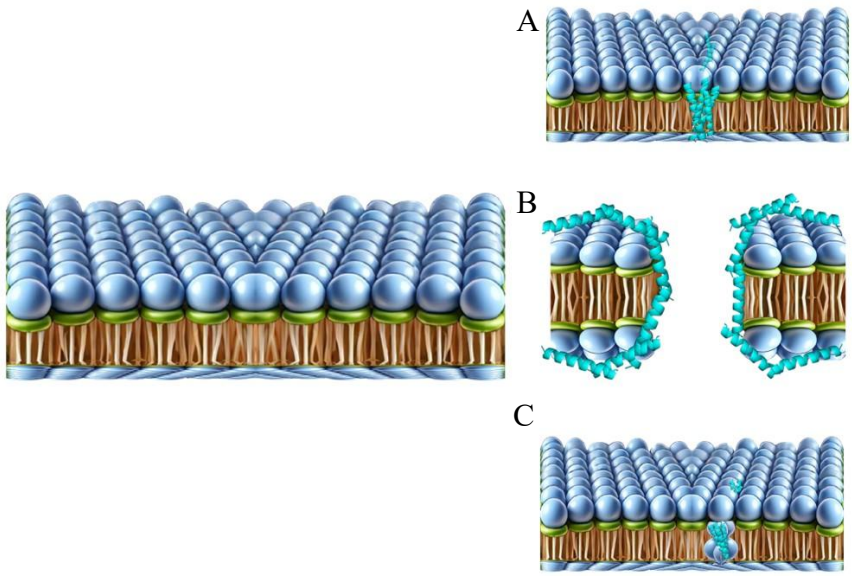

Fig. 1.5 Mechanisms of action of AMPs on bacterial membranes. Left: Intact lipid bilayer. Right: Three AMP models of membrane disruption: (A) Toroidal Pore Model, where AMPs form a pore lined with lipid headgroups; (B) Carpet Model, in which AMPs coat the membrane surface, causing disintegration; and (C) Barrel-Stave Model, where AMPs insert to form a transmembrane channel, destabilizing the membrane integrity. AMP model peptide is depicted in cyan.

The above-described mechanisms underline the versatility of AMPs, which is clearly evident in peptides like Buforin II, PR-39, and Indolicidin. Buforin II penetrates bacterial cells and binds to DNA and RNA, inhibiting replication and transcription. PR-39 disrupts cellular repair mechanisms by targeting DNA repair enzymes, while Indolicidin interacts with bacterial DNA, causing fragmentation and cell death. [43–45] This dual ability improves the effectiveness of AMP and decreases the likelihood of resistance, as cells must alter multiple molecular targets to evade AMP activity.[46]

Besides therapeutic uses, AMPs show potential in food preservation by inhibiting bacterial spoilage and extending product shelf life without the need for chemical preservatives, aligning with consumer preferences for natural additives.[47] In agriculture**,** AMPs have shown efficacy as bio-pesticides, enhancing plant resistance to pathogens while reducing dependence on synthetic pesticides. [48]The potential for aquaculture applications is similarly valuable, with AMPs being used to control disease in farmed fish and shrimp, reducing the need for antibiotics and mitigating the risk of antimicrobial resistance spreading in aquatic environments.[49] Considering the above-described features of AMP, the design of synthetic analogues with potential applications is a hot and innovative field of research. Recently, the application of advanced tools such as high-capacity screening and computational modelling allow the design of AMPs analogues with improved specificity, reduced toxicity and lower production costs. Moreover, advances in peptide engineering and recombinant synthesis have enabled the development of AMP-based

coatings for biomedical devices, providing pathogen resistant surfaces that can reduce the risk of infections associated with medical devices. This application is particularly relevant in clinical settings, where device-related infections pose a significant challenge. In the environmental field, AMPs offer promising solutions for water purification through filters that exploit their antimicrobial properties to combat microbial contamination and provide a sustainable solution against water pathogens.[50] [51]

1.2.2 AI techniques for AMPs discovery

Several ML algorithms have been used for AMPs prediction and classification in the past with remarkable results including random forests, support vector machine, k-nearest neighbors, XGBoost and others[52]. Such implementations established the potential of ML in computational AMPs discovery and paved the way for the current generation of computational tools used in the field. With the growing popularity of DL, neural networks have also been employed in AMPs discovery. DL architectures originally designed to handle sequential data, used commonly in natural language processing (NLP) for their ability to handle long-range context dependencies in text, were particularly easy to adapt for use in modelling the complex "language" of protein sequences. Among these, **convolutional neural networks** (CNNs), **recurrent neural networks** (RNNs), **variational autoencoders** (VAEs), **generative adversarial networks** (GANs) **and transformer-based models** have been the most commonly utilized and their main features and applications are briefly recapitulated here.

- **Convolutional Neural Networks**

Convolutional Neural Networks (CNNs) are a class of deep neural networks designed for image processing and analysis. As for the artificial neurons composing simple deep neural networks, the structure of the CNN architecture was originally inspired by biology, more specifically the visual cortex of cats, leading to the first precursor of this class of neural networks, the neocognitron.[53,54] The fundamental operation in CNNs is the "convolution", which essentially consists in a dot product between a learnable kernel matrix and a portion of the input (Figure 1.6). By sliding multiple kernels across the whole input and applying an activation function (usually rectified linear unit, ReLU), the convolution layers construct an activation map, which is then passed to a pooling layer to extract the most important features of the input data. After a number of convolutions and pooling operations, the resulting tensor is flattened and passed to one or more fully connected layers to generate the final output values. It has been observed that different kernels of the convolutional layers hierarchically learn during the training process, to perform more specialized roles; the kernels in the first layers are mainly activated by local features like edges with specific orientations, while the latter ones can recognize more complex shapes and objects. This process bears some resemblance to what has been observed for image processing by the mammalian visual cortex, in which individual neurons were shown to be receptive to specific features in a region of the total visual field (its receptive field).

The pattern recognition capabilities of CNNs have been widely utilized in image processing, driving the development of numerous models for tasks such as image classification and semantic segmentation. While image processing remains the most common application, CNNs are not limited to this domain and have also been applied to various types of structured data, including NLP, audio processing, time series analysis, and more.

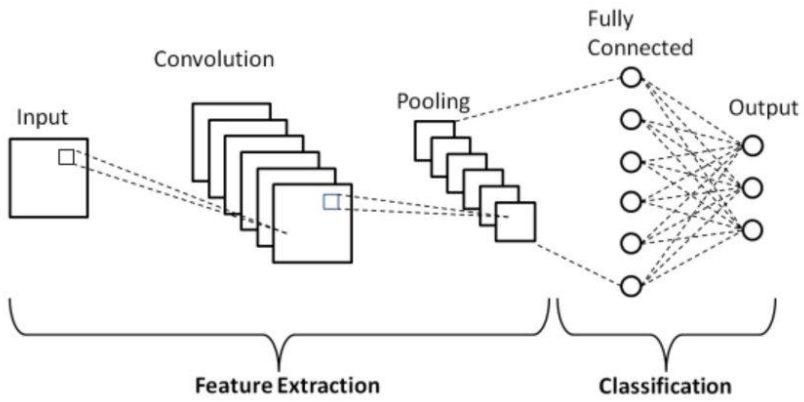

Fig. 1.6 Architecture of a Convolutional Neural Network (CNN). The pipeline is divided into two main phases: Feature Extraction and Classification. In the feature extraction phase, convolutional and pooling layers process the input image to identify significant patterns. In the classification phase, fully connected layers transform the extracted features into final predictions. Adapted from: *A High-Accuracy Model Average Ensemble of Convolutional Neural Networks for Classification of Cloud Image Patches on Small Datasets* by Van Hiep Phung and Eun Joo Rhee, *Appl. Sci.* 2019, 9(21), 4500.[55]

In addition to their success in traditional domains, CNNs have found significant applications in protein modeling, where their ability to capture spatial and sequential patterns is particularly advantageous. For instance, CNNs have been effectively used to predict protein secondary structure from amino acid sequences.[56] Similarly, contact map prediction, which involves identifying spatial proximities

between residues in the folded protein, has been performed using CNN architectures by incorporating both local and global sequence features.[57] In function prediction, CNNs have demonstrated the ability to classify proteins based on sequence features, enabling the identification of functional domains or subfamilies.[58] AMP prediction and classification have also been performed using several notable CNN architectures and their variants, enabling the identification and design of novel peptides with therapeutic potential.[59–62]

- **Recurrent Neural Networks and Long Short-Term Memory Networks (LSTMs)**

Recurrent Neural Networks (RNNs) are a type of artificial neural network designed to handle sequential data by processing it in a step-wise manner while retaining information from previous steps in the sequence. RNNs can do this by employing a so-called "hidden state" that serves as a sort of memory, capturing context from earlier inputs (Figure 1.7).[63] This allows RNNs to manage sequences of variable lengths and take temporal dependencies within the data into consideration, making them particularly suitable for tasks where context or sequence is important, such as natural language processing and time series analysis. Despite their good performance, RNN training was often found to be difficult because of vanishing gradients.[64] In addition to propagating errors through the layers of the network, RNNs also require propagation of the error through time for effective training. This can result in the multiplication of gradients progressively smaller in value, making it very difficult for

the network to learn long-term relationships in the input data, particularly with small initial weights and long sequences.[65]

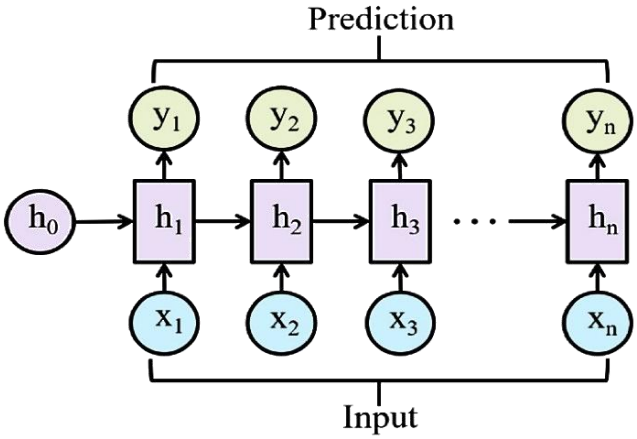

Fig. 1.7 Diagram of a neural network structure illustrating the flow from input layer to output layer through hidden layers. The diagram highlights the connectivity and hierarchy within the network, serving as a conceptual foundation for understanding Recurrent Neural Networks (RNNs). Adapted from: Recurrent Neural Networks: A Comprehensive Review of Architectures, Variants, and Applications by Mienye et al, Information 2024, 15(9), 517.

Long Short-Term Memory (LSTM) networks were originally designed to address the vanishing gradient problem of RNNs, by modifying the original architecture in a way that allows control over the flow of information between the different time steps. LSTMs are formed by a cell and three gates (input, forget and output) (Figure 1.8). Forget gates decide how much of the input is retained by multiplication by a scaling factor between 0 and 1. Input gates choose which parts of the input information should be retained by the cell state. Finally, output gates determine which parts of the cell state should influence the output at the current time step by selectively allowing information to pass through, based on a sigmoid activation

function. This gating mechanism enables LSTMs to retain relevant information over long sequences, effectively addressing the vanishing gradient problem inherent in traditional RNNs. The key intuition is to enable the network to learn which information should be remembered and which should be forgotten depending on the context, enabling a deeper understanding of the patterns and relationships within the input sequence. An alternative architecture based on a different gating mechanism known as gated recurrent unit (GRU) has also been proposed and was shown to have similar performance to LSTMs. There are numerous examples of both RNN and LSTM models trained to perform many tasks useful in real-world scenarios, given their natural ability to understand sequential inputs. These include machine translation, sentiment analysis, speech recognition, text generation, video analysis and many others. The use of these architectures in the realm of AMPs has also lead to several notable works including the design of non-hemolytic AMPs, AMPs with reduced mortality in experimentally-induced sepsis and the discovery of novel bacteriocins, among many others.[66–70]

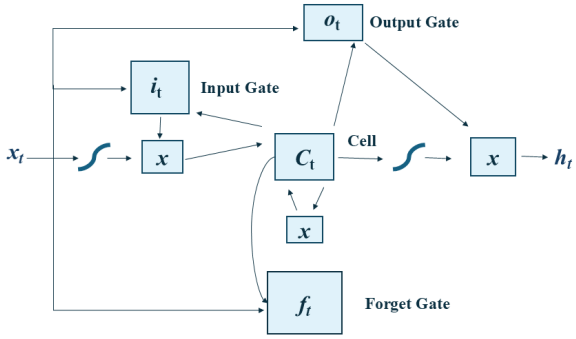

Fig. 1.8 Diagram of a standard Long Short-Term Memory (LSTM) cell, illustrating the flow of data through its components. It highlights the key gates—**Input Gate (i_t)**, **Forget Gate (f_t)**, and **Output Gate (o_t)**—which regulate the cell state (CtC_tCt) and hidden state (hth_tht). The gates control the addition, removal, and output of information, allowing the LSTM to manage long-term dependencies effectively. The input x_t and recurrent input h_t interact with the gates, ensuring precise information flow.

- **Variational Autoencoders** and **Generative Adversarial Networks**

Variational Autoencoders (VAEs) are a class of deep generative models that combine neural networks with principles from Bayesian inference to learn meaningful, continuous representations of data. VAEs are formed by two distinct neural networks joined together: the first, known as encoder, reduces input data dimensionality and compresses it into a vector in the latent space that is then decoded back into the original input by a second neural network, the decoder (Figure 1.9). Unlike traditional autoencoders, which encode data into deterministic latent variables, VAEs approximate a probability distribution in the latent space, enabling them to generate new data points by sampling from this distribution.[71] A key feature of VAEs is their use of a probabilistic framework to ensure smooth latent representations. In practice, training of VAEs is achieved through the

use of a loss function composed of a reconstruction term, which quantifies the difference between the original input and the decoded one, and a regularization term known as the Kullback-Leibler (KL) divergence.[72] This regularization ensures that the learned latent space aligns with a predefined prior distribution, typically a gaussian.

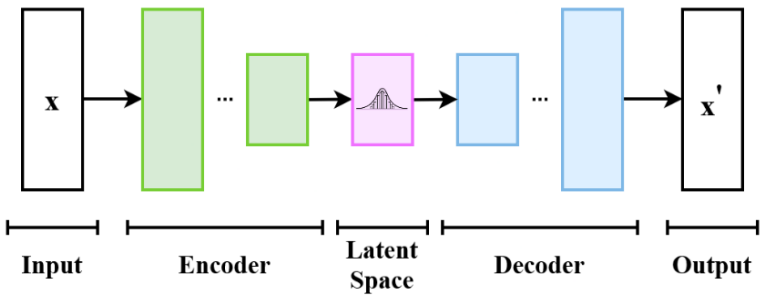

Fig.1.9 Illustration of a Variational Autoencoder (VAE) architecture. The input data x is compressed by the Encoder into a probabilistic latent space representation. The latent space is characterized by a Gaussian distribution, enabling sampling. The Decoder then reconstructs the data from the latent representation to produce the output x′, closely matching the input. This process enables both data reconstruction and generation.

VAEs have been widely adopted for applications in data generation and representation learning across diverse fields. In computer vision, they are used for generating realistic images, image denoising, and anomaly detection. [73] In natural language processing (NLP), VAEs are applied for generating coherent text and modelling language dynamics.[74] In scientific research, VAEs have gained prominence for analysing high-dimensional biological data, including single-cell transcriptomics and structural biology.[75] Their generative capabilities make them useful for exploring data spaces and designing novel candidates in fields such as drug discovery and material design.

In the realm of AMP discovery, VAEs have emerged as powerful tools for generating novel peptide sequences with desired properties. By encoding known AMP sequences into a continuous latent space, VAEs can interpolate between existing sequences, enabling the generation of novel peptides that maintain sequence and functional similarities to known AMPs.[76] For instance, VAEs have been employed to design peptides with enhanced antimicrobial activity or reduced cytotoxicity by conditioning the latent space on specific peptide properties.[10] Several models, sometimes with hybrid architectures, and variable latent spaces have been found to accelerate the discovery process by narrowing the experimental search space sequences with high therapeutic potential.[77,78]

GANs, or **Generative Adversarial Networks**, are a class of DL models tailored for the creation of new data samples that realistically mimic a given dataset. Introduced by Goodfellow et al. in 2014, GANs involve two neural networks, a generator and a discriminator, engaged in a minimax game.[79] The generator seeks to produce realistic data samples, while the discriminator works to distinguish real data from generated data. This adversarial interplay continues until the generator achieves outputs ideally indistinguishable from real samples.

GANs have been extensively utilized across fields due to their ability to generate realistic data. In computer vision, they have applications in image synthesis, super-resolution, and style transfer. In the medical domain, GANs generate synthetic imaging data for training models and improving rare disease detection. Additionally, in natural

language processing, GANs are employed for tasks such as text generation and language translation. Their generative capabilities also extend to scientific disciplines like drug discovery and material science, aiding in the design of novel molecular structures.

In the realm of antimicrobial peptide (AMP) discovery, GANs have proven capable in designing novel sequences with antimicrobial properties,[80–82] generating new peptides that are structurally and functionally akin to known ones, yet exhibiting unique characteristics. Furthermore, conditional GANs (cGANs) allow for tailored generation by specifying desired attributes, such as the target microorganism, mechanism of action[83] and reduced cytotoxicity.[83]

- **Transformer-Based Models**

The Transformer is a relatively new architecture, proposed by Vaswani et al. which excels in tasks requiring the understanding of sequential and structured data.[84] At its core, the Transformer utilizes self-attention to assign varying levels of importance to different parts of a sequence, enabling it to capture both local and global dependencies. This has been shown to be particularly advantageous in NLP applications, where this type of model has redefined the current state-of-the-art, delivering the stunning performance exhibited by modern chatbots in a wide range of tasks ranging from coding to text summarization, translation and even poetry. Additionally, they are faster than RNN-based model to train and not as unstable as GANs, which are often plagued by unstable training dynamics. Several models of this kind, sometimes directly lifted from those used in NLP, have been applied to protein sequence

modelling, where understanding the interplay between amino acids is crucial for elucidating sequence-function relationships.[85–88] By examining the entire sequence simultaneously, Transformers model the contributions of individual residues and their interactions, allowing for a comprehensive understanding of the functional dynamics within proteins. Transformers are not only effective for tasks such as classification and property prediction but also play a pivotal role in generative modelling.[89–91] These capabilities have been exploited to generate new peptide sequences that exhibit properties similar to known AMPs. This generative capability has also been adapted for multi-objective optimization, enabling the generation of sequences that simultaneously maximize the likelihood of possessing multiple desired features. This approach addresses the inherent trade-offs between competing objectives, making simultaneous optimization a significantly more complex and challenging task.

Specific tools like **HydrAMP** and **AMPlify** represent cutting-edge applications of DL in AMPs research. HydrAMP employes a VAE to generate and optimize AMP sequences, focusing in particular on balancing critical physico-chemical properties for antimicrobial efficacy and stability. This tool facilitates the design of new AMPs by incorporating peptide properties into a low-dimensional latent space, allowing the generation of new sequences with improved characteristics. Instead, AMPlify uses an LSTM model to predict the activity of AMPs.[92] Its architecture allows the model to focus on the most relevant segments for antimicrobial properties. In the following

paragraphs, details on HydrAMP and AMPlify algorithms are described.

1.3 HydrAMP

HydrAMP is a sophisticated DL tool developed specifically for the design and optimization of antimicrobial peptides (AMP), which leverages advanced machine learning methodologies to predict peptide efficacy with remarkable accuracy.[93] As a conditional variational model of autoencoder, HydrAMP is designed to generate new peptide sequences that are different in length, polarity and positive residue distribution from a known prototype sequence. The process begins with pre-processing of input data, in which a large set of known AMPs is used to train the model. This data set typically includes detailed information on peptide sequences, their physico-chemical properties and experimental bioactive profiles. The model extracts critical characteristics from these data, such as amino acid composition, hydrophobicity, net charge, amphipathicity and structural motifs, which are essential to predict the peptide's ability to damage bacterial membranes. By incorporating these characteristics into its predictive framework, HydrAMP ensures that the peptides generated are not only new but also have antimicrobial efficacy characteristics.[94] After training, HydrAMP creates sequences of de novo peptides with the appropriate characteristics and evaluates each one on how likely it is to be effective against micro-organisms. The model also uses post-processing filters to eliminate sequences that are subject to oxidation or present synthetic problems, ensuring that only strong candidates move forward. First-

level sequences can be experimentally validated through biological tests such as minimum inhibitory concentration (MIC) tests, confirming their antimicrobial properties (Figure 1.10).[95]

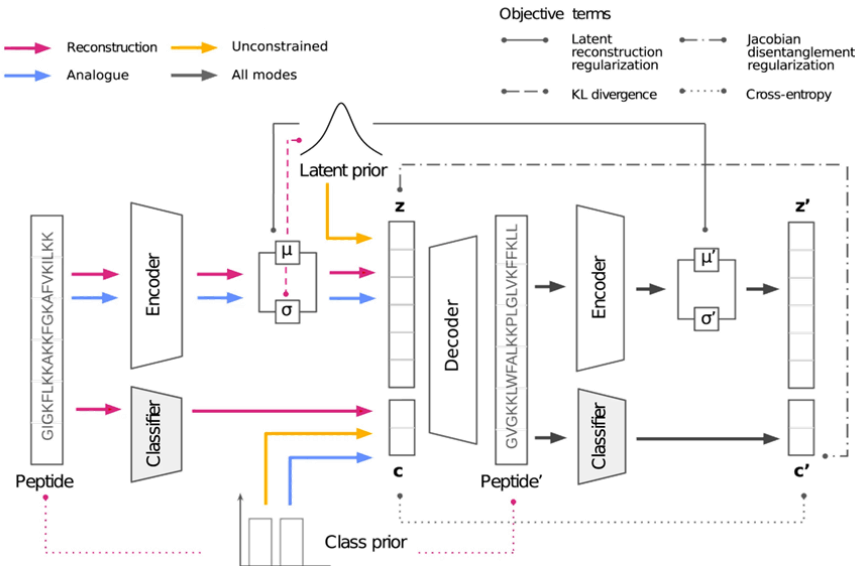

Fig. 1.10 Data stream for the HydrAMP model formation, showing the optimization pipeline used to develop antimicrobial peptides. Adapted from Szymczak et al., "Discovering highly potent antimicrobial peptides with deep generative model HydrAMP," Nature Communications, 14, 1453 (2023), DOI: 10.1038/s41467-023-36994-z.

HydrAMP exemplifies the potential of integrating DL and bioinformatics in the discovery of novel antimicrobial peptides. By leveraging sophisticated neural network architectures and focusing on critical sequence features, HydrAMP accelerates the identification of effective AMPs, providing valuable insights into the relationship between peptide structure and function (Figure 1.11).[96] This innovative approach not only enhances the efficiency of peptide discovery but also paves the way for developing next-generation

antimicrobial agents capable of addressing the pressing challenges posed by antibiotic resistance.

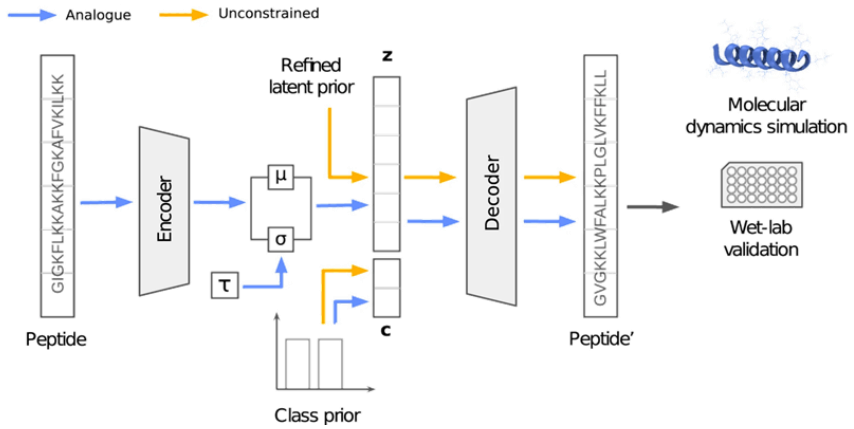

Fig. 1.11 Process of peptide generation by the HydrAMP model, illustrating steps to obtain highly effective antimicrobial peptides. Adapted from Szymczak et al., "Discovering highly potent antimicrobial peptides with deep generative model HydrAMP," Nature Communications, 14, 1453 (2023), DOI: 10.1038/s41467-023-36994-z.

1.4 AMPlify

AMPlify is a DL-based tool designed for the prediction and optimization of antimicrobial peptides (AMPs). It employs advanced machine learning techniques to analyze peptide sequences, enabling the identification of novel candidates with enhanced antimicrobial properties.[97] Having been trained on datasets including both AMP and non-AMP sequences, AMPlify rates each sequence according to its antibacterial likelihood. Beginning with feature encoding, where peptide sequences are converted into numerical representations that capture fundamental characteristics related to antimicrobial activity, using techniques such as one-hot encoding and more advanced

physicochemical property analyses, the operational framework of AMPlify consists of several key components (Figure 1.12). Important mechanisms behind antimicrobial action include peptides interacting with bacterial membranes or upsetting cellular processes, which depend on these properties.

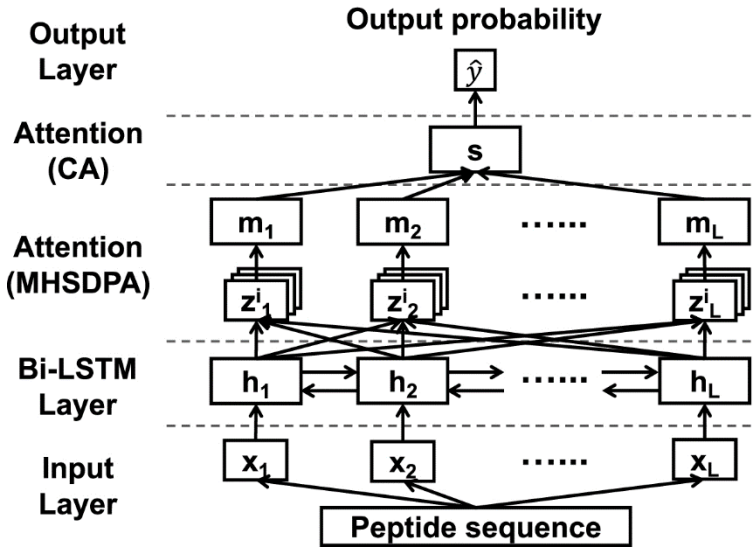

Fig. 1.12 AMPlify deep learning model architecture for AMPs prediction. Each peptide sequence is processed through a Bi-LSTM layer and multi-head, contextual attention mechanisms to generate a final representation and predict the likelihood of antimicrobial activity. Adapted from Li et al., "AMPlify: attentive deep learning model for discovery of novel antimicrobial peptides effective against WHO priority pathogens," BMC Genomics, 23, 77 (2022).

During model training, AMPlify typically employs architectures like Bi-LSTM and Attention Layer, which are trained on extensive datasets of known AMPs to learn complex patterns associated with antimicrobial efficacy.[98] Once trained, the model evaluates new peptide sequences, generating quantitative scores that reflect their likelihood of exhibiting antimicrobial activity, thereby facilitating the prioritization of candidates for experimental validation. By

examining the interactions between certain amino acid substitutions and variations in activity, AMPlify also offers information on possible alterations that can improve the antibacterial features of peptides. The novelty of this DL tool is the innovative integration of two cutting-edge techniques, called Bi-LSTM (Bidirectional Long Short-Term Memory) (Figure 1.13) and Attention Layer. Bi-LSTM allows the model to better capture long term dependencies and interactions between elements in a sequence, making it particularly effective for tasks where the relative position of elements - such as amino acids in peptide sequences - plays a crucial role.

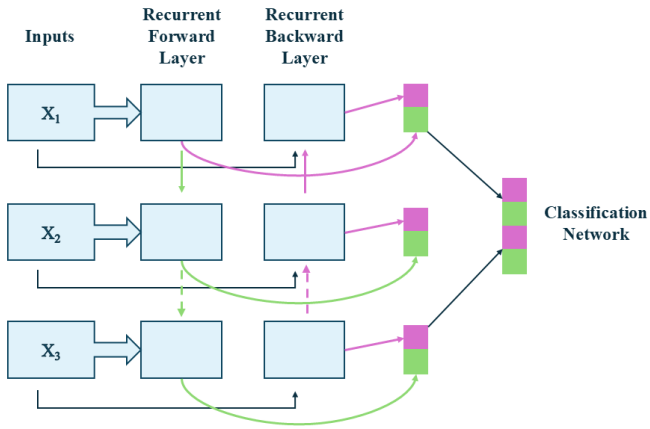

Fig. 1.13 Diagram of a Bi-LSTM architecture, illustrating how input sequences (X_1, X_2, X_3) are processed through recurrent forward and backward layers. The outputs are concatenated and passed to a classification network for final predictions.

Bi-LSTM captures both local and long-range dependencies within the peptide sequences by analyzing them in forward and backward directions. In combination with a level of focus, this architecture

allows the model to focus on specific regions of the peptide sequence that are related to antimicrobial activity (Figure 1.13). By prioritizing these regions, the model can identify and optimize peptide sequences with the highest potential for efficacy. Feature extraction plays a central role in this process, as it identifies important features such as hydrophobicity, net charge and structural motifs such as alpha-helix, which are often associated with membrane-active peptides. These features provide insight into how a peptide might interact with bacterial membranes, a crucial factor in its ability to disrupt the microbial integrity of cells.

1.5 Are the DL - predictions validated?

As described above, DL models have revolutionized AMPs research, allowing the prediction of new sequences with potential antimicrobial activity, stability, and selectivity with high accuracy. DL methods, especially those that use CNNs, RNNs, and VAEs, have been very good at finding AMPs. Wang et al. conducted one of the pioneering studies. [70] They applied an LSTM generative model to design AMP efficacy against *E. coli*. The model was trained on a large dataset of peptides with antibacterial activity and produced a series of new peptide sequences, which were synthesized and tested in the laboratory. The novel AMPs were classified as antimicrobial with accuracies between 70% and 90%. More recently, another validation has been given by Zhao et al., who developed models based on convolutional networks, to create advanced tools for AMP generation. [99] These models are designed to detect local patterns and patterns within peptide sequences, using CNNs for sequence

structure analysis. Predictions obtained by DL tools were experimentally validated, demonstrating that the peptide candidates generated show antimicrobial properties against a range of pathogenic bacteria, including those resistant to antibiotics. CNNs have made it possible to find patterns in peptide sequences that are important for their biological activity. Experiments have confirmed that these models can be used to make functional and specific AMPs. Moreover, by leveraging the VAEs, Das et al. developed potential antimicrobial sequences, focusing not only on functionality but also with optimized chemical and physical characteristics compared to natural peptides. [100] The peptides generated by this VAE were synthesized and tested in the laboratory, confirming that a high percentage of them showed significant antimicrobial activity. The results highlighted the importance of DL in de novo peptide generation, demonstrating that VAEs models can produce naturally occurring but equally effective AMPs.

1.6 Aim of the thesis: Section 1

As highlighted in the previous paragraphs, advanced DL tools represent a revolution in the discovery and optimization of antimicrobial peptides (AMPs), offering accurate and targeted predictions that can have a positive impact in the development of new molecules both therapeutically and environmentally important. [101] This PhD thesis aims to develop new candidate AMPs, optimizing their structural and functional properties for specific applications, including the preparation of functionalized membranes acting as

antimicrobial filters for industrial, clinical and environmental contexts.

Specifically, in this section, the computational approach used to develop new AMPs is described. In detail, HydrAMP To algorithm was used to generate novel peptide sequences that were subsequently scored respect their antimicrobial probability using AMPlify DL algorithm. The probability scores were used to rank and select the most promising candidates for further evaluation. This combination leverages the generative capabilities of HydrAMP and the predictive accuracy of AMPlify to streamline the discovery process, facilitating the identification of candidates that are not only novel but also exhibit a high likelihood of antimicrobial activity.

This section includes also the wet lab approaches used to verify the accuracy and reliability of DL predictions, therefore assuring the genuine antibacterial activity of the proposed AMP candidates. These approaches include the determination of the peptide antimicrobial activity on different bacterial strains. Moreover, a detailed biophysical characterization on model membranes, by combining differential scanning calorimetry, circular dichroism, and fluorescence spectroscopy, was carried out on most active sequence.[102]

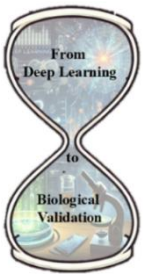

Fig. 1.14 Workflow of the Section: From Computational Design to Biological Validation

Chapter 2

Results and Discussion

2.1 Novel Antimicrobial Peptides via Deep Learning

Deep learning (DL) has proved to be very promising, particularly for the identification and research of new antimicrobial peptides (AMPs). By leveraging large data sets and complex neural network architectures, DL allows the identification of patterns and relationships within peptide sequences that correlate with antimicrobial activity.[103] This capability is crucial given the growing need for effective antimicrobial agents in the face of increasing antibiotic resistance. In this thesis, two DL tools have been used: HydrAMP and AMPlify; both of which utilize DL methodologies to predict the efficacy of AMPs. HydrAMP is specifically designed for the generation of novel peptide sequences with optimized properties such as enhanced stability and solubility. It generates a large library of candidates that can then be screened for antimicrobial potential. On the other hand, AMPlify is a tool designed for the prediction and optimization of antimicrobial peptide sequences through advanced machine learning algorithms. It analyzes large datasets of existing sequences, identifying patterns and characteristics common to peptides with antibacterial activity.

2.1.1 Combining AMPlify and HydrAMP for the Discovery of Novel Antibacterial Peptide Sequences

The integration of AMPlify and HydrAMP represents an innovative approach to accelerate the discovery of new antimicrobial peptide sequences. This aims to overcome the limitations of traditional methods for the selection or design of antibacterial peptides. While conventional approaches often require long time and considerable

resources to identify and test new compounds, the combination of these two tools allows for more accurate prediction and selection of peptides with antibacterial potential, reducing the need for extended experimental screening. The majority of AMPs targeting membrane bilayers typically exhibit sequences rich in cationic residues (Arg, Lys, His). Further, they share amphiphilic structure, in which cationic and hydrophobic residues, as Phe, Trp, Ile, and Leu, are clustered in different spatial regions. In particular, many AMPs are most active when are rich in Arg and Trp residues, thanks to their properties that enhance the interaction with microbial membranes.[104] The positive charge of Arg facilitates the interaction with the negatively charged membranes of bacteria, while Trp improves the insertion of the peptide in the membrane due to its hydrophobic nature.[105,106]

This thesis has been aimed at the development of novel Trp-rich AMP sequences with enhanced activity and selectivity (Figure 2.1).

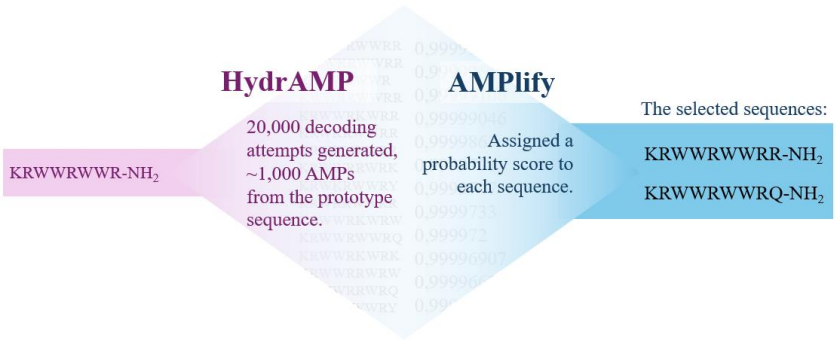

Fig. 2.1 Workflow illustrating the generation and selection of peptide sequences. A total of 20,000 decoding attempts resulted in approximately 1,000 potential antimicrobial peptides (AMPs) derived from the prototype sequence. The AMPlify model was employed to assign probability scores to each sequence, enabling the identification and selection of optimized candidates for further analysis.

Peptides design and selection started from a prototype peptide sequence, KRWWRWWR-NH_2, referred to as AMP1, which is a derivative of the already reported antimicrobial peptide Ac-RWWRWWR-NH_2.[107] The prototype sequence was chosen for its simplicity and residue repetition that would facilitate the development of new sequences by the analogue generation protocol of HydrAMP model. [93] The input sequence was rationally modified by addition of a Lys residue at the N-terminus. Indeed, as the final goal of this work is developing an antimicrobial membrane, the incorporation of a Lys residue at the N-terminus was done to allow chemical conjugation of the peptide to polymeric materials. Additionally, the presence of the Lys residue provides a reactive site that can enhance the versatility and potential for further functionalization of the peptide.

Initial candidate pool was created using the analogue generation protocol, with 20,000 total decoding attempts and temperature equal to 5.0, leading to approximately 1,000 potential AMPs derived from the prototype sequence. This library of AMP candidates was subsequently analyzed to remove duplicates. AMPlify program was employed to evaluate the antibacterial potential of each sequence, ranking the candidates based on their predicted likelihood of effectiveness Further selection was done by analyzing the sequences according to the following consideration. To prevent oxidation during peptide synthesis, using a Python script, sequences containing sulfur amino acids (Cys and Met) were removed, and peptide length was limited to eight to ten residues.[108,109] Moreover, sequences

containing three or more consecutive tryptophan residues were eliminated because of the difficulties during the solid-phase peptide synthesis (SPPS).[110,111] In addition, sequences that had more than 50% hydrophobic residues were eliminated because of their likely poor solubility and possible adverse synthesis interactions.[112] Following this filtering process, the sequences were ranked by AMPlify. Table 1 reports the set of generated sequences along with their corresponding log scores and associated probabilities. The log score is regarded as an absolute measure for evaluating the likelihood that a given sequence exhibits antimicrobial activity. Although there is no specific reference parameter for these scores, a higher log score directly correlates with an increased probability that the sequence possesses antimicrobial properties. Thus, sequences with elevated log scores were considered to have a stronger potential for antimicrobial effectiveness. All sequences exhibit probability scores significantly beyond the 0.5 threshold employed by AMPlify to differentiate AMPs from non-AMPs, clustering over 0.9. This outcome is unsurprising because, as noted by the authors, the absence of experimental data about antimicrobial activity on closely related sequences significantly impacts DL model training, hence limiting AMPlify's efficacy in distinguishing them.[97] Nonetheless, minor variations in antibacterial likelihood among the sequences can be emphasized by examining the AMPlify log-scaled score (Table 1). The two most similar sequences, specifically sequence "KRWWRWWRQ" and "KRWWRWWRR", which differ solely in the C-terminal residue, have AMPlify log scaled scores of 56.23 and 43.46, respectively (Table 1). To ascertain if the projected log-scaled

AMPlify scores accurately reflect varying antibacterial activity, we selected these sequences, designated AMP2 and AMP3, respectively, for wet lab experimentation.

Table 1. Peptide sequences with potential antimicrobial properties. Each sequence is characterized by specific parameters including length, charge, hydrophobicity and presence of key amino acids, with expected activity scores.

Sequence	Charge	Hydrophobicity	AMP Score	Log_Score
KRWWRWWRR	**5**	-2,833333333	0.999998	56.23
KWWKRWWRR	5	-2,766666667	0.999997	54.61
RRWWRWWR	4	-2.7	0.999991	50.49
KWWRRWWRR	5	-2,833333333	0.999990	50.21
KRWWRKWRR	6	-3,166666667	0.999986	48.63
KRWKRWWRR	6	-3,166666667	0.999977	46.40
KRRWRWWRR	6	-3,233333333	0.999975	45.97
KRWWRRWRK	6	-3,166666667	0.999973	45.73
KRWKRWWRY	5	-2,811111111	0.999972	45.53
KRWRRWWRR	6	-3,233333333	0.999969	45.09
KRWWRKWRW	5	-2,766666667	0.999966	44.72
KRWWRWWRQ	**4**	-2,722222222	0.999955	43.46
KRWWRKWRK	6	-3,1	0.999951	43.11
KRWWRRWRW	5	-2,833333333	0.999950	42.98
KRWWRRWRQ	5	-3,122222222	0.999933	41.77
KRWRRWWRY	5	-2,877777778	0.999928	41.45
KRWWYRWRK	5	-2,811111111	0.999920	40.95
KRWWRRWK	5	-3	0.999907	40.31
KRWWRWRRKW	6	-2,94	0.999901	40.05
KRWWQWWRR	4	-2,722222222	0.999873	38.98
KRWKRWWRW	5	-2,766666667	0.999866	38.74
KRWWRWQRR	5	-3,122222222	0.999835	37.84
KRRWRWWRRR	7	-3,359999999	0.999824	37.54
KRWRRWWRW	5	-2,833333333	0.999774	36.46
KRRWRWWRKK	7	-3,24	0.999682	34.98
KRWQRWWRR	5	-3,122222222	0.999602	34.00
KRRWRWWRKR	7	-3,3	0.999576	33.72
KRRWRWWRHK	6	-3,169999999	0.999568	33.65
KRWKRWWRKW	6	-2,88	0.999549	33.45
KRWKRWWRQ	5	-3,05555555555	0.999538	33.35
KRWRRWWRKW	6	-2,93999999999	0.999406	32.26
KRRWRWWQR	5	-3.12222222222	0.999372	32.02
KRWRRWWRQ	5	-3.12222222222	0.999146	30.68
KRRWRRWRKR	8	-3.66	0.998908	29.62
KRRWRWWQRR	6	-3.26	0.984675	18.15
KRRWRWWQKR	6	-3.2	0.976649	16.32

These sequences are particularly interesting for the following reasons:

- Optimal Amphipathic Profile: both sequences present an ideal balance between hydrophobic residues (W) and positively charged (K and R). This characteristic makes them highly amphipathic, that would favor the insertion in the bacterial membrane thanks to the hydrophobic region that interacts with lipids and the charged region that binds with the surface of the membrane.[113]
- High Charge: with a net charge of +5 and +4, these sequences can easily interact with negatively charged membranes of bacterial cells. The positive charge is crucial for antimicrobial activity, as it increases electrostatic attraction and facilitates penetration of the peptide through the membrane.[114]
- Small variations to test specificity: The small variation between "KRWWRWWRR" and "KRWWRWWRQ" allows exploring the effect of a single residue change on the overall behaviour of the peptide. This choice is based on the observations reported in the work of Amplify, where the authors highlight the difficulty of distinguishing very similar sequences and the usefulness of testing small variations to assess their effectiveness. [97] Thus, this approach aims to collect new data to understand how such a slight modification can affect activity.

As AMP2 was predicted to be less active than AMP3 and some other sequences listed in the table, this selection was made with two main objectives:

1. To provide a practical validation of the differences in log score and predicted antimicrobial activity.
2. To investigate the effect of the Gln residue on antimicrobial activity.

The incorporation of Gln residues in AMP sequences provides several limitations that can reduce their overall effectiveness. Primarily, Gln does not contribute to the peptide's net cationic charge, which is essential for strong electrostatic interactions with the negatively charged components of bacterial cell membranes. This reduction in positive charge can weaken the peptide's ability to bind effectively to microbial membranes, thus reducing its capacity to disrupt membrane integrity, a key mechanism of antimicrobial action. Additionally, glutamine's polar but non-hydrophobic nature may impair the peptide's amphipathic balance, which is crucial for integrating into lipid bilayers and forming pore-like disruptions or causing membrane thinning.[115] This can result in decreased antimicrobial activity, especially when compared to peptides with higher concentrations of hydrophobic and cationic residues.

The selection of antimicrobial peptide sequences was carried out also considering the helical wheel prediction.[116] The helical wheel is a graphical representation tool used to visualize the spatial arrangement of amino acids along an α-helix in proteins and peptides. It is particularly useful for understanding the structural and functional properties of antimicrobial peptides, many of which have a helical conformation that makes them effective against bacterial membranes. It's important that the sequences maintain an optimal

balance between hydrophobic and cationic residues. This structural configuration is essential for the peptide activity, as it facilitates the formation of a well-defined amphipathic α-helix with hydrophobic and cationic residues orientated on the opposite sides.[117] This distribution significantly increases the peptide's antimicrobial activity by promoting mechanisms such as pore formation and membrane thinning, which are critical for effective broad-spectrum bacterial killing. The selected sequences are illustrated in Figure 2.2 underlining how minor modifications in amino acid composition or positioning can impact the structure and function of the peptide.

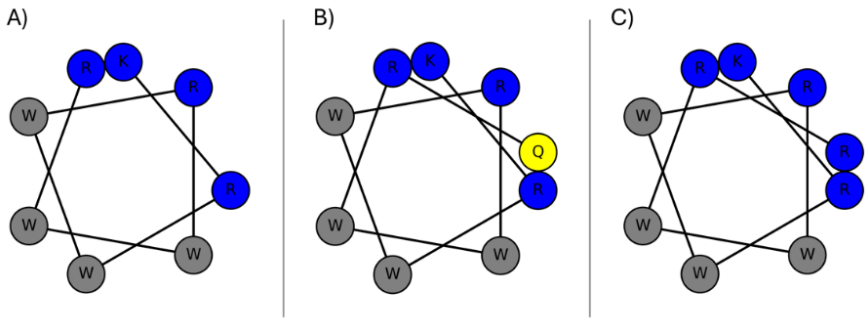

Figure 2.2. Helical wheel projection diagrams for AMP1 (A), AMP2 (B) and AMP3 (C) antimicrobial peptides.

Panel A of the figure shows the helical wheel projection of the prototype sequence. The peptide has an amphipathic arrangement, with positive residues on one side of the helix and the hydrophobic residues on the opposite side. This distribution is fundamental in the case of AMPs because it allows the interaction with bacterial membranes.

In panel B, the Gln residue in AMP2 peptide changes the original charge distribution, potentially reducing its ability to interact with the negative charges of the bacterial membranes. Thus, it can also cause a reduction of antimicrobial activity.

In panel C, there is the helical wheel prediction of the novel peptide AMP3. The addition of a residue of Arg doesn't alter the amphipathic nature, with Arg and Lys residues on one side and Trp residues on the opposite side.

2.1.2 Incorporation of Non-Natural Amino Acids into Peptide Sequences

Considering the predictions made using DL- tools and the analysis of alpha-helical wheel projections, the AMP3 sequence emerged as the best candidate for further modifications. AMP3 was then rationally modified by the introduction of a tail of one or two 6-aminohexanoic acid (Ahx) residues at the N-terminus, resulting in the generation of the sequences named AMP4 and AMP5 (Table 2). However, being Ahx an unnatural amino acid, the AMPlify score for these sequences could not be calculated.

Table 2. Sequences of AMPs, with AMP3 serving as the reference peptide without Ahx. AMP4 and AMP5 incorporate respectively two and one Ahx residues.

AMP3	**K-R-W-W-R-W-W-R-R-NH$_2$**
AMP4	**K-*Ahx*-*Ahx*-R-W-W-R-W-W-R-R-NH$_2$**
AMP5	**K-*Ahx*-R-W-W-R-W-W-R-R-NH$_2$**

The Ahx residues were inserted to act as a linker to increase the distance between the peptide and the membrane support. This modification offers several advantages, enhancing the functional properties of the peptide.[118] The Ahx may act as a flexible linker, allowing the peptide to have a higher mobility upon immobilization, thus reducing the steric hindrance that would happen by peptide conjugation to supports. [42]

All the peptides described were synthesized using SPPS and purified by preparative RP-HPLC. Their identity was confirmed by LC-MS (Figure 2.4) and their antimicrobial activity was subsequently assessed following the protocols explained in Experimental Methods Section.

RP-HPLC chromatograms (280 nm trace) of pure peptides are presented in Figure 2.3. Each peptide exhibited a distinct retention time (RT), as summarized in the results below:

- **AMP1:** Eluted at R_T = 13.10 min
- **AMP2:** Eluted at R_T = 13.02 min
- **AMP3:** Eluted at R_T = 12.88 min
- **AMP4:** Eluted at R_T = 14.30 min
- **AMP5:** Eluted at R_T = 13.48 min

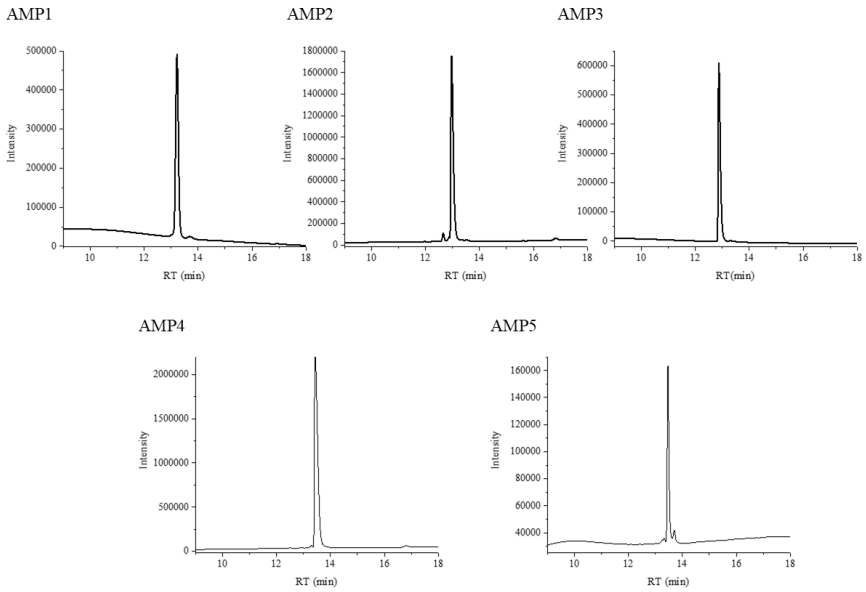

Fig. 2.3 Analytical RP-HPLC chromatograms for AMP1 to AMP5 (trace at 280 nm) showing distinct retention times (RT).

The theoretical and experimental mass values for the synthesized antimicrobial peptides are compared in Table 3 below:

Table 3. Comparison of theoretical and experimental mass values for the synthesized antimicrobial peptides.

Peptide	Theoretical mass values (g/mol)	Experimental mass values (g/mol)
AMP1	1358,6	1358,1
AMP2	1485,8	1486,2
AMP3	1514,3	1513,8
AMP4	1742,0	1741,0
AMP5	1626,9	1625,3

In the following figures are presented the ESI-MS spectrum of pure AMP1, AMP2, AMP3, AMP4 and AMP5 peptides.

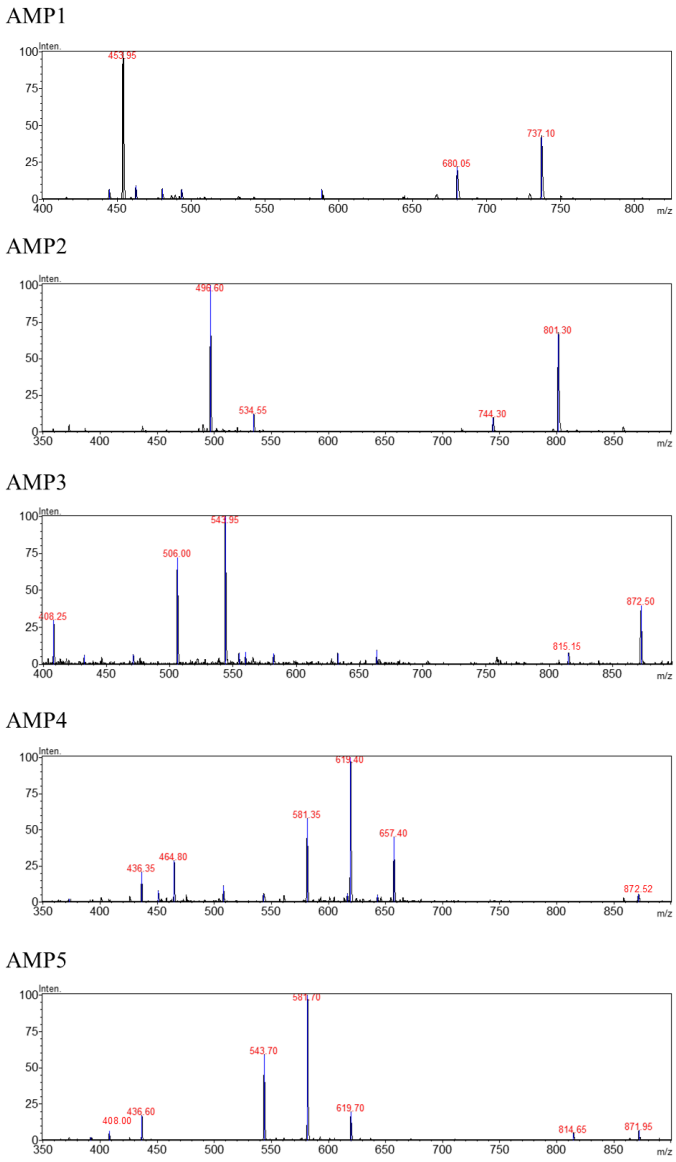

Fig. 2.4 ESI-MS spectra for AMP1 to AMP5 highlighting m/z peaks corresponding to specific ions.

As shown in Figure 2.4, the m/z ions $[M+2H^+]^{2+}$, $[M+3H^+]^{3+}$ and $[M+4H^+]^{4+}$ were detected for each peptide analyzed, corresponding to the theoretical values predicted.

Key details for each peptide are as follows:

- **AMP1:** the peaks at 453.95 and 680.05 represent $[M+2H^+]^{2+}$ and $[M+3H^+]^{3+}$ ions, respectively. The peak at 737.10 represents the $[M+2H^+ + TFA]^{2+}$ ion, indicating an adduct formed with one molecule of trifluoroacetic acid. The experimental mass value (1358,1 g/mol) agrees with the theoretical value (1358,62 g/mol).
- **AMP2:** the peaks at 744,30 and 496,60 represent $[M+2H^+]^{2+}$ and $[M+3H^+]^{3+}$ ions, respectively. The peak at 801,30 represents the $[M+2H^+ + TFA]^{2+}$ ion, while the peak at 534,55 represents the $[M+3H^+ + TFA]^{3+}$ ion indicating an adduct formed with one molecule of trifluoroacetic acid. The experimental mass value (1486,2 g/mol) agrees with the theoretical value (1485,8 g/mol).
- **AMP3:** the peak at 506,00 represents $[M+2H^+]^{2+}$ ions. The peaks at 408,25 and 543,95 and 815,15 represent respectively the $[M+4H^+ + TFA]^{4+}$, $[M+3H^+ + TFA]^{3+}$, $[M+2H^+ + TFA]^{2+}$ ion indicating an adduct formed with one molecule of trifluoroacetic acid. The peak at 872,50 represents the $[M+2H^+ + 2TFA]^{2+}$ due to an adduct formed with two molecules of trifluoroacetic acid. The experimental mass value (1514,3 g/mol) agrees with the theoretical value (1513,84 g/mol).
- **AMP4:** the peaks at 436,35, 581,35 and 872,52 represent $[M+4H^+]^{4+}$, $[M+3H^+]^{3+}$ and $[M+2H^+]^{2+}$ ions, respectively. The peak at 464,80 represents the $[M+4H^+ + TFA]^{4+}$ ion. The

peak at 619,40 represents the $[M+3H^{+}+TFA]^{3+}$, while the peak at 657,40 is the $[M+3H^{+}+2TFA]^{3+}$ due to an adduct formed with two molecules of trifluoroacetic acid. The experimental mass value (1741,04 g/mol) agrees with the theoretical value (1742,03 g/mol).

- **AMP5:** the peaks at 408,00, 543,70 and 814,65 represent $[M+4H^{+}]^{4+}$, $[M+3H^{+}]^{3+}$ and $[M+2H^{+}]^{2+}$ ions, respectively. The peak at 436,60 represents $[M+4H^{+}+TFA]^{4+}$ ion. The peak at 581,70 and 871,95 represents the $[M+3H^{+}+TFA]^{3+}$ and $[M+2H^{+}+TFA]^{2+}$, due to an adduct formed with one molecule of trifluoroacetic acid. The peak at 619,70 is the $[M+3H^{+}+2TFA]^{3+}$ due to an adduct formed with two molecules of trifluoroacetic acid. The experimental mass value (1741,04 g/mol) agrees with the theoretical value (1742,03 g/mol).

2.2 Minimum Inhibitory Concentration (MIC)

The antimicrobial activity evaluation was performed during a research period at Imperial College London, where advanced methodologies and facilities enabled reliable analysis. In order to confirm the DL prediction, the MIC was evaluated for all the peptides synthesized. The MIC is a crucial measure to assess and compare the antimicrobial activity of different compounds.[119] The activity of the five novel peptides was investigated against both Gram-Positive and Gram-Negative bacterial strains. The MIC values for each peptide are reported in Table 4. All peptides showed activity, but their potency varied notably based on the considered bacteria.

Table 4. MICs values for AMPs against several bacterial strains, comparing peptides with and without Ahx insertion.

	AMP1	**AMP2**	**AMP3**
E. coli	31	62	15
S. aureus	31	-	31
P. aeruginosa	250	250-500	125
Enterobacteria	>1000	>1000	>1000

	AMP4	**AMP5**
E. coli	62	31
S. aureus	-	31
P. aeruginosa	125	62
Enterobacteria	>1000	>1000

* All MIC values are expressed in μM.

Against *E. coli*, the peptides exhibited a MIC value of 31 μM, 62 μM, and 15 μM for AMP1, AMP2, and AMP3, respectively, indicating that AMP3 resulted in the most active among the tested bacteria. AMP3 also emerged as the best candidate against *P. aeruginosa,* which is notorious for its antimicrobial resistance, exhibiting a MIC value of 125 μM, more active than AMP1 and AMP2. When analyzing the efficacy against the Gram-positive *S. aureus,* AMP1 and AMP3 demonstrated similar efficacy, with MIC values of 31 μM, while AMP2 showed no detectable activity. The peptides AMP4 and AMP5, bearing the Ahx linker, showed a comparable activity with AMP3. This suggests that while the introduction of Ahx aimed to improve peptide flexibility and membrane interaction, it may not have an effect on the peptides' activity.

These results evidenced the effectiveness of the approach in developing highly active AMPs. Using these small peptide

sequences, modification of just one residue appears crucial for the activity. The biological characterization confirmed the computational prediction. Indeed, the sequence containing Gln as one extra residue at the C-terminus appears to be less active, in line with the predicted AMPlify log score. On the other hand, the addition of an extra Arg at the C-terminus provided a very active sequence. The lower MIC value for AMP3 indicates a stronger antibacterial effect and broad-spectrum antimicrobial properties, being effective with low MIC values toward both Gram-positive and Gram-negative bacteria, making it a promising candidate for the biophysical characterization on model membranes.

Expanding the evaluation to Mycobacterium species, the peptides were tested against several strains, including *Mycobacterium smegmatis*, *Mycobacterium abscessus*, *Mycobacterium avium*, and *Mycobacterium chelonae* (Table 5). The results showed that all the peptides had a significant antimicrobial activity against *M. smegmatis,* while no efficacy is reported for all peptides against the remaining strains.

Table 5. MICs values of AMP1 to AMP5 against *Mycobacterium strains.*

	AMP1	**AMP2**	**AMP3**
M. smegmatis	15-30	15-30	8
M. abscessus	>3000	>3000	>3000
M. avium	>3000	>3000	>3000
M. chelonae	>3000	>3000	>3000

	AMP4	**AMP5**
M. smegmatis	15	15
M. abscessus	>3000	>3000
M. avium	>3000	>3000
M. chelonae	>3000	>3000

* All MIC values are expressed in μM.

The selective antimicrobial activity of the peptides against *M. smegmatis* is reasonable due to the different cell envelope composition and membrane properties. *M. smegmatis* has the mycolic acid-rich cell wall characteristic of mycobacteria. Its cell envelope is relatively more permeable than that of pathogenic species such as *M. abscessus*, *M. avium*, and *M. chelonae*. These latter pathogenic species have a more robust and thicker outer layer rich in mycolic acids, making them highly impermeable and resistant to antimicrobial agents, including peptides. The structural differences in the cell envelope also involve variations in surface lipids and glycolipids, such as glycopeptidolipids (GPLs), which can influence membrane properties and resistance levels across different species.[120] Moreover, differences in surface charge and membrane composition among *Mycobacterium* species could influence the electrostatic interactions with cationic antimicrobial peptides. Peptides are more likely to interact with bacterial species that have a

higher negative surface charge or a membrane composition that favors the insertion and activity of amphipathic peptides. These factors explain why antimicrobial peptides demonstrate selective activity against *M. smegmatis* while being ineffective against other, more resistant mycobacterial species.

2.3 Biophysical Characterization of AMP3

To gain deeper insight into the peptide-membrane interaction mechanism, peptide AMP3 was selected for further biophysical studies due to its broader-spectrum antibacterial activity compared to the other peptides. Specifically, the interaction of AMP3 with POPE/POPG (7/3 mol/mol) liposomes, which serve as a model for *E. coli* bacterial membranes, was investigated.

2.3.1 AMP3 interacts with bacterial membrane models

Most known antimicrobial peptides have as a primary target the lipid matrix of bacterial membrane. Similarly, peptide AMP3 was evaluated for its ability to bind the biomembrane models that resemble bacterial membranes by Trp fluorescence emission measurements in order to determine the mole fraction partition constant (K_x), that represents an index of the interaction between the peptide and model membranes. In order to evaluate the K_x, a peptide solution at a fixed concentration (6 μM) was titrated with a suspension of large unilamellar vesicles (LUVs) made of POPE/POPG (7/3 mol/mol). Then, changes in the fluorescence emission from the Trp residues of AMP3 were followed.[121] Unfortunately fluorescence intensities of AMP3 at low lipid

concentrations was found to be not reproducible since a decrease of the signal intensity with time was observed. Instead, at high lipid concentration, the signal appears to be stable. Most likely, at low lipid concentrations peptide-induced aggregation of liposomes occurred, leading to the lack of reproducibility of the recorded spectra. Of note, a similar behaviour was also observed for the peptide CA(1-7)M(2-9) with PE/PG vesicles.[122] Despite this problem, analysis of the emission spectrum of the peptide in the absence and in the presence of 550 μM lipids revealed interesting features (Figure 2.5). There is evidence of a blue shift of about 13 nm in the position at the peak of emission combined with a strong increase in the fluorescence intensity. This can be explained by the fact that the peptide can interact with the bacterial model membrane and the Trp residues are experiencing a more hydrophobic environment, possibly suggesting a partial penetration of the peptide in the membrane.

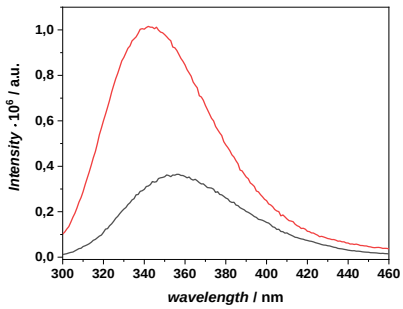

Fig. 2.5 Fluorescence emission spectra of AMP3 in the absence (black line) and in the presence (red line) of POPE/POPG LUVs.

To better understand the interaction and determine the actual K_x, an alternative approach was used, by fluorescence quenching experiments, utilizing acrylamide as a quencher (for details see

Experimental Methods section). Acrylamide, a water-soluble molecule, effectively quenches the fluorescence of Trp residues but lacks the ability to partition into the membrane. Consequently, in a mixture of peptides and lipids, acrylamide predominantly quenches the fluorescence of peptides in their free (unbound) form. As the peptide exists in either a bound or unbound state, the fraction and concentration of the free peptide were estimated by analyzing the data through a modified Stern-Volmer equation:

$$\frac{F_0}{\Delta F} = \frac{1}{f_a K_a [Q]} + \frac{1}{f_a}$$

In this equation, F_0 is the fluorescence intensity of the sample in the absence of acrylamide. Instead, $\Delta F = F - F_0$ is the difference in the intensity of the sample in the presence and absence of acrylamide, respectively.[123] The parameters K_a and f_a are the dynamic quenching constant (also denoted as the Stern-Volmer constant) and the fraction of free peptide (accessible to the quencher), respectively. The dynamic quenching constant describes quantitatively the ability of acrylamide to turn off the fluorescence emission of the accessible fluorophore. Instead, [Q] is the concentration of acrylamide. Thus, from such data analysis, it is possible to evaluate the fraction of free peptide that, multiplied by the total concentration of the peptide gives the concentration of unbound peptide. From the definition of mole fraction partition constant, it is possible to calculate the value of K_x.

$$K_x = \frac{[P_b]/[L]}{[P_f]/[W]}$$

In the equation above, $[P_b]$, $[P_f]$, $[L]$ and $[W]$ represent the molar concentrations of the membrane-bound peptide, the free peptide in the aqueous phase, lipids, and water, respectively. By leveraging this approach and analyzing the data results with the modified Stern-Volmer equation, is possible to evaluate the unbound peptide fraction that is accessible to the quencher (f_a); the latter allowed the determination of the value K_x. Figure 2.4 reports the fluorescence emission spectra recorded at increasing acrylamide concentrations, fixing the solution of the peptide AMP3 (at 3 μM) mixed with a POPE/POPG LUVs (30μM). Figure 2.7 reports the modified Stern-Volmer plot, obtained from the data reported in Figure 2.6.

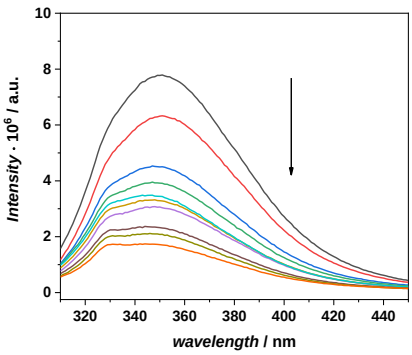

Fig. 2.6 Fluorescence emission spectra of a solution of AMP3 (3 μM) mixed with a lipid suspension of POPE/POPG LUVs at total lipid concentration of 30 μM. The arrow indicates the direction of increasing concentration of acrylamide showing the quenching of fluorescence emission.

Analysis of figure 2.6 highlights that the Trp residues in the peptide are increasingly quenched, implying that they are accessible to the quencher, likely due to their positioning near the peptide surface or in a more solvent-exposed region. The pattern indicates that as quencher concentration increases, the peptide's tryptophan residues

become less shielded, potentially reflecting changes in peptide conformation or its interaction with surrounding lipid membranes, where alterations in exposure may affect quenching efficiency.

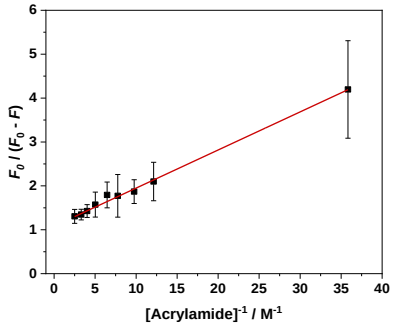

Fig. 2.7 Modified Stern-Volmer plot obtained using the data reported in Figure 2.4. The peptide solution (AMP3 at 3 µM) was mixed with POPE/POPG LUVs at a lipid concentration of 30 µM. The red line represents the best fit of the experimental data according to the modified Stern-Volmer equation described in the Material and Methods section.

The experiment was also repeated changing the ratio between the peptide and the lipids. Figure 2.8 reports the data obtained using the following conditions: AMP3 concentration 3 µM and a higher lipid concentration 150 µM.

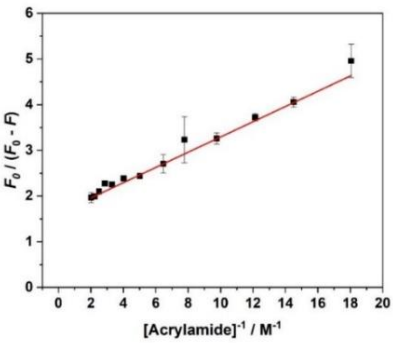

Fig. 2.8. The modified Stern-Volmer plot obtained from the titration with acrylamide of a solution containing AMP3 3 µM mixed with PE/PG LUVs at total lipid concentration of 150 µM.

Table 6 reports the data obtained by the two analyses. The *Kx* values obtained from both experiments were comparable, thus indicating that the quenching efficiency of accessible tryptophan residues remains high, even with increased peptide insertion into the membrane.

Table 6. Fraction of free peptide (f_a) obtained from the analysis of fluorescence quenching data using the modified Stern-Volmer equation for the two explored concentrations. From these values, the mole fraction partition constant (K_x) was calculated.

System	f_a	K_x	R^2
AMP3 3 µM + POPE/POPG 30µM	0.9244 ± 0.026	(1.53± 0.56) · 10^5	0.9681
AMP3 3µM + POPE/POPG 150µM	0.6154 ± 0.008	(2.37± 0.04) · 10^5	0.9821

The CD spectra of the peptide AMP3 was recorded to examine the conformational behaviors in solution and upon model membrane binding (Fig 2.9). The peptide was analyzed in two different conditions: the black line indicates the peptide in 10 mM phosphate buffer pH= 7.4, while the red line represents the peptide in the presence of POPE/POPG LUVs. In the CD spectrum, two minima were observed: one around 225 nm and one around 201 nm. In particular, the band at around 225 nm is due to the Trp´s contribution, as also observed in other Trp-rich peptides while the band at around 200 nm, on the other hand, is characteristic of disordered peptides.[124–127] However, a negative band around 230 nm has been often correlated to Trp rich peptides with turn structures, that can be also tentatively assigned to AMP3.[125,128–130] In the presence of

POPE/POPG vesicles, at lipid-to-peptide ratio of 10, no drastic changes in the shape of the spectrum of AMP3 were observed. However, changes in the intensities of the two bands were detected (Figure 2.9). [39,131] This observation may suggest that AMP3 interacts with model membranes and this interaction causes small conformational changes. Unfortunately, due to the strong Trp contributions it is not possible to unambiguously assign the conformation adopted by the peptide both in neat buffer and in the presence of model membranes.

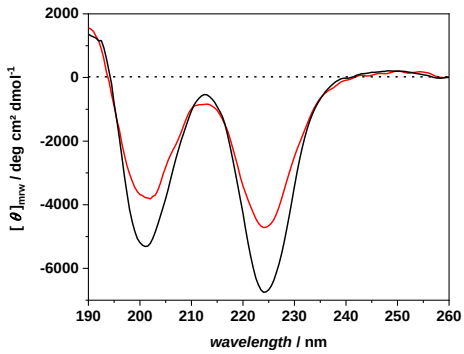

Fig. 2.9 Far-UV circular dichroism spectra of AMP3 peptide (60 µM) in neat buffer conditions (black line) and in the presence of POPE/POPG LUVs (red line) at total lipid concentration of 600 µM.

2.3.2 The effects of AMP3 on bilayer stability

To delve deeper into the interaction of peptides with membranes, the effect of AMP3 on POPE/POPG bilayers stability was studied. The Differential Scanning Calorimetry (DSC) measurements of POPE/POPG multilamellar vesicles (MLVs) were carried out in absence and in presence of AMP3, at a lipid-to-peptide ratio of 50, 25 and 10, respectively. The obtained thermograms are reported in Figure 2.10.

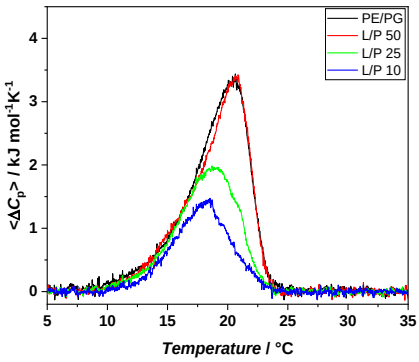

Fig. 2.10 DSC thermograms of POPE/POPG (7/3 mol/mol) MLVs at total lipid concentration of 1 mM in the absence (black line) and in the presence of AMP3 peptide at the lipid-to-peptide ratio of: 50 (red line), 25 (green line) and 10 (blue line).

In close correlation with DSC data, Table 7 reports the thermodynamic parameters associated with gel-to-liquid phase transition of the liposomes.

Table 7. Thermodynamic parameters associated to the gel-to-liquid phase transition of POPE/POPG MLVs obtained by means of differential scanning calorimetry. Normalization per total moles of lipids.

System	T_m / °C	[a]ΔH_m / kJ mol^{-1}
POPE/POPG	20.6 ± 0.1	19.6 ± 2.0
+ AMP3 at L/P = 50	20.9 ± 0.1	18.5 ± 1.9
+ AMP3 at L/P = 25	18.7± 0.3	12.3 ± 1.2
+ AMP3 at L/P = 10	18.5± 0.3	8.1 ± 0.8

The DSC thermogram of POPE/POPG vesicles was centered at 20.6 °C and it was characterized by an enthalpy change (ΔH_m) of 19.6 kJ mol^{-1}, in agreement with previously reported data in the literature.[132] Interaction with the AMP3 peptide led to a slight increase in the main transition temperature (T_m), while the enthalpy change remained constant within the experimental errors. The sharper peak suggested an increase in the transition cooperativity; this effect could be attributed to the AMP3 preferential interaction with the negatively charged headgroups of POPG lipids. This interaction on the membrane surface promotes the formation of a more homogeneous PE-rich domain that has the phase transition at higher temperature and with increased cooperation due to the reduced heterogeneity of the lipid environment. As the peptide concentration was increased to an L/P = 25, an important effect was detected, including a notable decrease in both T_m and ΔH. Therefore, the DSC peak looks more intricate, and it seems composed of at least two partially overlaid transitions, indicating that lipid domains are formed within the bilayer. This phenomenon is consistent with the behaviour observed

for several other cationic peptides, which are known to induce phase separation in mixed lipid systems.[133–135] The peak observed at lower temperature could correspond to a POPG-rich domain, while the peak at higher temperature might represent a POPE-rich domain, given the known transition temperatures of these individual lipids (~24 °C for POPE and ~-5 °C for POPG). The reduction in the overall enthalpy change compared to that of pure liposomes and conditions with L/P = 50 suggests that AMP3 penetrates the membrane to some degree, disrupting the packing of the lipids, a characteristic also observed in studies involving poly-Lys peptides with PG membranes.[136] At L/P = 10, the highest peptide concentration explored, a further reduction of the ΔH_m was observed, although the T_m value was unaffected. Interestingly, the higher-temperature peak, present at lower peptide concentrations, disappeared. This could be explained by the accumulation and deeper penetration of AMP3 molecules within the PE-rich domain, leading to a significant disruption of lipid packing and a loss of the characteristic higher-temperature phase transition. While it may initially appear surprising that the cationic AMP3 has a more pronounced effect on the PE-rich domain than on the PG-rich domain, several factors must be considered:

1. Both lipid species are distributed across the different domains, allowing the peptide to interact throughout the membrane.
2. PE lipids, characterized by their smaller headgroups, induce a negative curvature in the membrane, which

could facilitate the peptide's insertion into the bilayer by creating regions of increased membrane flexibility.

The results obtained from the DSC analysis suggest that the peptide AMP3 was able to insert into the bilayer. This interaction implies a degree of affinity and potential integration within the membrane structure, likely influencing the organization or stability of the lipid components. However, the precise extent to which AMP3 penetrates the membrane remains unclear. It is not clear whether AMP3 integrates deeply into the hydrophobic core or remains closer to the lipid headgroup region, interacting with the bilayer surface. For this reason, additional fluorescence experiments were performed. These experiments were carried out using the probes Laurdan and DPH embedded in POPE/POPG vesicles. These probes are important tools in fluorescence because they allow to study both the organization and the dynamics of lipid membranes. Laurdan (6-dodecanoyl-2-dimethylaminonaphthalene) was used to study phase transition into the lipids because it is influenced by polarity and water molecules.[137] When Laurdan is in a hydrated region of the membrane, it emits at longer wavelengths, while in a less hydrated region it emits at shorter wavelengths. This phenomenon shift is quantified by the generalized polarization (GP) parameter, given by the formula:

$$GP = \frac{F_{437} - F_{500}}{F_{437} + F_{500}}$$

where F_{437} and F_{500} were the fluorescence intensities in the Laurdan emission spectra at 437 nm and 500 nm, respectively. [138] Calculation

of GP values by this approach makes it possible to quantify the different phases into the bilayer. On the other hand, DPH (1,6-Diphenyl-1,3,5-Hexatrien) probe penetrates the membrane and measures the fluidity of the internal hydrophobic region. It provides detailed information on lipid mobility through anisotropy measurements, which reflect the degree of order and freedom of movement of the lipid tails. The following figures (Figure 2.11 and Figure 2.12) report the generalized polarization (*GP*) of Laurdan and DPH anisotropy (< *r* >) as function of peptide concentration. The red dashed lines do not represent data fitting but are intended as a guide for the eye.

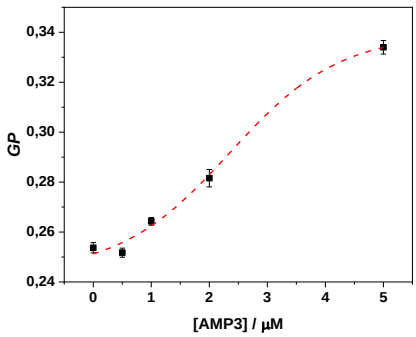

Fig. 2.11 Generalized polarization (*GP*) of the probe Laurdan embedded in POPE/POPG LUVs as function of AMP3 concentration.

An inspection of Figure 2.11 reveals that the *GP* value significantly increases with peptide concentration; indeed, in the absence of the peptide, the value results 0.25, while adding [AMP3] = 5 µM, which corresponds to L/P = 10, the values increase to around 0.33. This may suggest that the peptide binding and localization occurs at the level of headgroups of lipids: through its interaction, the peptide promotes

the dehydration of the surface, and then, partially penetrating the bilayer, it induces a higher degree of order in this membrane region. Figure 2.12 reports DPH anisotropy. Due to its high hydrophobicity, the DPH probe splits deeply into the hydrophobic core of the bilayer. The experiment was conducted exploring an AMP3 range of concentrations up to 5 μM, L/P = 10. Interestingly, no significant changes in DPH anisotropy were observed, which means that the peptides didn't perturb the interior of the membrane.

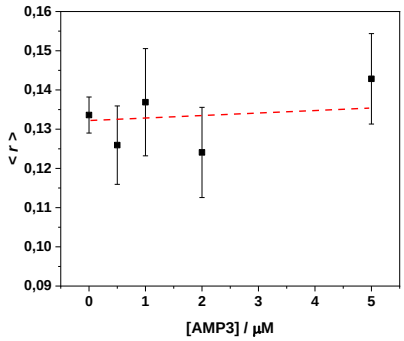

Fig. 2.12 Fluorescence anisotropy (< *r* >) of DPH in POPE/POPG unilamellar vesicles as function of peptide concentration. The fluorescence experiments were performed at the temperature of 25 °C.

The data collectively indicate that AMP3 exerts a concentration-dependent effect on both the microscopic and mesoscopic characteristics of the lipid bilayer. At low peptide concentrations, AMP3 primarily localizes on the bilayer surface, interacting with headgroup regions without significant penetration. As AMP3 concentration increases, there is evidence of domain formation within the bilayer, likely due to peptide-peptide interactions that promote lateral segregation. This segregation facilitates partial insertion of AMP3 into the membrane, while the peptide remains

largely localized near the headgroup regions, altering the bilayer's organizational structure and potentially influencing its stability and fluidity. These findings suggest that the interaction of AMP3 with the bilayer involves both surface-associated and insertion mechanisms that vary with peptide concentration, hinting at concentration-dependent modulation of the membrane's biophysical properties.

Chapter 3

Section 1: Conclusion

DL methods were crucial to identify and optimize the AMPs sequence, in particular in the identification of the peptide named AMP3, which represents an intriguing candidate for its antimicrobial activity and ability to interact with bacterial membranes. Deep neural network analysis facilitated the exploration of a vast space of potentially active sequences, enabling a rapid and targeted selection into the most active peptides. The use of advanced DL models, such as RNN and conditional autoencoders, facilitated the discovery of AMP3. The latter, identified among thousands of sequences obtained in silico, was selected based on the high score attributed by the DL model to its potential activity.

Experimental analysis confirmed the DL prediction; indeed, AMP3 has shown high antimicrobial efficacy against both Gram-positive and Gram-negative bacteria, including *E. coli, S. aureus, and P. aeruginosa*. The results of the MIC assays showed that AMP3 has bactericidal activity at low concentrations, further supporting the reliability of DL in predicting complex biological properties.

DL simulations also guided the choice of amphipathic peptide configuration, optimizing the arrangement of hydrophobic residues and loads to facilitate selective interaction with bacterial membranes. The balance between hydrophobicity and positive charge, predicted as ideal for optimal antimicrobial action, has been experimentally confirmed, with AMP3 showing a high ability to interact with bacterial membranes. Predictive analysis has thus facilitated the identification of a sequence allowing the peptide to enter the bacterial membrane effectively.

Moreover, it was possible to study the effect of small variations in the amino acid sequence. It has been observed that residues such as Arg and Trp, essential for antimicrobial activity, are optimally arranged in the structure of AMP3, increasing the ability of the peptide to bind to the bacterial membrane and penetrate it. On the other hand, the inclusion of a Gln in place of an Arg resulted in a decrease in antimicrobial activity, in line with DL prediction.

In conclusion, the use of DL has not only accelerated the discovery of AMP3 but also demonstrated its transformative potential in antimicrobial research. Enabling fast, accurate and reliable identification of bioactive peptides, DL offers a revolutionary approach to combat antimicrobial resistance.

Based on these results, this sequence was anchored to a polymer support in order to obtain an antimicrobial membrane (see section 2)

.

Chapter 4

Experimental Methods

4.1 Computational methods

The process started with the use of HydrAMP, an advanced model based on conditioned variational auto-encoders (cVAE). This tool has allowed to generate a large set of peptide sequences optimized for specific parameters such as net charge and hydrophobicity. Starting from the AMP1 prototype peptide (KRWWRWWR-NH2), candidate sequences were generated using HydrAMP. An initial candidate pool was created using the analogue generation protocol, with 20,000 total decoding attempts and temperature equal to 5.0, leading to approximately 1,000 potential AMPs derived from the prototype sequence. HydrAMP created a continuous latent representation of the sequence space, generating new combinations that meet the required characteristics. Peptide lengths was limited to 8–10 residues, and an overall charge restricted between +4 and +10. After generation, the sequences were analyzed using AMPlify, a prediction model based on integrated bi-LSTM networks with attention mechanisms.

AMPlify evaluated each sequence, assigning a predictive score that reflected the likelihood of antimicrobial activity. The formula used by AMPlify to calculate the log score is: -10*log(1-probability score). This step also identified key regions of the sequences that contribute most to antimicrobial activity, providing valuable insights for further optimization.

After the analysis with AMPlify, a filtering process was applied based on the following criteria:

- Removal of duplicate sequences.
- Elimination of sequences containing residues problematic for synthesis, such as cysteine (Cys) and methionine (Met).
- Exclusion of sequences with a length greater than 10 residuals.
- Rejection of sequences with excessive hydrophobicity (>50%).
- Filtering sequences which are difficult to synthesize, such as those with more than three consecutive Trp residues.

The computational workflow was structured in the following main steps:

- Initial generation of sequences with HydrAMP, controlling relevant physico-chemical parameters.
- Predictive evaluation with AMPlify to classify sequences according to their potential antimicrobial efficacy.
- Sequence filtering to ensure synthetic feasibility and compliance with design requirements.
- Selection and optimization of the best candidates, including introduction of targeted modifications to improve functionality or stability.

4.2 Solid Phase Peptide Synthesis and Purification

The synthesis of the selected AMP sequences obtained through DL methods was carried out with solid phase methodology. SPPS is a commonly used technique for the synthesis of peptides. By

sequentially coupling amino acids on a solid support, SPPS enables the production of peptides with high yield and purity.

4.2.1 Peptide synthesis

The peptides were synthesized using an automatic ABI 433A peptide synthesizer (Applied Biosystem, Foster City, CA, USA) with 0.25 mmol Fmoc-protocols on a 0.25 mmol scale. The C-terminal was amidated, while the N-terminal was free. The resin used was Rink Amide Resin with a substitution of 0.54 mmol/g.

The following protected amino acids were used:

Fmoc-Trp(Boc)-OH, Fmoc-Lys(Boc)-OH, Fmoc-Arg(Pbf)-OH, and Fmoc- Gln(Trt)-OH.

Standard synthetic protocols were followed for the deprotection, activation, coupling, and capping cycles. These steps were repeated with each successive amino acid addition until the complete assembly of the peptide chain. After the synthesis was completed, the resin was washed four times with dichloromethane (DCM), NMP, isopropanol, and methanol, and then dried.

4.2.2 Cleavage and deprotection

Two deprotection protocols were employed, as the initial procedure had low yield. The protocols are detailed below:

Protocol 1: Peptide cleavage from the resin, accompanied by side chain deprotection, was performed using a solution mixture of 95% trifluoroacetic acid (TFA), 2.5% triisopropylsilane (TIS), and 2.5% water (v/v/v, 40 mL total volume). The reaction was conducted for

one hour at 0 °C, followed by an additional hour at room temperature, under slight magnetic stirring. Then, the resin was filtered, and the cleavage solution was collected under vacuum in a glass flask. The resin was quickly washed with TFA to ensure complete peptide removal. The solution was concentrated to a reduced volume, and the crude peptide was immediately precipitated by adding five volumes of cold diethyl ether relative to the peptide solution. The precipitate was collected by centrifugation, with the supernatant carefully decanted, followed by two washes with three volumes of cold diethyl ether. The peptide was then dried to remove residual ether, re-dissolved in water, and lyophilized.

Protocol 2: A two-step deprotection and cleavage process was implemented, optimized specifically for Rink amide resin. Initially, the resin was placed in a glass funnel fitted with a fine sinter to enable controlled solvent flow. It was then treated with a 10% TFA solution in dichloromethane (DCM), allowing the cleavage solution to percolate through the resin. Subsequently, a 5% TFA solution was used to rinse the resin thoroughly, promoting effective peptide removal due to the continuous addition of the acid. Continuous solvent flow was maintained to prevent incomplete cleavage, which can occur in static conditions. To enhance cleavage efficiency, 1-5% TIS was incorporated into the mixture. The final stage of deprotection was conducted using 95% TFA, with 2,5 % of TIS and 2,5 % of water used as a scavenger. Excess TFA/DCM was eliminated under reduced pressure, and the crude peptide was precipitated in cold diethyl ether, followed by drying under vacuum.

4.2.3 Peptide analysis and purification

The identity of the crude peptide was determined by analytical reverse-phase high-performance liquid chromatography (RP-HPLC) analysis, using a Shimadzu LC-10ADvp system equipped with an SPDM10Avp diode-array detector. Electrospray ionization ion trap time-of-flight mass spectrometry (ESI-IT-TOF) spectra were acquired on a Shimadzu LCMS-IT-TOF system, interfaced via ESI, with data acquisition and processing carried out using the Shimadzu LC-MS Solution Workstation software.

Peptide purification was carried out with a Shimadzu LC-8A preparative HPLC system (Shimadzu, Kyoto, Japan) featuring an SPD-M10AV UV-Vis detector. A Reverse Phase (RP) Vydac C18 column (250 cm x 22 mm; 10 µm) was employed, eluting with a linear gradient of H2O 0.1% TFA (eluent A) and acetonitrile 0.1% TFA (eluent B) at a flow rate of 23 mL/min. A gradient from 5% to 70% of solvent B was applied for optimal separation from undesired by-products. Peptide purity and identity were evaluated through RP-HPLC-MS analyses using a Shimadzu LC-10ADvp equipped with an SPDM10Avp diode-array detector. Mass spectra were recorded on a Shimadzu LC-MS-2010EV system with ESI interface and a quadrupole mass analyzer. A Vydac C18 column (150 mm x 4.6 mm, 5 µm) was used, eluting with the same gradients employed for purification—over 30 min at a flow rate of 1 mL/min in LC analyses and over 60 min at a flow rate of 0.5 mL/min in LC-MS analyses. ESI-MS analyses were performed in the positive ion scanning mode, covering the 400–1800 Th range of m/z.

4.3 Antimicrobial activity determination

Antimicrobial activity was evaluated for all the synthesized peptides. The minimum inhibitory concentration (MIC) is defined as the lowest concentration of an antimicrobial agent that prevents visible growth of a microorganism after overnight incubation. It serves as a quantitative measure of the effectiveness of a compound against a specific bacterial strain, with lower MIC values indicating higher antimicrobial potency.

4.3.1 Bacterial strain and Growth Conditions

In this study, a total of seven bacterial strains were used: *Escherichia coli* ATCC 25922, *Staphylococcus aureus* ATCC 29213, *Pseudomonas aeruginosa* ATCC 27853, *Enterobacteria, Mycobacterium smegmatis*, *Mycobacterium avium*, *Mycobacterium chelonae*. All bacterial strains were cultured in Mueller-Hinton Broth (MHB; Becton Dickinson Difco, Franklin Lakes, NJ, USA) and on Tryptic Soy Agar (TSA; Oxoid Ltd., Hampshire, UK). For each experiment, the bacteria were inoculated and grown overnight in MHB at 37°C. The following day, cultures were transferred to fresh MHB and grown to the mid-logarithmic phase.

4.3.2 Antimicrobial Activity

The determination of the minimum inhibitory concentration (MIC) using the two-fold broth microdilution method involves several key steps. First, bacterial strains were cultured in an appropriate growth medium, Mueller-Hinton Broth (MHB) for *E. coli, S. aureus, P. aeruginosa* and Enterobacteria, while Tryptic Soy Agar was used for

Mycobacterium, in both cases were incubated overnight at 37°C. The overnight culture was then diluted in fresh broth to achieve a standardized inoculum, adjusted to approximately 2×10^6 CFU/mL. The antimicrobial compound was serially diluted in a two-fold manner in MHB, preparing a series of wells in a 96-well plate, where each successive well contains half the concentration of the compound compared to the previous one starting from a concentration of 1mM for each peptide. An equal volume of the prepared bacterial inoculum was then added to each well containing the antimicrobial dilutions, usually 100 µL of the bacterial suspension to 100 µL of the antimicrobial solution, resulting in a final concentration of approximately 1×10^6 CFU/mL. Positive control wells (bacteria without the antimicrobial agent) and negative control wells (broth only) were included to validate the test. The plate was then covered and incubated at 37°C for 24 hours. Following incubation, wells were examined for visible signs of bacterial growth, typically indicated by turbidity. The MIC is defined as the lowest concentration of the antimicrobial agent that prevents visible growth.

4.4 Bio-Physical characterization

4.4.1 Circular Dichroism (CD)

Circular dichroism (CD) spectra of the peptides were recorded using a JASCO J-715 spectropolarimeter (Jasco Corporation, Tokyo, Japan). The measurements were performed in a 0.1 cm path-length quartz cuvette, with the spectra averaging over three scans. The instrument was set with the following parameters: a scan speed of 20

nm/min, a response time of 4 seconds, and a bandwidth of 2 nm. The temperature during the measurements was maintained at 25 °C through a Peltier system. Peptide samples were prepared in a 10 mM sodium phosphate buffer at pH 7.4, with a peptide concentration of 60 μM. The peptide CD spectra were collected both in the absence and presence of LUVs at lipid concentrations of LP10. For each sample, a background blank (buffer or lipid suspension alone) was subtracted to account for any extraneous signal.

4.4.2 Differential Scanning Calorimetry

Differential Scanning Calorimetry (DSC) experiments were performed by means of a nano-DSC from TA Instruments (New Castle, DE, USA) Since multi lamellar vesicles (MLVs) have a high peak resolution, they were used in all DSC studies. The calorimetry vessel was filled with 700 μL of 1 mM vesicle suspension (POPE/POPG 70/30), with and without peptide at the lipid-to-peptide ratio of 50, 25 and 10. Instead, the refence cell was filled with the sodium phosphate buffer. The experiments were performed over a temperature range of 20–50 °C, at scan rate of 1 °C/min. A separate buffer *vs.* buffer scan was also collected and subtracted from the lipid *vs*. buffer scan. The obtained data were analyzed by means of NanoAnalyze software supplied with the instrumentation. The reported enthalpy changes of lipid phase transitions were normalized by total moles of lipids. Origin software (OriginLab, Northampton, MA, USA) was used to visualize the data.

4.4.3 Liposome preparation

Liposomes for various experiments were prepared through a multi-step process. Lipids stock solutions were prepared by weighting appropriate amounts of lipids and dissolving them in a chloroform/methanol (2/1 vol/vol) mixture. These stock solutions were used to prepare liposomes composed of POPE/POPG (7/3 mol/mol) by mixing appropriate amounts of the two lipids dissolved in the organic mixture. To form lipid films, the organic solvent was removed using a stream of dry nitrogen gas. The lipid films were kept under vacuum for approximately 5 hours to ensure the complete removal of any residual organic solvent. Then, the lipid films were hydrated with a given volume of NaP buffer and vigorously vortexed to produce a suspension of Multi Lamellar Vesicles (MLVs). Typically, liposomes suspensions with a total lipid concentration of 5 mM (final volume 1 mL) were prepared. For the preparation of large unilamellar vesicles (LUVs), the MLVs suspensions were extruded 31 times, through a 100 nm polycarbonate membrane using a mini-extractor (from Avanti Polar Lipid Inc., Alabaster, USA). For the preparation of labeled vesicles (with the probes Laurdan or DPH), the fluorescence probes dissolved in DMF (Laurdan) or chloroform (DPH) were added to the organic mixture containing lipids and then, the same procedure as described above was followed. For DPH, the lipid-to-probe ratio was 150. Instead, for Laurdan, the lipid-to probe ratio was 30. The resulting LUVs suspensions were subsequently used to study peptide binding.

Steady-state Fluorescence Spectroscopy

All the fluorescence experiments were performed by means of a Fluoromax-4 from Horiba Scientific (Edison, USA) at the temperature of 25 °C using a quartz cuvette with a path length of 1 cm.

Binding Experiments

To evaluate the interaction of the AMP3 peptide with POPE/POPG large unilamellar vesicles (LUVs), two experimental approaches were employed. The first approach involved monitoring changes in the fluorescence intensity of AMP3, due to the Trp residues, by recording emission spectra of the peptide in solution. The concentration of AMP3 was fixed at 6 μM, while the lipid concentration varying in the range 0 to ~1 mM. The excitation wavelength was set at 280 nm, and emission spectra were collected over a range of 300 to 450 nm. The slit widths for the excitation and emission wavelengths were adjusted to 8 nm and 10 nm, respectively. To minimize distortions in the emission spectra caused by light scattering from the liposomes, polarizers were used during the titration experiments[121,139]. However, the data proved to be non-reproducible, likely due to aggregation of AMP3-induced liposomes at a low lipid-to-peptide ratio. For this reason, a second approach was followed, and the K_x was evaluated by performing quenching experiments by using acrylamide (for details, see the paragraph below). The experiments were conducted as follows: a solution of 3 μM of AMP3 was mixed with a vesicle's suspension of POPE/POPG LUVs at total lipid concentration of 30 μM and 150 μM. The samples

were then titrated with an aqueous solution of acrylamide at 25 wt% where the same amount of peptide and lipids were also present to avoid their dilution during the addition. The emission spectra were recorded from 310 nm to 450 nm, with the excitation wavelength set at 295 nm and using a 1-cm path length quartz cuvette with a magnetic stirrer bar. The fluorescence intensity of the sample in the presence of acrylamide was corrected for its absorbance at the wavelength of excitation, as previously described[140]. All the experiments were performed in 10 mM sodium phosphate buffer, pH 7.4 and at the temperature of 25 °C.

Laurdan generalized polarization (GP)

Fluorescence emission spectra of the probe Laurdan embedded in POPE/POPG LUVs were recorded upon excitation at 340 nm and collecting the intensity in the range 390-620 nm. The lipid concentration was 50 μM and the lipid-to-probe ratio was 30. Emission spectra in the presence of AMP3 peptide at concentrations of 0, 0.5, 1, 2, 5 and 10 μM were recorded. The generalized polarization (GP) parameter was evaluated through the equation:

$$GP = \frac{F_{437} - F_{500}}{F_{437} + F_{500}}$$

where F_{437} and F_{500} were the fluorescence intensities in the Laurdan emission spectra at 437 nm and 500 nm, respectively. All the experiments were performed in a 10 mM sodium phosphate buffer, pH 7.4 and at the temperature of 25 °C.

DPH fluorescence anisotropy

Fluorescence anisotropy experiments were carried out for the probe DPH embedded in POPE/POPG LUVs. Anisotropy of DPH was evaluated at 427 nm upon excitation at 355 nm. The total lipid concentration was 50 μM and the lipid-to-probe ratio was 150. Experiments were carried out for liposomes in the absence of AMP3 peptide and in its presence at the concentrations of 0, 0.5, 1, 2, 5 and 10 μM. All the experiments were performed in a 10 mM sodium phosphate buffer, pH 7.4 and at the temperature of 25 °C

Section 2

Peptides and Polymers: Engineering Antimicrobial Membranes

Chapter 1

Introduction

1.1 Harnessing Antimicrobial Peptides for Sustainable Surface Protection

In an era where antimicrobial resistance poses a critical global challenge, developing functionalized surfaces with antimicrobial peptides offers an innovative and sustainable solution to reduce microbial contamination across industries.[141] Indeed, AMPs are becoming a crucial component in material science researches focusing on the development of surfaces capable of actively preventing contamination and infection in various fields.[142,143] Inspired by natural defense mechanisms, AMPs are distinguished by their selective mechanism: they can target directly harmful pathogens, leaving non-target cells intact, a characteristic that enhances their effectiveness. Their versatility also allows them to be used on a variety of materials, from polymers to metals, textiles, and ceramics, transforming everyday surfaces into protective barriers against bacteria, viruses, and fungi (Figure 1.1).[144] This adaptability makes them valuable in improving the safety and durability of materials in different applications (Figure 1.2).

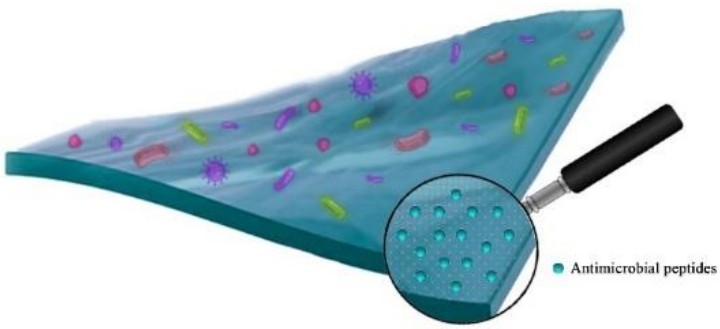

Fig. 1.1 Functionalized surface with antimicrobial peptides: cartoon representation of AMPs that actively target and neutralize microbial threats, including bacteria, viruses and fungi.

For example, AMP coatings on medical devices can help significantly to reduce infections in hospital environments. Their use in food packaging can extend the shelf life of perishable products without the need for chemical additives.[145] The AMPs are also distinguished by their biodegradability, which addresses the environmental challenges posed by many traditional antimicrobial treatments. By preventing biofilm formation and controlling microbial growth, they help to create safer and more reliable materials that meet the specific needs of high-risk environments such as health care facilities, food production facilities and biotechnology laboratories. Their ability to combine effectiveness and sustainability makes them a milestone for the development of new generation antimicrobial-based materials.[146,147]

- **Applications in the Medical Sector**

In the medical field, materials functionalized with AMPs show considerable potential for improving the safety and effectiveness of high-contact devices. Materials such as wound dressings, sutures and implantable devices benefit greatly from the functionalization with AMPs, which provide prolonged antimicrobial protection and reduce the risk of infection even in the presence of prolonged exposure. Wound dressings enriched with AMPs, for example, release antimicrobial agents continuously, creating a sterile environment around the wound.[148,149] This prolonged action not only prevents infections but also accelerates the healing process, as it keeps the area free of external contamination, thus reducing the risk of secondary infections and improving recovery times and quality. This benefit is

particularly important in patients with chronic wounds or difficulty in healing, where infection prevention can be a key factor in the outcome of treatment. For implantable devices, AMPs prevent bacterial adhesion and biofilm formation, two factors that can compromise the functionality of the device and require its premature removal. As biofilms pose a significant threat to the life of implants, the use of surfaces functionalized with AMPs extends the useful life of these devices, reducing the need for replacements and improving the experience and safety for patients. This application is particularly beneficial for patients at risk of post-operative infections, offering a safe and long-lasting alternative to conventional antimicrobial treatments.[150]

- **Applications in the Food Industry**

In the food industry, antimicrobial surfaces functionalized with AMPs offer significant advantages for food safety, as they help to reduce microbial contamination in processing areas and on food contact surfaces.[151] Coating based on AMPs on these surfaces inhibits bacterial growth, improving the preservation of food and reducing the risk of contamination that can compromise consumers health. This application responds to the growing demand for safe and sustainable food handling practices, especially in food processing and production facilities where microbial contamination is a high risk.[152] Furthermore, surfaces functionalized with AMPs can help to prolong the shelf life of food products, reducing the likelihood of spoilage and waste, thus improving the sustainability of the entire production process.[153]

- **Aspects of Environmental Sustainability**

The effectiveness of AMPs is not limited to antimicrobial protection but extends to environmental sustainability. As biodegradable compounds, AMP degrades naturally without leaving toxic residues, unlike conventional antimicrobial treatments. This minimizes ecological damage and aligns with the objectives of companies seeking to reduce the environmental impact of their products. In addition, their production processes can often be designed to use renewable resources and environmentally friendly methods, reducing dependence on harmful chemicals and lowering the overall carbon footprint. These properties position AMPs as a forward-looking solution for sustainable applications.[154]

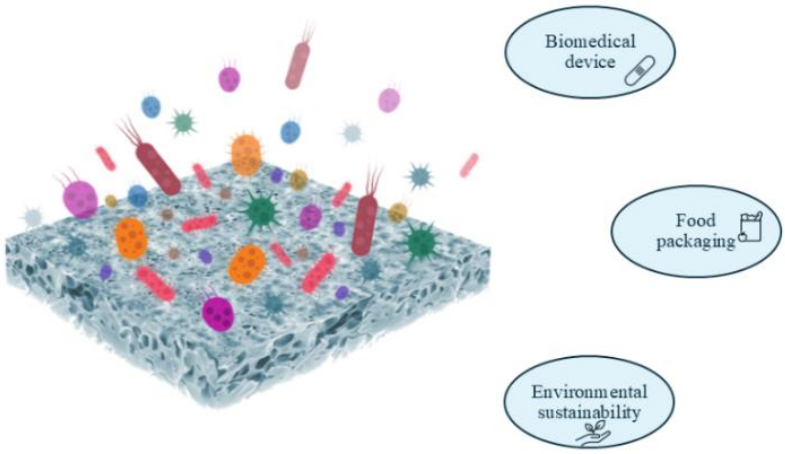

Fig. 1.2 Antimicrobial membranes as versatile tools for diverse applications: This illustration highlights their potential in critical fields such as biomedical devices, food packaging, and environmental sustainability. These advanced materials enhance healthcare safety, improve food preservation, and contribute to eco-friendly microbial control solutions.

1.2 Biohybrid materials and functionalization methods

Based on the remarks, the functionalization of materials with antimicrobial peptides represents an innovative and environmentally friendly solution for developing surfaces with advanced antimicrobial properties.

AMPs can be applied for the development of a variety of useful bioactive materials. Bioactive hybrid materials represents an important progress in the field of biomaterial science, aimed to develop surface with antimicrobial properties.[155,156] To obtain hybrid materials based on AMPs with desired characteristic, is important that the synthetic process is made up by controlled reactions aimed at preserving the bioactivity of the peptides.

Indeed, despite the many benefits and promising applications of AMPs in materials science, there are still several challenges that require further exploration and optimization. One of the main challenges is the long-term stability of AMPs once they are integrated into materials. Environmental factors such as heat, humidity and UV exposure can degrade the peptides, reducing their effectiveness over time. Strategies such as encapsulation in protective coatings or integration into resistant polymer matrices could mitigate these effects, extending their functionality in different environments. The integration of AMPs with smart materials, capable of responding to environmental stimuli such as temperature or pH variations, could lead to the development of adaptive surfaces, able to activate antimicrobial properties only when necessary.[157] In addition, ensuring biocompatibility and minimizing potential

cytotoxic effects is crucial, especially for medical applications.[158] Careful evaluation of their interaction with cells is also necessary, and strategies to modify peptides to increase their selectivity towards microbial membranes without damaging host cells are needed. The development of hybrid systems, combining AMPs with other biocompatible materials such as hydrogels or biodegradable polymers, is a promising solution to achieve this balance. [159–161] Material functionalization employs various methods, and the choice is based on the intrinsic properties of both peptides and polymer surface as well as the intended application. Recent studies have focused on optimizing functionalization strategies to enhance material performance and bioactivity.[162,163]

In the following, some of the most advanced and promising approaches for achieving efficient and durable peptide-based surface functionalization are discussed.[164,165]

Integration of peptides into materials by covalent interactions can be obtained by methods such as *grafting to*, *grafting from,* and *grafting through* (see Figure 1.3). These procedures allow to control the distribution and stability of peptides, improving the effectiveness of antimicrobial coatings in medical and industrial applications.[166]

- ***Grafting to:*** This strategy involves synthesizing a polymer separately and then attaching peptides via covalent bonds to functional groups on the polymer. While it offers the advantage of high peptide density and precise control of bioactive sites, it can encounter steric limitations. The accessibility of inner functional groups can be reduced, which may affect binding

efficiency. Thiol-mediated conjugation represents a specific approach of this strategy for immobilizing AMPs onto various surfaces by leveraging the reactivity of thiol groups to form stable covalent bonds with thiol sensitive functionalities inserted on the surfaces. Surfaces such as silica or polymers are typically activated via treatments like UV/ozone exposure or chemical modifications, to introduce reactive groups capable of interacting with thiol-bearing AMPs. Conjugation is achieved primarily through two approaches: *Thiol-Ene Click Chemistry*, a photochemical reaction enabling rapid AMP attachment, and *Thiol-Maleimide Conjugation*, a one-pot reaction that facilitates AMP immobilization on maleimide-functionalized surfaces, improving the efficiency and stability of the peptide attachment process. [167,168]

- ***Grafting from:*** The peptides act as initiators for the polymerization process, where monomers are added around the peptide, allowing controlled growth of the polymer chain. This method supports customization of polymer size and architecture, producing a stable peptide-polymer conjugate. However, the polymerization conditions must be strictly controlled to maintain the structure and bioactivity of the peptides, limiting some application areas. In the context of advanced polymerization techniques, Atom Transfer Radical Polymerization (ATRP) serves as a prime example of a well-controlled and versatile polymerization method. ATRP is a living radical polymerization process catalyzed by a transition metal complex, which generates radicals from an initiator molecule containing halogen atoms.

The initiator, typically an alkyl halide, facilitates the growth of polymer chains from each halogen atom within its structure. The key to ATRP's precision lies in the equilibrium between propagating radicals and dormant species. This equilibrium is maintained by the reversible formation of radicals from dormant species and their exchange with the transition metal complex. As a result, ATRP enables the production of polymers with a low polydispersity index, ensuring uniform chain lengths and access to high molar mass polymers.[169,170]

- ***Grafting through:*** In this approach, peptides are incorporated directly into the polymer's monomeric units and serve as building blocks during polymerization (Figure 1.3). The peptide must be functionalized with at least one "polymerizable" group. It allows the synthesis of polymers with a high level of peptide repeats, giving the final polymer completely new characteristics resulting from the properties of the peptide. This strategy is theoretically customizable since different peptides bearing a polymerizable part can be combined in a desired ratio and copolymerized entirely with the same chemistry. This technique ensures that bioactive sites on the peptide remain accessible while allowing specific control over concentration and orientation. This results in a homogenous distribution of bioactive peptides along the polymer, yielding a highly functionalized material with enhanced antimicrobial or bioactive properties. This strategy is particularly useful for biomedical applications, as it provides a high degree of peptide density and uniformity in bioactivity across the surface. An effective example of this approach is interfacial

polymerization, in which the peptide acts as a macromonomer. It involves a chemical reaction at the interface between an aqueous solution containing one monomer and an organic solution containing a second monomer. The reaction takes place by condensation, with the monomers spreading towards the interface, where they chemically bind to form a thin polymer film. During interfacial polymerization to form the functionalized fiber, the antimicrobial peptide is dissolved in the aqueous phase. This allows the incorporation of the peptide into the polymeric structure during the reaction at the interface. The result is a functionalized fiber with integrated antimicrobial properties thanks to the presence of the peptide. This technique has been used to create filtration membranes, protective coatings and microcapsules, due to the possibility of controlling the thickness and properties of the polymer by adjusting the reaction conditions. [171,172]

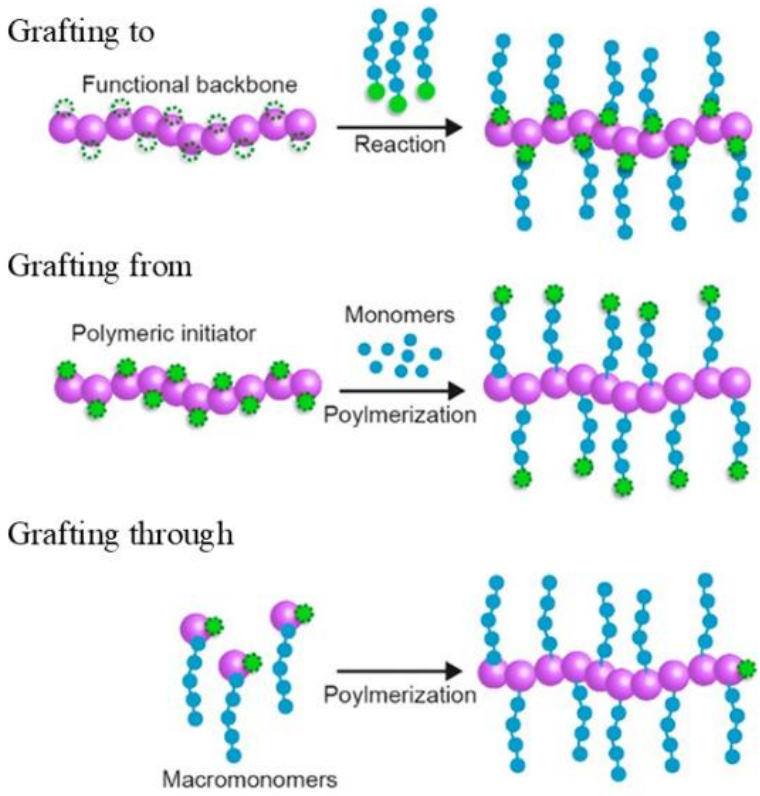

Fig. 1.3 The three primary grafting strategies for polymer functionalization: (1) grafting-to, where functional groups on the backbone react with complementary functional monomers; (2) grafting-from, where polymerization occurs from initiators attached to the backbone; and (3) grafting-through, where macromonomers are polymerized directly. The peptide chains are depicted in cyan while the polymer structure is depicted in pink. Adapted from Varlas et al., Getting into Shape: Reflections on a New Generation of Cylindrical Nanostructures' Self-Assembly Using Polymer Building Blocks[173].

An alternative to covalent functionalization methods is non-covalent functionalization, a strategy which is equally relevant and worthy of attention. The non-covalent functionalization is usually achieved by adsorption via weak interactions on activated, or non-activated polymers. [166] Some examples of this approach are described below.

- **Self-Assembled Hybrid Peptide-Polymer Systems**

Hybrid systems based on peptides and polymers can self-assemble in well-organized structures such as nanofiber and hydrogel, which are able to retain or even increase bioactivity and mechanical stability. These supramolecular architectures, which reflect natural biological structures, are effective for developing biosensors and antimicrobial films. The combination of natural and synthetic peptides in these systems provides enhanced interaction with cells, making them ideal for wound treatment and tissue regeneration.[173]

- **Surface engineering**

The regulation of the orientation and density of peptides on the surfaces is crucial for optimizing interactions with cells or pathogens. Multi-functional hydrogel studies, such as those based on star-structured polyethylene glycol (starPEG) integrated with AMP, show that these materials improve cell adhesion and support tissue integration. Enzyme- or mechanical stress-sensitive peptides for controlled degradation, essential for applications in drug delivery systems and tissue supports, may be incorporated. [174]

In summary, functionalizing surfaces with antimicrobial peptides presents a multifaceted approach to preventing bacterial adhesion and infection. The integration of advanced conjugation techniques, careful selection of peptides, and thorough evaluation of

biocompatibility and efficacy are essential steps in developing effective antimicrobial coatings for various applications.[175,176]

1.3 Bioactive hybrid materials for membrane development

The development of advanced membranes has become a cornerstone in addressing global challenges in medicine, environmental sustainability and industrial processes. Membranes act as a versatile platform, allowing targeted solutions for critical applications such as filtration, water purification, antimicrobial protection and controlled substance release.[177] Their ability to be designed at the micro and nanometric scale makes them particularly suitable for integrating functionalities such as antimicrobial activity, increased mechanical resistance and customized permeability.

Membranes are an integral part of a wide range of applications due to their ability to selectively separate, filter and interact with various substances.[178,179] In the healthcare sector, antimicrobial membranes are essential for infection prevention, especially in wound dressings, implantable devices and filtration systems. In environmental engineering, membranes play a key role in water and air purification, responding to the urgent need for sustainable and effective filtration technologies.[180] The incorporation of bioactive agents, such as AMPs, amplifies their usefulness by transforming membranes into active systems capable not only of filtering contaminants but also of actively neutralizing microbial threats. This functionalization is particularly important in an era of increasing antimicrobial

resistance, where traditional approaches to disinfection and sterilization are becoming less effective.[181]

Understanding the principles behind membrane development has highlighted the need to examine advanced techniques for membrane production. Among these, two approaches of particular relevance are **electrospinning**, which allows to obtain membranes with a nanofibrous structure and highly controllable characteristics, and **phase inversion**, a well-established methodology that allows the formation of defined morphologies through the regulation of process parameters.[182,183]The main aspects of both techniques are described in the following paragraph.

1.3.1 Electrospinning in membrane manufacture

Electrospinning is a highly versatile technique to produce nanofiber membranes with unique structural and functional characteristics. This technique involves the application of a high voltage to a polymer solution or a molten mass, generating a load jet that extends and solidifies into ultrafine fibers deposited on a collector. The resulting membranes have nanoscale characteristics, including high porosity, interconnected pore structures and a huge surface-area-volume ratio, making them ideal for applications requiring efficient interaction with their environment. The advantages of electrospinning for the development of antimicrobial membranes are manifold.[184,185] Nanofibrous structures may maximize the exposure of functional agents such as antimicrobial peptides (AMP), ensuring their antimicrobial efficacy and making them particularly suitable for biomedical applications. The high porosity of these membranes also

allows for excellent breathability, which is critical in applications such as air filtration and protective fabrics. In addition, electrospinning provides precise control over fiber morphology, allowing adjustment of mechanical properties, pore size and fiber alignment to meet specific application requirements.[186]

1.3.2 Characteristic of phase inversion

Phase inversion, unlike electrospinning, produces dense and asymmetrical membranes characterized by controlled porosity and high mechanical strength.[187] Phase inversion involves the transition of a polymer solution from a liquid to a solid state through controlled demisting, usually achieved by solvent evaporation, immersion in a non-solvent bath or temperature change. The process produces membranes with a gradient structure, often characterized by a dense top layer supported by a porous substrate, which provides an excellent balance of selectivity and mechanical durability.

Phase inversion membranes are particularly suitable for applications requiring precise control of filtration and separation processes [184]. Their asymmetric structure allows for selective permeability, making them ideal for water treatment, gas separation and medical filtration devices. When functionalized with AMP, these membranes offer dual functionality: physical separation of contaminants and active microbial neutralization. The dense top layer acts as a barrier to particles, while the embedded AMPs actively disrupt microbial cell membranes, improving the mechanochemical properties. Phase inversion membranes are also robust and can withstand harsh

operating conditions, such as high pressures and prolonged exposure to harsh environments.[183,188]

1.4 Aim of the thesis: Section 2

This section illustrates the approaches applied in this PhD project to develop an advanced antimicrobial membrane. The peptide sequences generated by DL-tools and deeply characterized, as discussed in section 1, were assayed for real-world applications by investigating their behavior upon immobilization on Nylon, by a grafting through strategy. Part of these activities were performed in collaboration with SAATI S.p.A. The AMP3 peptide has been identified as the most promising sequence in the series of candidates, because of its high and broad antimicrobial activity, and demonstrated ability to interact effectively with bacterial membranes (*Section 1*). Thus, this sequence was selected for practical implementation and development of the biohybrid material.

By exploiting the presence of the lysine residue at the N-terminus of the AMP3 sequence, it was possible to insert this peptide into nylon by the grafting through strategy.

Complete characterization of the functionalized membrane was performed, assessing their structural integrity, chemical stability and, most importantly, antimicrobial efficacy. The insertion of AMP3 into the polymer converts the Nylon 6,6 into a bioactive and functional barrier that inhibits the proliferation of bacteria Direct tests on clinically relevant bacterial strains provide convincing evidence of the membrane's ability to inhibit microbial growth.

Chapter 2

Results and Discussion

AMP3 for the development of biohybrid materials.

Based on the consideration discussed in the previous sections and in line with the objective of developing an antimicrobial bioactive membrane, a Peptide-Nylon hybrid biomaterial was synthesized and characterized. To this end, the *Grafting through strategy* was selected as it offers several significant advantages compared to alternative methods, including post-functionalization. By immediately incorporating the functional component into the polymer matrix during polymerization, the necessity for further operations is eliminated, thereby decreasing both time and costs. Besides guaranteeing a uniform distribution of the functional component within the matrix, mitigating the reactivity fluctuations characteristic of post-functionalization, and ensuring consistent properties across the membrane, covalent integration achieved by grafting through strategies enhances chemical and physical stability, thereby diminishing the likelihood of release or degradation of the functional component. In contrast, post-functionalization may result in weaker bonds and a subsequent decline in efficacy. This technique more effectively maintains the original qualities of the material, including crystallinity, thermal stability, and mechanical characteristics, hence preventing modifications that may arise from post-functionalization. It enables regulation of the integrated component quantity, enhancing process efficiency and minimizing waste. Ultimately, grafting through strategy could be more readily scalable and reproducible at an industrial level, since it allows the production of the polymer in one stage, thus diminishing the number of operation steps needed for post-functionalization.

The AMP3 peptide (KRWWRWWRR-NH_2), derived from DL tools, was integrated within the polymer nylon matrix. In the following paragraph, the behaviour of nylon and the synthesis of AMP3-Nylon are discussed.

2.1 Nylon: A Versatile Polymer for Industrial and Biomedical Applications

Nylon is a synthetic polymer composed of repeating amide bonds, typically derived from monomers such as hexamethylenediamine and adipic acid (in the case of Nylon 6,6) or from the condensation of caprolactam (in the case of Nylon 6). It is widely used for applications ranging from clothing to medical devices due to its numerous distinctive advantages over other polymers.[189] Nylon differs from other polymers thanks to its mechanical resistance, a great advantage compared to polymers such as polyethylene and polypropylene, which have lower performance in terms of strength. Nylon has optimal thermal stability, keeping its structure even at high temperatures. This advantage is especially significant in industrial settings were materials encounter temperature fluctuations. Nylon maintains its strength at around 200°C, making it suitable for applications requiring durability in hot environments. Thanks to its chemical structure, Nylon can be easily modified to achieve specific properties such as moisture resistance or reduced friction. This versatility is not common in many other polymers and allows Nylon to be adapted for applications. The possibility of using strategies such as functionalization with reactive groups or integration with biomolecules allows for customized materials with unique properties

that combine bioactivity and mechanical durability. In fact, this has made the polymer emerge also for biocompatibility; this important characteristic allows the use of the polymer in medical stuff. The use of functionalized Nylon with peptides and other bioactive molecules has shown promising developments in applications such as sutures, dressings, and prosthetics. For example, Nylon can be modified to have antibacterial properties or improve cell adhesion, which is essential for implantable medical devices. Due to its ability to be chemically modified, it can be adapted to meet specific industrial and biomedical needs, proving itself a valuable resource in many sectors.

2.1.1 Comparison of Nylon 6,6 and Nylon 6,10

To achieve the aim of the work, preliminary studies were performed by synthesizing both Nylon 6,6 and Nylon 6,10 using the interfacial polymerization strategy (see details in the Experimental Section). Nylon 6,6 is obtained from hexamethylenediamine and adipic acid, while Nylon 6,10 is synthesized from hexamethylenediamine and sebacic acid. The comparison between Synthesized Nylon 6,6 and Nylon 6,10 highlights key differences in their physico-chemical properties due to the changes in molecular structure and length of monomeric chains. Indeed, the sebacoyl chloride for Nylon 6,10 having a longer carbon chain than the adipoyl chloride, gives to Nylon 6,10 a greater flexibility but also a lower crystalline density than Nylon 6,6.[190]

Both polymers were characterized by several techniques. The wide-angle X-ray diffraction profiles (WAXS) of the polymers obtained were made using a MALVERN PANALYTICAL EMPYREAN.

WAXS analysis confirmed the semi-crystalline nature of both polymers, showing for Nylon 6,6 two main diffraction peaks at 2θ of about 20.2° and 24.0°, associated with the crystalline form α, which guarantees high rigidity and structural stability. Nylon 6,10 shows peaks at 2θ of 20.13° and 24.11°, with a weak presence of crystals at 21.3°, indicative of a less dense and more flexible structure.[191,192] (Figure 2.1)

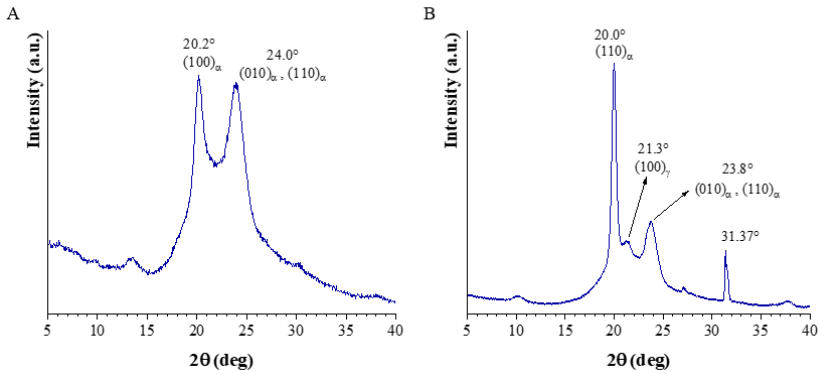

Fig. 2.1 X-ray diffraction (WAXS) profiles of Synthesized Nylon 6,6 (A) and Nylon 6,10 (B), showing distinct crystallinity patterns. Nylon 6,6 displays prominent α-phase peaks, while Nylon 6,10 reveals additional peaks indicating minor γ-phase content, reflecting structural differences due to monomer composition.

These obtained data, in combination with the DSC thermogram (Figure 2.2), highlight the notable differences of the polymers' fusion points. The DSC analysis was performed with the METTLER DSC 822. DSC thermograms of first heating, cooling and second heating were recorded using a scan speed of 10°C/min.

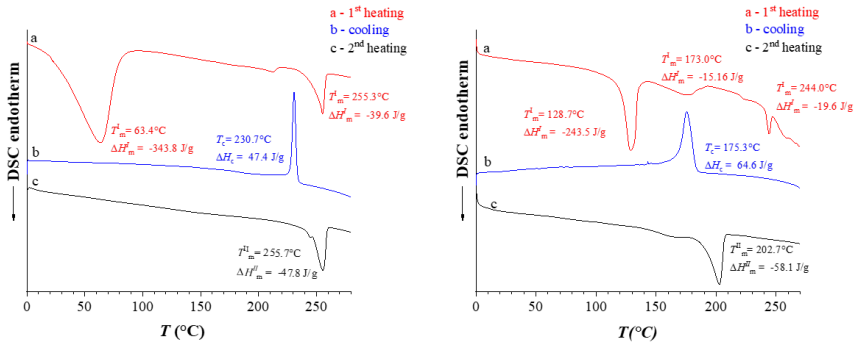

Fig. 2.2 DSC thermograms for Synthesized Nylon 6,6 (left) and Nylon 6,10 (right) show the first heating (a), cooling (b), and second heating (c) cycles. Differences in melting and crystallization temperatures highlight the distinct thermal behaviors and stability of each polymer.

Regarding Synthesized Nylon 6,6 there are two primary endothermic peaks in the initial heating thermogram (Figure 2.2, curve a). The first peak at about 63°C is probably due to the removal of volatile compounds from the sample, while the second peak at about 255°C is due to polymer melting. The polymer crystallizes from the melt at about 231 °C (Figure 2.2, curve b) and then remelts during subsequent heating (Figure 2.2, curve c) at about 256 °C. Table 1 reports the parameters derived from the DSC analysis.

Table 1 Values of temperatures and enthalpy of first and second fusion (T^{I}_m ΔH^{I}_m T^{II}_m ΔH^{II}_m) and crystallization (T_c ΔH_c) of the sample of Synthesized Nylon 6,6.

	T^{I}_m (°C)	ΔH^{I}_m (J/g)	T_c (°C)	ΔH_c (J/g)	T^{II}_m (°C)	ΔH^{II}_m (J/g)
Synthesized Nylon 6,6	63.4	-343.8	230.7	47.4	255.7	-47.8
	255.3	-39.6				

For Synthesized Nylon 6,10 in the first heating thermogram (Figure 2.2, curve a), there are two endothermic peaks. The first peak at about 129°C and the second peak at 244°C are probably due to the removal of volatile compounds from the sample; the polymer melting occurs at about 173°C. The polymer crystallizes from the melt at about 175 °C (Figure 2.2, curve b) and then remelts during the next heating (Figure 2.2, curve c), at about 202 °C. The parameters obtained from the DSC analysis are shown in Table 2. These values indicate that Synthesized Nylon 6,6 is preferred for applications requiring resistance to intense thermal conditions.

Table 2 Values of temperatures and enthalpy of first and second fusion (T^{I}_{m} ΔH^{I}_{m} T^{II}_{m} ΔH^{II}_{m}) and crystallization (T_c ΔH_c) of the sample of Synthesized Nylon 6,10.

	T^{I}_{m} (°C)	ΔH^{I}_{m} (J/g)	T_c (°C)	ΔH_c (J/g)	T^{II}_{m} (°C)	ΔH^{II}_{m} (J/g)
Synthesized Nylon 6,10	128.7 173.0 244.0	-243.5 -15.16 -19.6	175.3	64.6	202.7	-58.1

Given its use in contexts that require high thermal and mechanical performance, it was considered a priority to characterize in detail the Synthesized Nylon 6,6, keeping the focus of investigations on this polymer to maximize the effectiveness of analyses in relation to the objectives of the project. Thus, further characterization was performed, including TGA and the measurement of intrinsic viscosity. The TGA is an analytical technique used to assess the thermal stability of the material by monitoring mass loss as a function

of temperature. In the case of Nylon, TGA allows thermal decomposition behaviour to be observed and the temperature at which the material begins to degrade to be identified. The TGA curve of the Synthesized Nylon 6, 6 (Figure 2.3), performed with PERKIN ELMER TGA 4000, shows a 10% loss in weight over a temperature range between 30°C and 73°C, corresponding to the removal of volatile components from the sample. The degradation temperature of the polymer, estimated as a temperature at which a loss in weight of 50% compared to the initial weight ($T_{50\%}$) is observed, is equal to 395°C. At 700°C there is a residue (10%) of undegraded sample.[193]

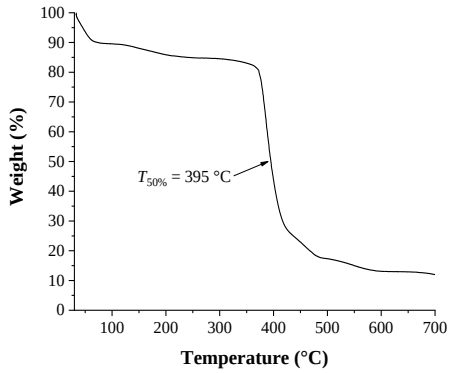

Fig. 2.3 Nylon 6,6 sample TGA curve recorded in the temperature range 30-700° under nitrogen flow (50 ml/min), using a scan speed of 10 °C/min.

Viscosity measurements were made at 25 °C using a capillary viscometer from Ubbelohde. For viscosity measurements, 90% formic acid was selected as the solvent because in this solvent the Mark-Houwink constants (*K* ed *a*) for Nylon 6,6 are tabulated at a temperature of 25°C.[194]

These constants are necessary for the calculation of the mean viscosity molecular mass (M_v) from the intrinsic viscosity [η] (Eq. 1).

$$[\eta] = KM_v^a \quad \text{(Eq. 1)}$$

Viscosity measurements were made by recording the efflux times of the pure solvent and the efflux times of 5 solutions of Synthesized Nylon 6,6 in formic Acid 90% at different concentrations, ranging from 0.1 to 0.5 g/dl. The specific, reduced, relative and inherent viscosities were evaluated from the efflux times of the pure solvent (t_0) and solutions at different concentrations (t). The results obtained are shown in Table 3.

Table 3 Viscosity measurement results: specific (η_{sp}), relative (η_{rel}) reduced (η_{red}) and inherent (η_{inh}) efflux times and viscosities calculated from the efflux times using the equations given in the table. t0 is the efflux time of the pure solvent; t is the efflux time of the solutions at different concentrations c.

c (g/dl)	**Efflux Time**	$\eta_{sp} = (t-t_0)/t_0$	$\eta_{rel} = t/t_0$	$\eta_{red} = \eta_{sp}/c$	$\eta_{inh} = \ln \eta_{rel}/c$
Blank	146.34				
0.101	160.79	0.099	1.099	0.977	0.932
0.201	176.08	0.203	1.203	1.01	0.920
0.302	194.21	0.327	1.327	1.08	0.937
0.403	204.32	0.396	1.396	0.98	0.828
0.497	223.03	0.524	1.524	1.05	0.840

The intrinsic viscosity [η], estimated by the average of the intercept with the ordinate axis of the two lines that best interpolates the data of the inherent (η_{inh}) and reduced (η_{red}) viscosity as a function of the concentration (Figure 2.4), is equal to (0.98 ± 0.05) dl/g.

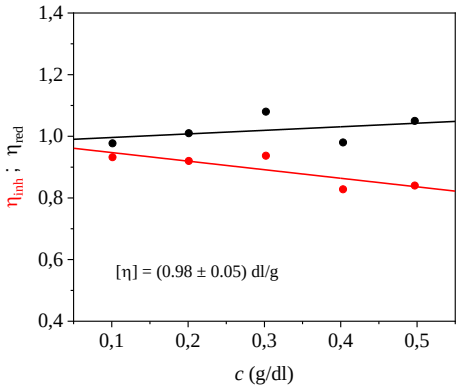

Fig. 2.4 Graph of inherent (η_{inh}) and reduced (η_{red}) viscosity as a function of concentration for the sample Synthesized Nylon 6,6 in formic acid 90% at 25 °C. Intrinsic viscosity [η] shown in the graph is the mean value of the intercept with the axis of the ordinates of the two lines interpolating the experimental data of η_{inh} and η_{red} as a function of concentration.

In conclusion, the comparison between Synthesized Nylon 6,6 and Nylon 6,10 shows that the choice of monomer significantly affects the structural, thermal and mechanical properties of the resulting polyamides. Synthesized Nylon 6,6, thanks to its more compact molecular structure and crystallinity, demonstrates superior thermal stability and mechanical strength.

2.2 AMP3-Nylon synthesis

Based on the previous results, Nylon 6,6 was selected for its exceptional mechanical strength and stability, qualities that facilitate effective integration with the peptide and ensure the durability of the composite material.[195] To prepare the AMP3-Nylon biomaterial, the *Grafting through strategy* was the method employed. The presence of the Lys residue at the N-terminus facilitates the incorporation of the peptide into the nylon structure.[196] In the polymerization reaction,

the aliphatic diamine is substituted by the peptide containing two primary amino groups: one provided by the N-terminal amine and the other by the amine group of the lysine side chain (Figure 2.5).

The synthesis of the bioactive nylon was performed by reacting adipoyl dichloride with peptide sequences combined with the 1,6-diaminohexane building block, resulting in modified nylon 6–6. A 1% mol of peptide relative to the diamine used in the polymerization process was used (see experimental methods). This method allows the AMP3 peptide to be directly incorporated into the polymer matrix through covalent binding. This means that the peptide becomes an intrinsic component of the Nylon network, with a uniform and stable distribution that can preserve its chemical and physical properties even under conditions of prolonged use. [197,198,199]

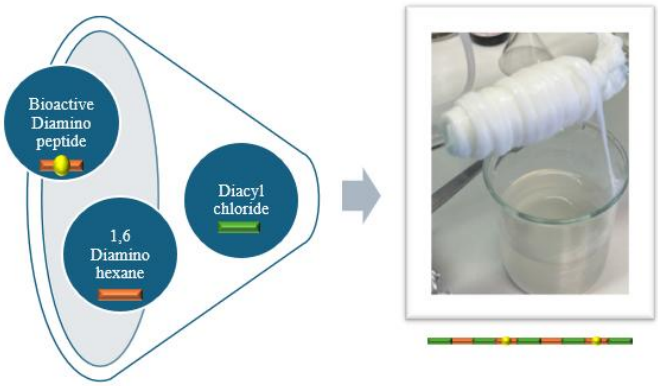

Fig 2.5 Schematic representation of the synthesis process for an AMP3-Nylon fiber. The reaction involves bioactive diamino peptide, 1,6-diamino hexane, and diacyl chloride as precursors. The resulting polymeric material is extracted as a continuous fiber, as shown in the experimental setup on the right, illustrating the formation of bioactive functionalized fibers.

2.3 AMP3-Nylon structural characterization

To fully assess the properties of the synthesized materials, a detailed characterization was performed on both the unmodified polymer and the peptide-functionalized polymer, also comparing them with Commercial Nylon 6,6. This analysis aimed to assess the structural, thermal, mechanical, and antimicrobial properties, providing a complete understanding of the effects introduced by peptide integration. By comparing the unmodified polymer with the functionalized counterpart, it was possible to determine to what extent the incorporation of the peptide affected the performance of the polymer. A combination of advanced analytical techniques has been employed to ensure robust and multidimensional characterization. The results provide critical information on the functionalization process and its impact on the overall properties of the material.

The UV-Vis analysis highlighted the incorporation of peptide into the Nylon compared to pure Nylon, as shown by the comparison between the two samples (Figure 2.6). The UV absorption spectrum of the AMP3-Nylon shows a distinct band at 280 nm, while it is absent in the un-functionalized Nylon. This band is attributable to the presence of the Trp residues in the bioactive peptide, which specifically absorb at this wavelength.[200] This comparison also suggests that the peptide retains its distinctive spectroscopic properties within the polymer matrix.

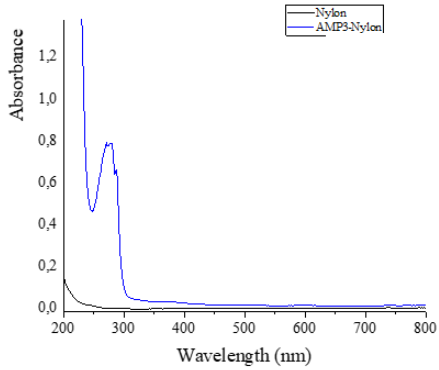

Fig. 2.6 UV spectrum of pure Nylon and AMP3-Nylon samples at a concentration of 1.5 mg/mL in TFE. The AMP3-Nylon sample shows an absorption band at 280 nm, attributable to the Trp residue present in the peptide, confirming the integration of the peptide into the Nylon matrix.

To evaluate the impact of the incorporation of the peptide into the Nylon matrix on the crystalline structure of Synthesized Nylon 6,6, the analysis WAXS was performed. It consents to obtain detailed information on the crystal arrangement, providing a complete study of the structural changes induced by the functionalization of the polymer. In the WAXS profile shown below (Figure 2.7), there are two main diffraction peaks emerging from a halo due to amorphous component scattering, confirming that the presence of the peptide does not alter the semi-crystalline nature of the polymer. In particular, the observed values of 2θ, equal to 20.2 and 24.0° (λ = 1.5418 Å), correspond to the reflections 100 and 010/110 of the form α of Nylon 6,6.

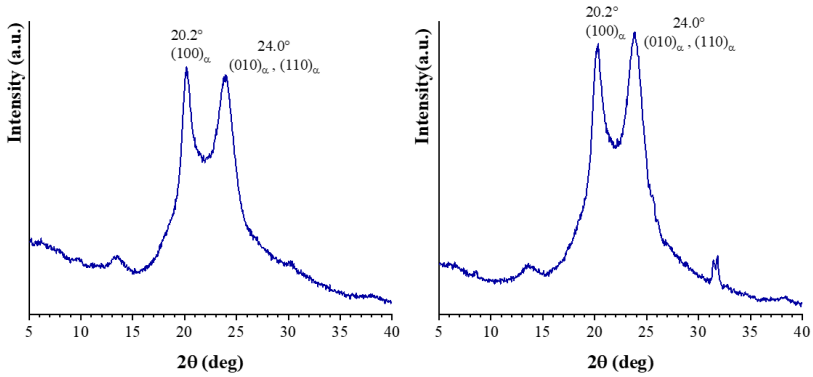

Fig. 2.7 WAXS profile of Synthesized Nylon 6,6 (right) and AMP3-Nylon 6,6 (left). The peak around 32° is due to the solid support used.

Moreover, the DSC analysis was performed on the functionalized polymer, and the results compared with the Synthesized Nylon 6,6. DSC thermograms of first heating, cooling and second heating were recorded using a scan speed of 10°C/min. The analysis of the Commercial Nylon 6,6, Synthesized Nylon 6,6 and AMP3-Nylon showed that the incorporation influences the vitreous transition (see Figure 2.8). AMP3-Nylon has a vitreous transition at lower temperatures than the sample without peptide, suggesting an increase in polymer matrix flexibility, probably due to an interaction of the peptide with polymer chains which reduces overall stiffness. In addition, the thermograms of Synthesized Nylon 6,6 and AMP3-Nylon exhibit an initial endothermic peak, attributable to the presence of a volatile component, which is absent during the second heating cycle. This behaviour likely indicates water absorption during the synthesis process, which is subsequently released upon initial thermal treatment. Finally, from the analysis of the thermograms obtained, it can be stated that the inclusion of the

peptide in the polymeric matrix does not affect the capacity of the polymer to recrystallize from the molten state. In fact, the peptide, although incorporated into the system, does not significantly interfere with the thermodynamic and kinetic processes that regulate the recrystallization of the polymer.

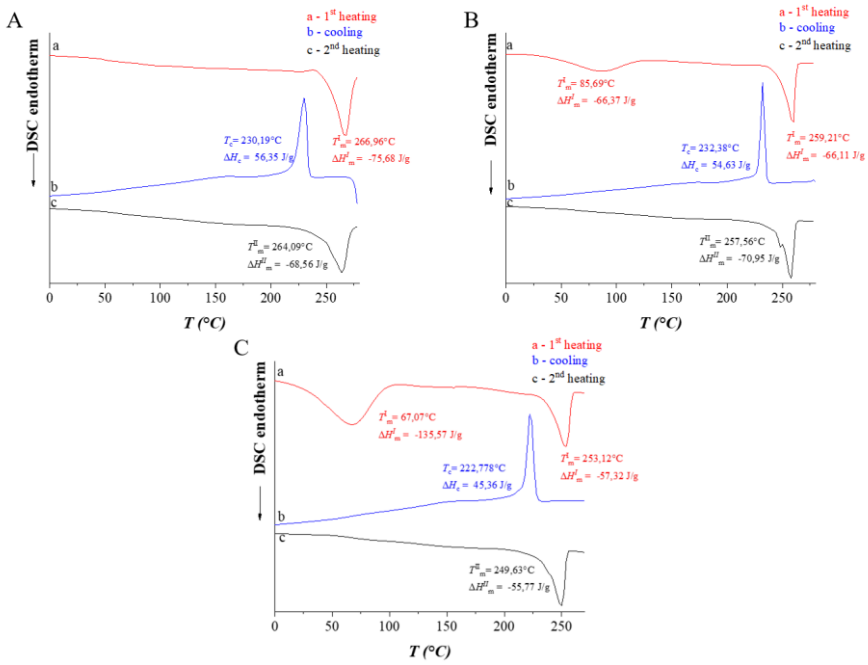

Fig. 2.8 Comparison of DSC thermograms for the samples: (A) Commercial Nylon 6,6, (B) Synthesized Nylon 6,6, (C) AMP3-Nylon. The labels (a), (b), and (c) correspond to the first heating, cooling, and second heating cycles, respectively. The graphs illustrate variations in thermal behaviour, highlighting differences in T_m , T_c and ΔH among the analyzed materials.

Table 4 reports the data obtained from DSC analysis.

Table 4 Comparison of cooling and melting temperatures between Commercial Nylon 6,6, synthesized one and AMP3-Nylon.

	T*c* (°C)	**T*m* (°C)**
Commercial Nylon 6,6	230,19	264,09
Synthesized Nylon 6,6	224,97	249,24
AMP3–Nylon	222,77	249,63

The characterization on the synthesized peptide-functionalized Nylon revealed that the incorporation of AMP3 into the Nylon 6,6 matrix successfully preserves the intrinsic structural and functional properties of the polymer. UV-Vis spectroscopy confirmed the effective integration of the peptide, as evidenced by the 280 nm absorption peak attributable to Trp residues. The WAXS analysis showed that the semi-crystalline nature of Nylon 6,6 remained unchanged, without any significant disturbance to its crystal structure. DSC analysis has evidenced subtle changes in thermal behaviour, particularly a reduction in the glass transition temperature of the peptide-functionalized polymer, indicating increased flexibility due to peptide integration. In addition, the ability of the polymer to recrystallize from the molten state remained intact, underlining the peptide's compatibility with the polymeric matrix. Together, these results confirm the success of the functionalization process.

2.4 AMP3-Nylon films preparation and characterization

To assess the feasibility of the biohybrid peptide-nylon material for industrial applications, a laboratory-scale proof of concept was established. This initial study aimed to synthesize and characterize polymers, produce films under controlled conditions and analyze their structural and functional properties. The results obtained provide indications of their scalability and suitability for further development. Films of Synthesized Nylon 6,6 and AMP3-Nylon were prepared. by drop-casting approach. To produce the films, 20.0 mg of polymer were dissolved in 1.0 mL of TFE. The solubilization process was facilitated using a magnetic stirrer plate and, where necessary, sonication was used to improve dissolution. To produce films, 1.0 mL of the resulting solution was distributed on weighing boats with a bottom surface of 3x3cm, placed on a rotating platform to ensure uniform distribution, and allowed to evaporate overnight under ambient conditions. The resulting films were then analyzed by SEM to assess their morphology and structure. Concurrently, the antimicrobial activity of the films was verified, demonstrating their functional potential.

SEM images (Figure 2.9) show the morphology of the top and bottom surfaces of the synthesized films. The upper surface appears more irregular, with a clear porosity distribution. This porous structure is attributed to the kinetics of solvent evaporation during film formation. Conversely, the lower surface has a more uniform and compact morphology. This is due to the interface between the

film and the substrate used during the evaporation process. However, the lack of porosity on the bottom surface could improve the mechanical strength and stability of the film. The difference between the two surfaces highlights the importance of process conditions, such as evaporation rate and interaction with substrate, in determining the final structure of the material.

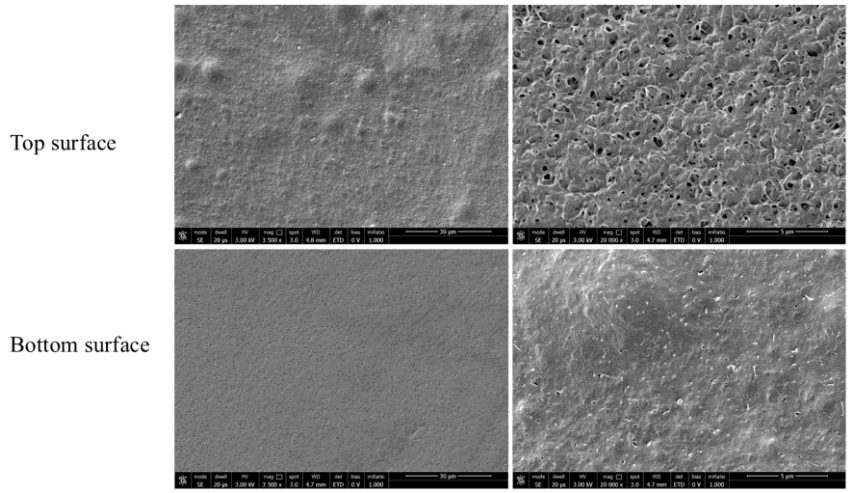

Fig. 2.9 SEM images of the Synthesized Nylon 6,6 films showing the porous top surface (upper panels) and the compact bottom surface (lower panels). The structural differences are attributed to evaporation kinetics and substrate interaction during film formation.

A preliminary analysis was conducted to assess the antimicrobial activity of the Synthesized Nylon 6,6 and AMP3-Nylon films against *E. coli*. The assay procedure involved applying 20 µl of a standardized bacterial suspension to the surfaces, followed by the assessment of bacterial viability at two time points: after 3 minutes (considered as t=0h) of wetting, which ensures that the inoculum is well adhered to the surface before measurements start, and after a 30-

minute (t=0.5h) exposure period. In the following table (Table 5) are shown the results of the essays.

Table 5. Bacterial viability after contact with Synthesized Nylon 6,6 and AMP3-Nylon membranes at different time intervals (t=0h and t=0.5h, 3 and 30 minutes, respectively). Values are expressed as a percentage of initial viability at t=0h for each condition.

1st	**SYNTHESIZED NYLON 6,6**	**AMP3-NYLON**
t=0h	100%	34,94%
t=0.5h	73,78%	45,67%
2nd	**SYNTHESIZED NYLON 6,6**	**AMP3-NYLON**
t=0h	100%	17,50%
t=0.5h	89,64%	37,74%

The percentages represent relative viability with respect to the initial condition, with t=0h for Synthesized Nylon 6,6 taken as a reference at 100%. Across both experiments, AMP3-Nylon consistently demonstrates a pronounced reduction in bacterial viability compared to Synthesized Nylon 6,6. At t=0h, bacterial viability for AMP3-Nylon is significantly lower (ranging from 17.50% to 34.94%), highlighting its immediate antimicrobial effect. At t=0.5, Synthesized Nylon 6,6 shows a bacterial viability between 73.78% and 89.64%, whereas AMP3-Nylon maintains a greater efficacy, with viability values ranging from 37.74% to 45.67%.

Despite some statistical variability between the two experimental series, these results suggest that the AMP3-Nylon has good antimicrobial activity, evident already at the initial time (t=0h) and maintained effectively over time, both in the first and second series

of experiments. The differences between t=0h and t=0.5h indicate that the antimicrobial effect of AMP3-Nylon is more persistent than the simple membrane of Synthesized Nylon 6,6, significantly reducing bacterial viability even with prolonged exposure.

2.5 AMP3-Nylon for the production of Antimicrobial Membranes

Based on the promising results, the preliminary investigation confirms the feasibility of Synthesized Nylon 6,6 and AMP3-Nylon films production as an initial step for future membrane development.

To explore the potential applications of the peptide-functionalized polymer, several membranes were prepared by using the AMP3-Nylon. This activity was performed in collaboration with SAATI S.p.A., where part of the research within this PhD project was carried out. SAATI S.p.A. is a multinational company that develops, produces and markets, highly advanced technical fabrics and chemical products for industrial use. The “Process Filtration” sector is particularly developed, with the production of filtration systems and materials applicable in different production processes, such as the chemical and mining sectors, but also of filters for wastewater and even the pharmaceutical field. Two distinct membrane fabrication techniques were herein employed: electrospinning and phase inversion. Each technique was used to produce membranes with unique structural and functional properties, allowing a comparative analysis of their performance. Electrospinning was selected to create nanofiber membranes with high surface and

interlinked porosity, ideal for maximizing antimicrobial activity through increased surface exposure. In contrast, phase inversion has been used to develop membranes with a denser structure and tailored pore distribution, offering better mechanical strength and selective permeability (Figure 2.10). These two approaches may provide a comprehensive platform for assessing how manufacturing techniques influence antimicrobial efficacy and the physical characteristics of the resulting membranes, considering factors such as materials, process parameters, and membrane morphology. Membrane porosity and filtration efficiency requirements further highlighted the distinct advantages of each method, necessitating a comparison to identify the most suitable solution. A detailed explanation of each technique is provided in the following paragraphs.

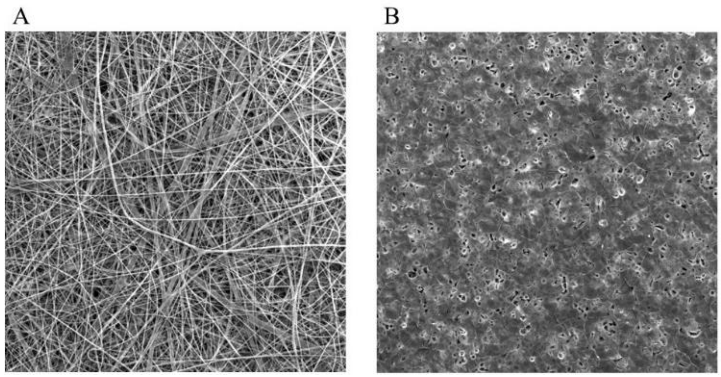

Fig. 2.10 SEM images of membranes produced using two different techniques. (A) Membrane obtained by electrospinning, characterized by a nanofibrous structure with interwoven fibers. (B) Membrane obtained through phase inversion, exhibiting a porous structure with heterogeneous pore distribution. These images highlight the significant morphological differences between the two manufacturing methods.

2.5.1 Electrospinning and Phase Inversion: Dual Techniques for Advanced Antimicrobial Membranes

The choice of electrospinning and phase inversion techniques for this study was guided by their complementary advantages and alignment with project objectives. Using these two independent approaches, it was possible to develop separate membrane prototypes, each one adapted to meet specific application needs [187]. These membranes are particularly advantageous for applications where rapid antimicrobial action and lightweight structures, such as protective fabrics and dressings, as well as for water purification, where both mechanical strength and antimicrobial functionality are critical. The integration of AMPs into membranes using these techniques represents a significant advance in materials science.[201] These functionalized membranes face multiple challenges, from reducing biofouling in filtration systems to antimicrobial protection in biomedical devices. In addition, the possibility of adapting membrane properties through choice of manufacturing technique extends their applicability in different fields.

2.5.2 Phase inversion membranes

The phase inversion (IP) technique is a widely used method for synthesizing membranes, known for its ability to produce materials with well-defined porosity and adjustable microstructures. When combined with advanced techniques such as Vapor-Induced Phase Separation (VIPS), Non-Solvent Induced Phase Separation (NIPS), Thermally Induced Phase Separation (TIPS), Diffusion-Induced

Phase Separation (DIPS).[202] This approach enables a high degree of control over membrane morphology and pore size.

The synthesis of membranes by phase inversion is based on the preparation of a polymeric solution, obtained by dissolving the polymer in an appropriate solvent. This solution is spread on a support and then immersed in a coagulation bath, usually water or non-solvent. During this phase, the exchange between solvent and non-solvent induces phase separation, leading to the formation of a characteristic porous membrane structure. At the end of the immersion, the membrane is carefully washed to remove any residue of solvent and then dried under controlled conditions in order to obtain the final product with specific characteristics, as regulated porosity and an asymmetric structure. In this work, Commercial Nylon 6,6 was used to conduct several tests, preparing polymer solutions with concentrations of 12 (as for electrospun membranes), 14, 16, 18 and 25% (w/w) (Figure 2.11). The polymer solutions were prepared at the appropriate concentrations (w/w) by dissolving the polymer matrix in a formic acid solution containing 2% TFA. The dissolution process was carried out in a glass flask using magnetic stirring at a speed of 300 rpm for 2 hours at 100°C. The objective was to analyze the structural characteristics of the membranes produced and identify the optimal formulation to achieve an ideal conformation. Unfortunately, the membrane obtained with a polymer concentration of 12% (w/w) was not included in the characterization because its preparation did not produce a satisfactory result from the

point of view of the structural quality and stability required for the analyses.[203]

Fig. 2.11 Membranes prepared with increasing polymer concentrations, from left to right: 14, 16, 18, and 25% (w/w). The images illustrate the effect of polymer concentration on the structural integrity and morphology of the membranes, with higher concentrations leading to thicker and more stable structures.

Morphological and structural characterization

This section presents a comprehensive evaluation of membranes produced with Commercial Nylon 6,6 at various polymer concentrations (14, 16, 18 and 25% w/w). The study focuses on how polymer concentration affects membrane morphology and mechanical integrity, providing information on the relationship between material composition and performance. This analysis was carried out to assess the best conditions for membrane synthesis functionalized with the peptide. As was done for electrospun membranes, this analysis highlights the distinct structural characteristics resulting from the phase inversion process, with particular emphasis on porosity, surface uniformity and overall stability. The membranes obtained were initially submitted to a morphological evaluation using SEM, to analyze in detail the structure, size and distribution of the pores present. (Figure 2.12)

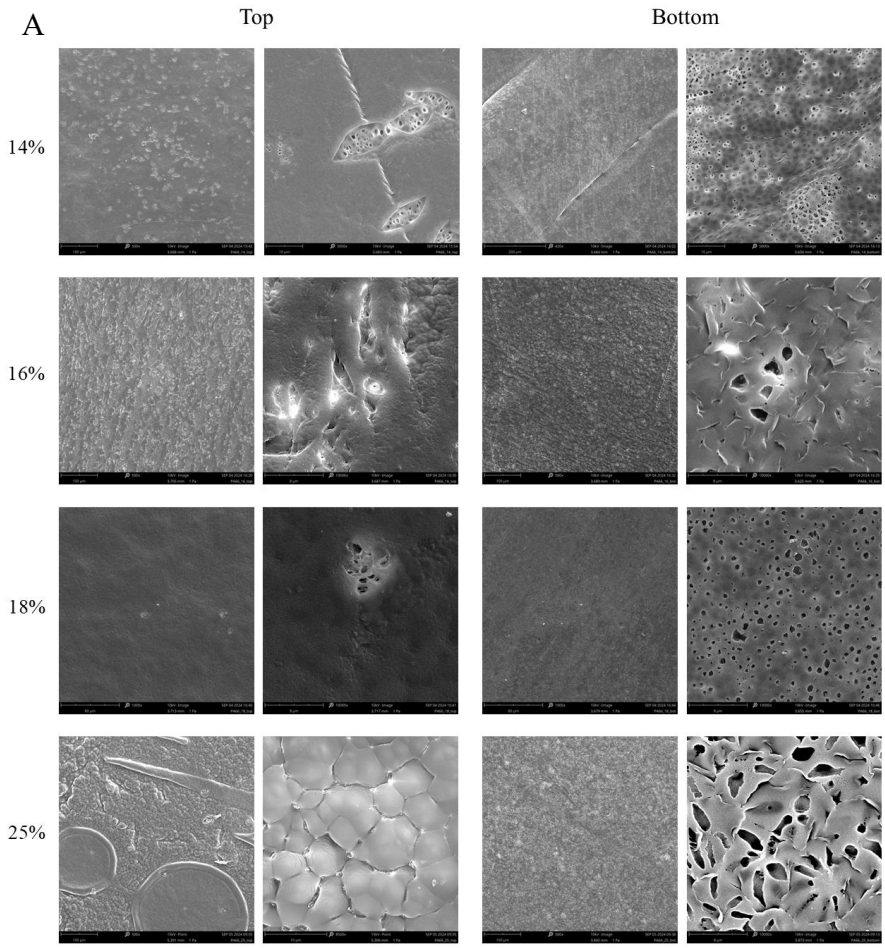

Fig. 2.12 SEM images illustrate (A) the top and bottom surfaces of membranes prepared with polymer concentrations of 14%, 16%, 18%, and 25% (w/w), along with the cross-section (B) of the 18% membrane. The images reveal the impact of polymer concentration on membrane morphology, highlighting differences in porosity, surface uniformity, and structural integrity across the samples.

SEM images show how the increase in polymer concentration significantly affects membrane morphology. The 14% (w/w) membrane has a relatively porous upper surface and a lower structure with more evident pores, indicating a lower overall density. At 16% (w/w), the upper surface becomes more compact with a reduction in porosity, while the lower part maintains a more even pore distribution. The 18% (w/w) membrane shows the optimal combination of compactness and porosity, with a dense upper surface and well-controlled porosity in the lower part, also confirmed by cross-sectional analysis, which reveals an asymmetric structure ideal for filtration applications. Finally, the 25% w/w membrane exhibits excessive density in both surfaces with greatly reduced porosity, making it less suitable for applications requiring permeability. To complete the structural analysis, the physical and functional properties of the membranes were evaluated. These included measurements of air permeability, contact angle, weight and thickness, which provide a deeper understanding of how the polymer concentration affects membrane performance and structural integrity (Table 6).

Table 6 Physical and functional properties of membranes produced with Commercial Nylon 6,6 at different polymer concentrations (14%, 16%, 18%, and 25% w/w), including air permeability (AP), weight (gsm), contact angles (top and bottom surfaces), and thickness (µm).

	(%) w/w	AP (l/m^2s^{-1}) @200Pa	AP (l/m^2s^{-1}) @1000Pa	gsm	Contact angle (°)	Thickness (µm)
Commercial Nylon 6,6	14	7,04	18	13,84	T: 59,64 B: 53,08	24
	16	4,26	14,5	26,904	T: 52,24 B: 47,62	28
	18	2	7,3	12,46	T: 57,6 B: 56,76	14
	25	1,4	3,6	33,14	T: 41,86 B: 62,92	32-38

These results show that an intermediate concentration, such as 18%, offers the best compromise between structural strength and functionality. Based on the results of tests conducted on membranes made from Commercial Nylon, it was decided to use a polymer concentration of 18% w/w for the preparation of membranes with Synthesized Nylon 6,6 and AMP3-Nylon. In addition, the VIPS technique has been applied to these membranes, allowing even more precise control over the formation of the porous structure, favoring the creation of a porosity gradient from the upper side to the lower. The main advantage of integrating VIPS is that it can further improve asymmetry and pore distribution, optimizing membrane functional properties, particularly for advanced biomedical and industrial applications.

Unfortunately, the membranes produced using Synthesized Nylon 6,6 and AMP3-Nylon have a not optimal morphology, characterized

by irregularities in the distribution of pores and in the overall structure as they were very thin (Figure 2.13).

Fig. 2.13 Comparison of membranes produced with Synthesized Nylon 6,6 (left) and AMP3-Nylon (right).

This result could be attributed to the limited amount of material available for the preparation of polymer solutions, which probably influenced the uniform formation of the membrane during the phase inversion process. Consequently, the analyses carried out on these membranes were limited to morphological characterization by SEM, since it was not possible to obtain sufficiently stable samples for further tests. Despite these limitations, the SEM images (Figure 2.14) show that the phase inversion procedure with VIPS is adequate, as it has allowed the preparation of a membrane characterized by high porosity and homogeneous pore distribution, confirming the potential of the preparation method used.

SEM images clearly show the morphological differences between Commercial Nylon 6,6 and Nylon membranes obtained by phase inversion, showing how this process affects the structure and porosity of the material. The surface of Commercial Nylon 6,6 appears relatively compact and disordered, with a limited and uneven pore

distribution. In contrast, Synthesized Nylon 6,6 and phase inversion Nylon show a more regular surface structure with a well-defined and distributed porous mesh, confirming the effectiveness of the phase inversion process in creating high porosity membranes. In cross sections, Commercial Nylon 6,6 is less porous and has a denser structure, while synthesized membranes show a more homogeneous pore distribution and greater internal porosity. These observations underline the success of the phase inversion process in membrane production with an optimized microstructure, ideal for applications requiring permeability, filtration or separation capacity.

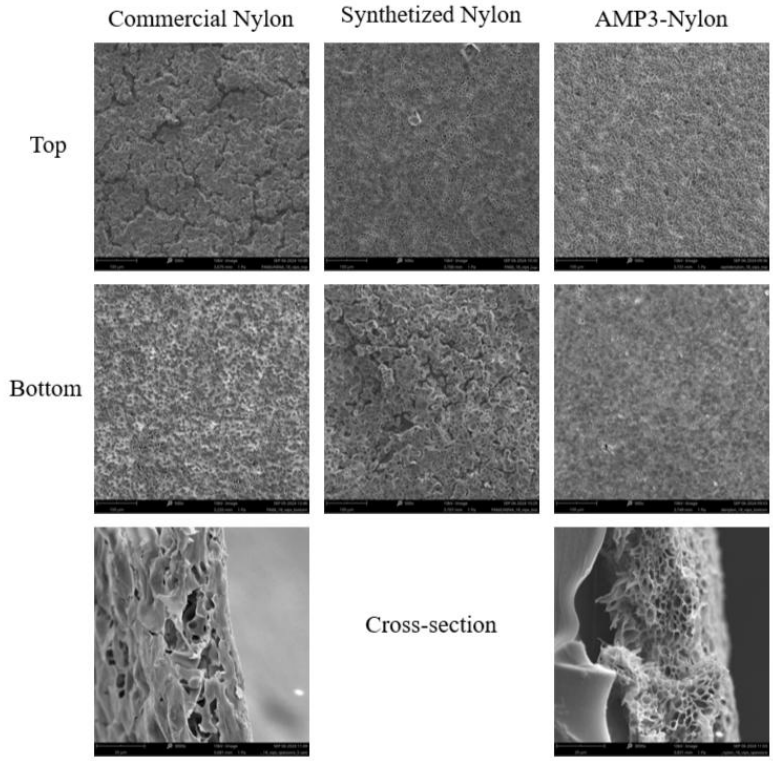

Fig. 2.14 SEM images of the top and bottom surface of Commercial Nylon 6,6, synthesized and AMP3-Nylon and the cross sections of Commercial Nylon 6,6 and AMP3-Nylon, obtained by phase inversion.

The antimicrobial activity of the membranes obtained by the phase inversion process could not be assessed, as the membranes have morphological properties which compromise their suitability for the tests envisaged, as shown in the images (Figure 2.13). In particular, the resulting structure is characterized by marked inhomogeneity and fragmentation of portions, which make it impossible to use as membranes in laboratory tests. The primary reason for these morphological defects could be the insufficient amount of material used during the preparation phase. The lack of material availability may have prevented the formation of a continuous and structurally stable membrane, leading to the appearance of non-uniform areas and a weak general structure. Another hypothesis is that it is plausible that an excessive solvent/non-solvent exchange rate or insufficient homogeneity of the solution contributed to the appearance of significant defects. [204]

2.5.3 Electrospinning membranes

This technique was chosen for its ability to generate high-porosity membranes with a potentially uniform distribution of the AMP3 peptide. In this paragraph the results obtained by applying this methodology are presented, with particular attention to the morphological characterization of membranes, their stability and their antimicrobial efficacy. These results provide an important basis for assessing the potential of membranes produced for medical and industrial applications.

The e-spin was carried out using ElMarco 1NS500. Three different polymer solutions were prepared: Commercial Nylon 6,6,

Synthesized Nylon 6,6 and AMP3-Nylon. For all the compounds, the same conditions were used (see Experimental Methods section for details). The polymer solutions were prepared at a concentration of 12% w/w by dissolving the polymer matrix in formic acid solution in a glass flask using magnetic stirring with a speed of 300 rpm for 2 h at 100°C. For Commercial Nylon, an additional 2% trifluoroacetic acid (TFA) was included to facilitate dissolution. The concentration of the polymer solution - in this case and in all subsequent cases - was determined using the Sartorius MA1600-1 thermogravimetric scale, a high precision instrument that allows to measure the mass change in the sample during controlled heating. Moreover, a critical parameter for electrospinning polymer solutions is their conductivity. Since the Nylon 6,6 dissolved in acids inherently produces conductive solutions, it is worth noting that the measured conductivity of the prepared solutions (>100 μS/cm), ensured the suitability for electrospinning. Once the polymer solution was homogeneous, was then transferred to an electrospinning process. Figure 2.15 illustrates the macroscopic membranes obtained through this process.

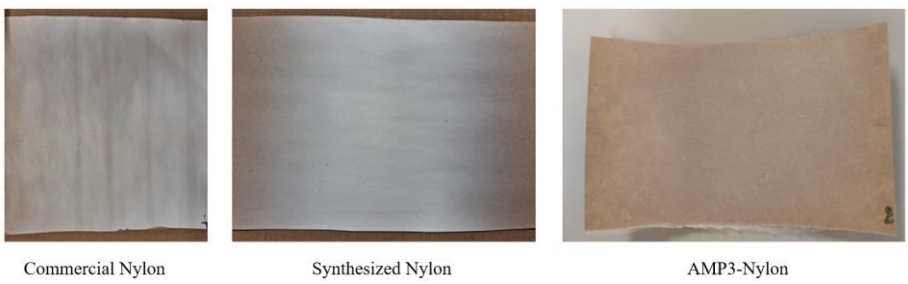

Fig. 2.15 Visual differences in structure and appearance between the produced samples.

Morphological and structural characterization

This section presents a detailed characterization of membranes prepared using Commercial Nylon 6,6, Synthesized Nylon 6,6 and AMP3-Nylon. The comparison aims to assess the impact of synthesis methods and peptide incorporation on membrane properties. Given the unique challenges posed by the limited availability of synthesized materials, the study focused on the delicate balance between maintaining membrane integrity and ensuring reproducibility during manufacturing. Particular attention was paid to their surface morphology, fiber arrangement and wettability, which are critical for applications such as filtration and antimicrobial purposes.

In the following table (Table 7) the structural characteristics of the obtained membranes are shown. Commercial Nylon 6,6 was employed to conduct multiple trials. Once the optimal conditions were established, membranes of Synthesized Nylon 6,6 and AMP3-Nylon were subsequently prepared. Due to the very limited quantities of Synthesized Nylon 6,6 and AMP3-Nylon available, the electrospinning process was conducted without moving the substrate, relying instead on material accumulation.

Table 7: Air permeability (AP), mass (m), and grammage (gsm) of electrospun samples. The mass was calculated using a sample size of 5x5 cm for all samples except for the AMP3-Nylon, which was measured on a 2.5x2.5 cm area.

	AP (l/m^2s^{-1}) @200Pa		m (g)	gsm	
	average	e%		average	e%
Commercial Nylon	11,4	4%	0,00476	1,9	1%
Synthesized Nylon	15,81		0,00661	2,6	
AMP3-Nylon	95,5		0,00106	1,7	

Due to the limited availability of material needed for the synthesis of both Synthesized Nylon and AMP3-Nylon, the membranes produced are particularly thin. To characterize the properties of these membranes, a series of in-depth analyses were carried out, aimed at assessing their intrinsic characteristics. The three samples were studied using SEM analysis in order to evaluate the surface morphology and obtain a thorough characterization of their fibrous structures (Figures 2.16 and 2.17). The SEM images show that the peptide does not alter the membranes formation during electrospinning (see Figure 2.16 and 2.17). This observation is consistent with findings by Gharaei et al., who reported that the incorporation of self-assembling peptides into electrospun PCL fibers did not significantly affect the fibrous morphology of the resulting membranes, ensuring structural integrity despite the addition of bioactive components.[205] Indeed, the composite structure observed in the three samples shows three kinds of fiber: microfibers, nanofibers and a spiderweb-like fibrous network. The only difference

is that Commercial Nylon 6,6 exhibits a uniform, tightly woven fiber structure, indicating controlled manufacturing processes, while Synthesized Nylon 6,6 and AMP3-Nylon show greater variability in fiber thickness and arrangement, with a less compact and more irregular morphology, reflecting differences in production methods. However, the similarity of the three types of fibers in all samples shows some reproducibility of the material suggesting that the addition of the peptide does not interfere with the ability of the material to generate a characteristic hierarchical structure. The results confirm that the electrospinning process maintains its effectiveness and reproducibility even in the presence of chemical modifications such as the incorporation of the peptide.

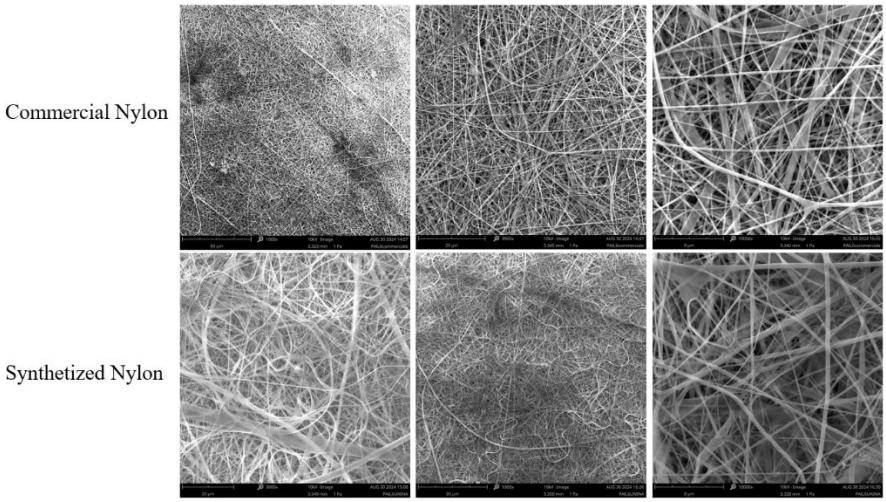

Fig. 2.16 The SEM images compare the microstructure of Commercial Nylon 6,6 (top row) and Synthesized Nylon 6,6 (bottom row) at increasing magnifications from left to right.

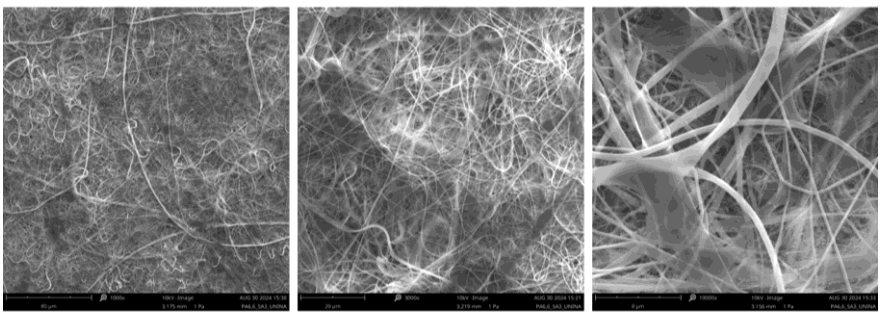

AMP3-Nylon

Fig. 2.17 SEM images of AMP3-Nylon fibers at three different magnifications. The structure reveals a network of interwoven fibers with increasing detail, showing uniformity at lower magnification and more intricate morphological features, including variations in fiber diameter and surface texture, at higher magnifications. These characteristics highlight the distinct microstructural properties of AMP3-Nylon.

Further, to better understand the characteristics, all the membranes obtained were characterized in terms of surface properties, focusing on contact angle and wettability. These tests were performed on all membrane types, both functionalized and non-functionalized, with multiple measurements for each sample to assess the hydrophilicity and hydrophobicity of their surface. These measurements are crucial to understanding how membranes interact with fluids - a property closely related to their effectiveness in the context of antimicrobial applications.

The results shown in Table 8 provide essential information on contact angle (Figure 2.18) of the different membranes tested: Commercial Nylon, Synthesized Nylon 6,6, and AMP3-Nylon.

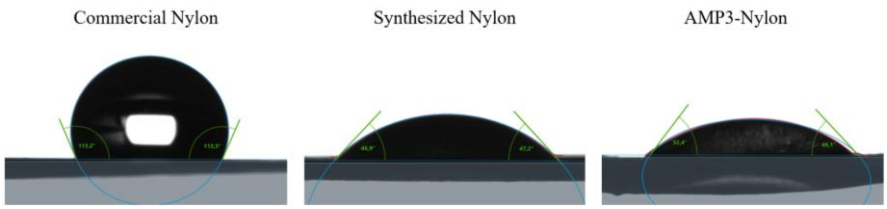

Fig. 2.18 The images illustrate the variation in hydrophilicity/hydrophobicity across the samples, with Commercial Nylon 6,6 showing a hydrophobic surface, while Synthesized Nylon 6,6 and AMP3-Nylon exhibit hydrophilic characteristics.

Table 8. Contact angle measurements of the different membranes obtained: Commercial Nylon 6,6, Synthesized Nylon 6,6, and AMP3-Nylon.

Sample	Contact angle (°)
Commercial Nylon 6,6	104,02
Synthesized Nylon 6,6	48,959
AMP3-Nylon	52,02

Contact angle measurement was performed using the KRÜSS Drop Shape Analyzer, a tool designed to characterize wettability and surface tension properties of solid and liquid surfaces by optical analysis of the shape of the drop. A small drop of water has been deposited on the well-prepared membrane for analysis. The integrated high-resolution camera captured the image of the drop immediately after deposition and the angle formed between the tangent to the drop surface at the point of contact with the solid and the surface itself was measured as the contact angle. This method also allowed a visual evaluation of the membrane water absorption behaviour. Figure 2.19 shows the response of Commercial Nylon 6,6 (A) and Synthesized Nylon 6,6 (B) to water drops. Unfortunately, an image of the AMP3-Nylon could not be captured as it broke immediately. The images clearly show that the Commercial Nylon 6,6 membrane does not absorb water, as the drop remains intact and spherical on the surface, reflecting its hydrophobic nature. In contrast, Nylon synthesized in the laboratory absorbs water, allowing the droplet to spread and integrate into the membrane structure. These observations are in line with contact angle measurements, which indicate that Nylon synthesized in the laboratory has hydrophilic properties, while Commercial Nylon 6,6 is hydrophobic.[206]

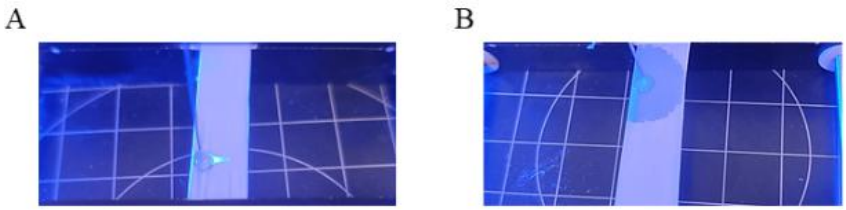

Fig. 2.19 Pictures showing the water absorption behaviour of (A) Commercial Nylon 6,6 and (B) Synthesized Nylon 6,6. The Commercial Nylon 6,6 repels water, as seen by the intact droplet, confirming its hydrophobic nature. In contrast, the Synthesized Nylon 6,6 absorbs water, indicating a hydrophilic surface.

Antimicrobial activity

After the structural and surface characterization of membranes, an antimicrobial activity assay was conducted to assess their effectiveness in reducing bacterial viability. All membranes obtained by the electrospinning procedure were tested against *E. coli*, following the protocol established in the proof-of-concept phase (see paragraph 2.4), to verify their antimicrobial potential. This evaluation focused on the immediate and long-term action of membranes in reducing bacterial survival, demonstrating their potential as innovative antimicrobial materials. Table 9 presents the results of two duplicate experiments, providing a complete comparison of antimicrobial efficacy.

Table 9 Comparison of bacterial viability (%) in the presence of membranes of Commercial Nylon 6,6, Synthesized Nylon 6,6 and AMP3-Nylon, in the two duplicates, at times t=0h and t=0.5h (3 and 30 minutes, respectively). The results show the antimicrobial efficacy of AMP3-Nylon compared to unmodified Nylon membranes, showing a significant and persistent reduction in bacterial viability over time.

1st	**COMMERCIAL NYLON 6,6**	**AMP3-NYLON**
t=0h	100%	14,62%
t=0.5h	102,47%	10,95%
2nd	**COMMERCIAL NYLON 6,6**	**AMP3-NYLON**
t=0h	100%	9,46%
t=0.5h	77,42%	6,03%
1st	**SYNTHESIZED NYLON 6,6**	**AMP3-NYLON**
t=0h	100%	19,55%
t=0.5h	135,34%	14,46%
2nd	**SYNTHESIZED NYLON 6,6**	**AMP3-NYLON**
t=0h	100%	17,57%
t=0.5h	123,59%	11,20%

The tables show the bacterial viability measured in contact with different membranes, including Commercial Nylon 6,6, Synthesized Nylon 6,6, and AMP3-Nylon, at times t=0h and t=0.5h. The results from two duplicates have been averaged to ensure consistency and reliability. Overall, the results clearly show the higher antimicrobial efficacy of AMP3-Nylon compared to unmodified Nylon samples.

In all conditions, AMP3-Nylon shows a marked reduction of bacterial viability already at the initial time, with values significantly lower than both Commercial Nylon 6,6 and Synthesized Nylon 6,6. At t=0h, bacterial viability in the presence of AMP3-Nylon is reduced to 9–19% of the reference value for both types of Nylon, suggesting an immediate and significant antimicrobial effect. Even at t=0.5h (after 30 minutes), AMP3-Nylon maintains this ability to

drastically reduce bacterial viability, with values ranging from 6% to 14%, demonstrating a constant and persistent antimicrobial effect over time.

On the other hand, Commercial Nylon 6,6 and Synthesized Nylon 6,6 fail to maintain a substantial reduction in bacterial viability. Commercial Nylon 6,6 shows an increase in bacterial viability in the first series at t=0.5h, while Synthesized Nylon 6,6 shows a clear tendency to promote bacterial growth, with values exceeding 100% of the initial viability. These results underline the limited effectiveness of unmodified Nylon membranes in controlling bacterial viability and highlight that peptide modification is crucial for achieving effective and prolonged antimicrobial action.

Overall, AMP3-Nylon emerges as the best choice to reduce bacterial viability quickly and durably, both at the early stages of exposure and after a prolonged period, demonstrating its potential for applications requiring materials with sustained antimicrobial activity. The presence of the peptide is therefore decisive in conferring superior antibacterial properties on Nylon membranes compared to their unmodified counterparts.

Chapter 3

Section 2: Conclusion

The work has highlighted the great potential of nylon as a polymer material due to its versatility, mechanical and thermal resistance, chemical stability and possibility of functionalization, making it suitable for applications ranging from industrial to biomedical areas. Following a structural characterization, Nylon 6,6 has shown greater thermal stability and rigidity due to its highly crystalline structure, while Nylon 6,10, while showing greater flexibility, has proved less suitable for applications requiring high thermal and mechanical performance. These results justify the choice to focus on Nylon 6,6 for functionalization with antimicrobial peptide AMP3, which was obtained through applications of DL. The synthesis of peptide-nylon was a crucial point in the project, allowing the AMP3 peptide to be stably integrated into the polymer matrix by means of grafting through strategy. The analysis carried out on the AMP3-Nylon confirmed the effectiveness of the functionalization: the UV-Vis spectrum confirmed the incorporation of the peptide, while the WAXS and DSC analyses showed that the semi- crystalline structure and the thermal properties of nylon 6,6 were not compromised by peptide integration. The membranes synthesized by electrospinning showed a nanofibrous structure with an adequate distribution of fibers. SEM images revealed that the incorporation of the peptide did not alter the ability of the nylon to form hierarchical structures, confirming the stability and reproducibility of the process. Wettability analyses showed a significant change in the hydrophilic nature of functionalized membranes, suggesting an improvement in their surface properties for antimicrobial applications. Antimicrobial activity tests conducted on AMP3-nylon membranes showed a

significant reduction in bacterial viability compared to unfunctionalized nylon, confirming the efficacy of de novo AMP3 peptide in conferring persistent antibacterial properties to the material. In parallel, the synthesis of membranes by phase inversion approach has made it possible to explore an alternative method for obtaining porous structures. However, the membranes obtained with functionalized nylon showed significant morphological defects. These aspects have limited the possibility of performing antimicrobial activity tests on such membranes. The electrospinning approach has proved most effective in producing functional membranes with promising structural and antimicrobial properties, while phase inversion requires further optimization. The main features of the process are influenced by the amount of material and the control of process parameters. However, the results obtained provide a solid basis for further development, with the aim of improving the scalability and performance of peptide-nylon membranes for advanced industrial applications. Indeed, electrospinning and phase inversion methods are particularly efficient for scaling the production of peptide-nylon antimicrobial membranes, satisfying both precision and throughput demands for industrial use.[207]

Electrospinning is proficient in producing nanofibrous membranes with exact shape, elevated porosity, and adjustable characteristics. This makes it optimal for the incorporation of antimicrobial peptides such as AMP3, which necessitate homogenous distribution throughout the nylon matrix to guarantee effective bioactivity.

Innovations like multi-needle and needleless systems, together with automation, have significantly enhanced production rates while ensuring structural integrity, an essential aspect for sustaining the functionality of peptide-loaded membranes.

Phase inversion provides intrinsic scalability owing to its suitability for continuous production. While our attempts were limited by material scarcity and did not achieve the desired results, this method should enable the regulated integration of the peptide into the nylon, preserving both structural integrity and bioactivity. By adjusting parameters such as polymer concentration, solvent systems, and coagulation conditions, phase inversion can reduce flaws and improve membrane performance.

These developments highlight the feasibility of moving peptide-nylon membranes from laboratory development to large-scale production, facilitating their industrial application in areas such as filtration, medicinal devices, and antimicrobial surface coatings.

Chapter 4

Experimental Methods

4.1 Compounds synthesis

Nylon belongs to a category of synthetic polyamides widely used in industrial and consumer applications for its mechanical, thermal and chemical resistance properties. Nylon polymers, derived from monomers containing amino groups and acids, are produced through polymerization processes which determine their structure and, consequently, the final properties.

4.1.1 Nylon Synthesis

Polyamide (PA) synthesis was carried out following the interfacial polymerization method, using different monomers depending on the polyamide. This method involves the use of two immiscible liquid phases: an aqueous phase and an organic phase. The aqueous phase contains the hydrophilic monomer, hexamethylenediamine, in solution with sodium hydroxide (NaOH) as a base to neutralize the hydrochloric acid (HCl) produced during the reaction. The organic phase, consisting of dichloromethane (DCM), contains in solution the hydrophobic monomer. The reaction takes place rapidly at the interface between the two phases, at room temperature, and the kinetic of polymerization is governed by the diffusion of monomers through the interface.

Nylon 6,6

Nylon 6,6 was synthesized from the monomers Adipoyl chloride and hexamethylenediamine:

$$C_6H_8Cl_2O_2 + C_6H_{16}N_2 \longrightarrow (C_{12}H_{22}N_2O_2)_n + 2HCl$$

A solution of sodium hydroxide (NaOH) 0.5 M has been prepared in which Hexamethylenediamine is added to give a 0.4 M solution; this solution has been poured slowly in the beaker containing dichloromethane (DCM) and Adipoyl Chloride with a final concentration of 0.4 M. It forms a film to the interface that is pinched with a tweezer and pulled out slowly, getting a thread that is wrapped on a glass rod. The polymer obtained was washed with distilled water several times and then dried in a vacuum.

Nylon 6,10

Nylon 6,10 was synthesized in the same way as PA 6,6, from the monomers Sebacoyl chloride and hexamethylenediamine:

$$C_{10}H_{16}Cl_2O_2 + C_6H_{16}N_2 \longrightarrow (C_{16}H_{30}N_2O_2)_n + 2HCl\ .$$

A solution of 0.4 M dichloromethane containing the monomer sebacoyl chloride was prepared; to this solution a solution of 0.5 M sodium hydroxide, containing 0.4 M hexamethylenediamine was added.

4.1.2 AMP3 – Nylon synthesis

The synthesis of AMP3-Nylon was carried out following a procedure like that used for the production of Nylon 6,6 by interfacial polymerization, with some important modifications. Whereas for Nylon 6,6 the aqueous phase contained only hexamethylenediamine, in the case of AMP3-Nylon both 1,6-diaminohexane and a peptide sequence with two amino groups were introduced into solution. Specifically, a 0.5 M solution of sodium hydroxide (NaOH) was prepared in the aqueous phase, into which the antimicrobial peptide

(AMP3) was dissolved. To achieve the desired biofunctionalization, the peptide was added at 1 mol% relative to the total amount of diamine used in the polymerization process. Hexamethylenediamine (1,6-diaminohexane) was then added to the solution to achieve a final concentration of 0.4 M. The organic phase, containing adipoyl chloride dissolved in dichloromethane, also remained unchanged. The reaction then took place at the interface between the two phases, where the primary amino groups of the peptide and diamine react with the chloride of the adipoyl, forming a polymeric film on the surface. This film was then collected and treated as described for Nylon 6,6, so it was washed several times with water and then dried under vacuum.

4.2 Membranes synthesis

4.2.1 Electrospinning

The electrospinning procedure was performed using ElMarco 1NS500. For the fabrication of polyamide nanofibres, SAATI SpA provided a PA66 powder, furthmore Synthesized-Nylon nanofibres and AMP3-Nylon were also manufactured. They were dissolved to form a 12% polymer solution in formic acid, with addition of TFA for Commercial Nylon 6,6, maintaining a magnetic stirring at 300 rpm for 2 hours at 100°C. To confirm the concentration of the polymer solution, the Sartorius MA1600-1 thermogravimetric scale was used. 1.0 g of polymer solution was taken and heated to 150 °C for 65 minutes. During the process, the mass of the sample was monitored in real time, allowing the loss of mass due to evaporation

of solvents present in the solution to be recorded. The residual fraction, corresponding to the non-volatile polymer content, was calculated as the ratio of the residual mass to the initial mass, allowing the determination of the polymeric concentration with high precision and reproducibility. Once the polymer solution was homogeneous, it was then transferred to an electrospinning process.

The electrospinning configuration employed a thin stainless-steel wire (0.2 mm) as the spinning electrode and a moving head to apply the polymer solution along the entire length of this wire. The solutions have been electrospun at room temperature (22 ± 1 °C) and stable relative humidity (19 ± 1 %), loaded into the moving head with a stainless-steel orifice of 0,6 mm, which was connected to a high-voltage supply to provide a negative bias continuous voltage up to 90 kV and a working voltage of 60 kV. To facilitate the delamination of the electrospun samples from the carrier, brown siliconized paper was used as the supporting substrate. The siliconized coating on the paper acts as a non-stick surface, ensuring easy removal of the polymeric material after the electrospinning process without damaging its structure.

4.2.2 Phase Inversion

The membranes were made using phase inversion technique. Polymer solutions were prepared at different concentrations of Commercial Nylon 6,6 (12%, 14%, 16%, 18%, 25% w/w) and polymer solutions of Synthesized Nylon 6,6, as well as a solution containing an 18% AMP3-Nylon combination. For Commercial Nylon solutions, the polymer was dissolved in formic acid with 2%

added trifluoroacetic acid (TFA), while the Nylon synthesized in lab and the AMP3-Nylon were dissolved exclusively in formic acid. All the solutions were stirred at 300 rpm for one hour at 100°C, except for the AMP3-Nylon solution which was stirred at room temperature.

For the preparation of the membranes, a PET carrier was used, which was fixed to a glass plate. The polymer solution was spread on the glass plate with a metal bar with a gap of 200 μm, maintaining a coating speed of about 3 seconds. The newly coated membrane was then immersed in a first bath of deionized water to allow phase inversion. After this phase, each membrane was subjected to a second wash in water for 20 minutes and finally to a final bath in water for one hour. The membranes were then dried in an oven at T= 70°C.

The addition of VIPS was applied to Commercial Nylon, Synthesized Nylon 6,6 and AMP3-Nylon 18% polymer solutions, after trial. After the solutions were drawn on the glass plates, they were placed in a climate chamber with controlled parameters (3 mins, RH 80%, T=60°C). The membranes were then immersed in a first water bath for 20 minutes to allow phase inversion, followed by two washing baths similar to those described above (20 minutes and 1 hour respectively). Finally, the membranes were dried in the oven at T= 70°C.

4.3 Chemical and structural characterization

4.3.1 Differential Scanning Calorimetry (DSC)

The thermograms of Nylon 6,6, Synthesized Nylon 6,6 and AMP3-Nylon were determined using a Mettler Toledo DSC1 calorimeter (Mettler Toledo, Milan, Italy); analyses were conducted under nitrogen atmosphere, weighting 5 mg of each sample in a standard 40 µL aluminum crucible and using an empty 40 µL crucible as reference.

Non-isothermal behaviour was studied using the following program: (i) heating at a rate of 10 °C/min from -25 to 280 °C; (ii) 5 min of isotherm at 250 °C; (iii) cooling from 280 to -25 °C at 10 °C/min (crystallization temperature, Tc and crystallization enthalpy, ΔH_c, were determined during cooling); (iv) 5 min of isotherm at -25 °C; and (v) heating from -25 to 280 °C at 10 °C/min (melting temperature, Tm, and heat of fusion, ΔH_f, were measured during heating).

4.3.2 Viscosity

After checking the percentage of the polymer solution, viscosity measurement was carried out. The polymers viscosity was controlled using rotational viscometer Anton Paar ViscoQC 10, with temperature controlled with PTD80. The sample is poured into the measuring container, ensuring that the shaft is completely covered and that the desired temperature is set to PTD 80. The T-Ready™ function indicates when the sample has reached thermal equilibrium. In this step, the measurement is started. During the measurement

process, the viscometer records the sample viscosity as a function of time, torque or temperature.

4.3.3 Air Permeability

The air permeability of samples obtained by electrospinning and phase inversion was analyzed using the Textest FX 3300 Air Permeability Tester, an international standard-compliant instrument for measuring the air permeability of flat materials. For each sample, a 5x5 cm square was cut out and firmly fixed on the instrument's test area to ensure accurate and reproducible measurements. The air permeability was measured by applying two different test pressures for phase-reversal samples (1000 Pa and 200 Pa), while a pressure of 200 Pa was used for electrospun yarns. In each case, the air flow through the material under the specified conditions was recorded. The same sample was then used for weight determination, by weighing the sample on a high precision analytical scale and relating the weight to the area of the sample. Results were expressed in gsm.

4.3.4 UV-Vis

UV-Vis absorption spectra were recorded with a Cary Varian 60 Spectrophotometer, equipped with a thermostatic compartment (Varian, Palo Alto, CA, USA), using a quartz cuvette with a path of 1 cm. The scans were performed at 25 °C from 200 to 800 nm, with a min-1 scan speed of 600 nm.

4.3.5 Scanning Electron Microscopy (SEM)

The SEM of Nylon films was analyzed at the Department of Chemical Sciences of the Federico II University of Naples, using the scanning electron microscope Nova NanoSEM 450, which guarantees high resolution and precision in surface characterization. SEM analysis of samples obtained by electrospinning and phase inversion at the SAATI S.p.A. in Appiano Gentile, were obtained using the Phenom ParticleX system, specially designed for the analysis of particles and microstructure.

In both cases, the samples were subjected to a preliminary metallization process to improve electrical conductivity and obtain high quality SEM images. The metallized samples were then analyzed to characterize their morphology and surface structure in detail.

General Conclusion

This work represents a significant step forward in the use of AI technologies, especially DL, applied to the design and development of innovative antimicrobial materials. New results have been found by combining advanced computer methods with experimental methods. These results open up new ways to design antimicrobial peptides (AMPs) and use them on functionalized materials. This interdisciplinary approach combines computational biology, materials chemistry, and microbiology to create solutions that meet concrete needs in the biomedical, industrial, and environmental fields.

Innovation in the computational design of antimicrobial peptides

Deep learning tools such as HydrAMP and AMPlify have proven to be highly effective in predicting how to obtain peptide sequences with optimal antimicrobial properties. These algorithms have overcome the limitations of traditional methods, offering a swift and efficient approach to explore the amino acid sequence space and pinpoint candidates with a high likelihood of biological success. This phase represents a turning point in AMP research, as it not only speeds up development times but also reduces the number of experiments needed to identify the most promising sequences. The synergy between HydrAMP and AMPlify highlighted the importance of an integrated approach, where generative and predictive models work together to select the best candidates. One of the distinguishing features of this work was the rigor in the experimental validation of computational predictions.

Biophysical and antimicrobial characterizations

The designed peptides were characterized by microbiological testing, such as finding the minimum inhibitory concentration (MIC) for a lot of different types of bacteria. The results confirmed the validity of the computational predictions, with AMP3 showing high antimicrobial efficacy against both Gram-positive and Gram-negative bacteria. Additional biophysical characterizations, such as model membrane interaction studies, have given us useful information about how the AMP3 peptide works. In particular, the work showed that the designed peptide interacts with model membranes of *E. coli*.

The development of functionalized antimicrobial membranes

The second part of the work successfully explored the immobilization of antimicrobial peptides on Nylon membranes, utilizing the innovative strategy of grafting through. This approach ensured a uniform and stable anchoring of the peptides, preserving their biological activity and ensuring a homogeneous distribution on the material's surface. The functionalized membranes obtained showed advanced physical properties. Furthermore, microbiological tests on membranes showed a significant reduction in bacterial viability, confirming the effectiveness of functionalization. These results make them ideal for antimicrobial applications in the biomedical and industrial fields.

Applications and Future Perspectives

The importance of this work lies in its ability to address some of the most pressing challenges in the field of safety and sustainability. Growing antimicrobial resistance is a global threat to public health, and the development of innovative solutions such as functionalized AMPs offers a sustainable and scalable approach to mitigate this problem. In addition, the applicability of antimicrobial membranes extends to several areas, including:
Biomedical fields: infection-resistant medical devices.
Food industry: *active* packaging to preserve the freshness of food.
Water treatment: antimicrobial filters for water purification.

The combination of artificial intelligence technologies, advanced chemical synthesis techniques, and biophysical characterization methods has opened new avenues in antimicrobial materials research. Integrating the use of DL to design custom peptides is a milestone in the field, demonstrating how AI can drive scientific innovation quickly and effectively.
In conclusion, the research activity carried out in this PhD thesis is an example of how the integration between artificial intelligence and materials science can lead to innovative solutions for complex global problems. The AMP designs and antimicrobial membranes developed not only meet current needs but also pave the way for further technological and scientific developments, thus providing a solid basis for future research and applications.

References

References

(1) Ngiam, K. Y.; Khor, I. W. Big Data and Machine Learning Algorithms for Health-Care Delivery. *Lancet Oncol.* **2019**, *20* (5), e262–e273. https://doi.org/10.1016/S1470-2045(19)30149-4.

(2) Araújo, S. O.; Peres, R. S.; Ramalho, J. C.; Lidon, F.; Barata, J. Machine Learning Applications in Agriculture: Current Trends, Challenges, and Future Perspectives. *Agronomy* **2023**, *13* (12), 2976. https://doi.org/10.3390/agronomy13122976.

(3) Chakraborty, C.; Bhattacharya, M.; Lee, S.-S.; Wen, Z.-H.; Lo, Y.-H. The Changing Scenario of Drug Discovery Using AI to Deep Learning: Recent Advancement, Success Stories, Collaborations, and Challenges. *Mol. Ther. Nucleic Acids* **2024**, *35* (3). https://doi.org/10.1016/j.omtn.2024.102295.

(4) Ben Ayed, R.; Hanana, M. Artificial Intelligence to Improve the Food and Agriculture Sector. *J. Food Qual.* **2021**, *2021* (1), 5584754. https://doi.org/10.1155/2021/5584754.

(5) Saharkhiz, S.; Mostafavi, M.; Birashk, A.; Karimian, S.; Khalilollah, S.; Jaferian, S.; Yazdani, Y.; Alipourfard, I.; Huh, Y. S.; Farani, M. R.; Akhavan-Sigari, R. The State-of-the-Art Overview to Application of Deep Learning in Accurate Protein Design and Structure Prediction. *Top. Curr. Chem.* **2024**, *382* (3), 23. https://doi.org/10.1007/s41061-024-00469-6.

(6) Wan, F.; Wong, F.; Collins, J. J.; de la Fuente-Nunez, C. Machine Learning for Antimicrobial Peptide Identification and Design. *Nat. Rev. Bioeng.* **2024**, *2* (5), 392–407. https://doi.org/10.1038/s44222-024-00152-x.

(7) Childers, M. C.; Daggett, V. Insights from Molecular Dynamics Simulations for Computational Protein Design. *Mol. Syst. Des. Eng.* **2017**, *2* (1), 9–33. https://doi.org/10.1039/C6ME00083E.

(8) Engqvist, M. K. M.; Rabe, K. S. Applications of Protein Engineering and Directed Evolution in Plant Research. *Plant Physiol.* **2019**, *179* (3), 907–917. https://doi.org/10.1104/pp.18.01534.

(9) Koretke, K. K.; Luthey-Schulten, Z.; Wolynes, P. G. Self-Consistently Optimized Energy Functions for Protein Structure Prediction by Molecular Dynamics. *Proc. Natl. Acad. Sci.* **1998**, *95* (6), 2932–2937. https://doi.org/10.1073/pnas.95.6.2932.

(10) Das, P.; Sercu, T.; Wadhawan, K.; Padhi, I.; Gehrmann, S.; Cipcigan, F.; Chenthamarakshan, V.; Strobelt, H.; dos Santos, C.; Chen, P.-Y.; Yang, Y. Y.; Tan, J. P. K.; Hedrick, J.; Crain, J.; Mojsilovic, A.

Accelerated Antimicrobial Discovery via Deep Generative Models and Molecular Dynamics Simulations. *Nat. Biomed. Eng.* **2021**, *5* (6), 613–623. https://doi.org/10.1038/s41551-021-00689-x.

(11) LeCun, Y.; Bengio, Y.; Hinton, G. Deep Learning. *Nature* **2015**, *521* (7553), 436–444. https://doi.org/10.1038/nature14539.

(12) Castiglioni, I.; Rundo, L.; Codari, M.; Di Leo, G.; Salvatore, C.; Interlenghi, M.; Gallivanone, F.; Cozzi, A.; D'Amico, N. C.; Sardanelli, F. AI Applications to Medical Images: From Machine Learning to Deep Learning. *Phys. Med.* **2021**, *83*, 9–24. https://doi.org/10.1016/j.ejmp.2021.02.006.

(13) Xu, J.; Li, F.; Li, C.; Guo, X.; Landersdorfer, C.; Shen, H.-H.; Peleg, A. Y.; Li, J.; Imoto, S.; Yao, J.; Akutsu, T.; Song, J. iAMPCN: A Deep-Learning Approach for Identifying Antimicrobial Peptides and Their Functional Activities. *Brief. Bioinform.* **2023**, *24* (4), bbad240. https://doi.org/10.1093/bib/bbad240.

(14) Nedyalkova, M.; S. Paluch, A.; Potes Vecini, D.; Lattuada, M. Progress and Future of the Computational Design of Antimicrobial Peptides (AMPs): Bio-Inspired Functional Molecules. *Digit. Discov.* **2024**, *3* (1), 9–22. https://doi.org/10.1039/D3DD00186E.

(15) Ovchinnikov, S.; Huang, P.-S. Structure-Based Protein Design with Deep Learning. *Curr. Opin. Chem. Biol.* **2021**, *65*, 136–144. https://doi.org/10.1016/j.cbpa.2021.08.004.

(16) Son, A.; Park, J.; Kim, W.; Lee, W.; Yoon, Y.; Ji, J.; Kim, H. Integrating Computational Design and Experimental Approaches for Next-Generation Biologics. *Biomolecules* **2024**, *14* (9), 1073. https://doi.org/10.3390/biom14091073.

(17) Chang, L.; Mondal, A.; Perez, A. Towards Rational Computational Peptide Design. *Front. Bioinforma.* **2022**, *2*. https://doi.org/10.3389/fbinf.2022.1046493.

(18) Kuhlman, B.; Dantas, G.; Ireton, G. C.; Varani, G.; Stoddard, B. L.; Baker, D. Design of a Novel Globular Protein Fold with Atomic-Level Accuracy. *Science* **2003**, *302* (5649), 1364–1368. https://doi.org/10.1126/science.1089427.

(19) Das, R.; Baker, D. Macromolecular Modeling with Rosetta. *Annu. Rev. Biochem.* **2008**, *77* (Volume 77, 2008), 363–382. https://doi.org/10.1146/annurev.biochem.77.062906.171838.

(20) Jumper, J.; Evans, R.; Pritzel, A.; Green, T.; Figurnov, M.; Ronneberger, O.; Tunyasuvunakool, K.; Bates, R.; Žídek, A.; Potapenko, A.; Bridgland, A.; Meyer, C.; Kohl, S. A. A.; Ballard, A. J.; Cowie, A.; Romera-Paredes, B.; Nikolov, S.; Jain, R.; Adler, J.; Back,

T.; Petersen, S.; Reiman, D.; Clancy, E.; Zielinski, M.; Steinegger, M.; Pacholska, M.; Berghammer, T.; Bodenstein, S.; Silver, D.; Vinyals, O.; Senior, A. W.; Kavukcuoglu, K.; Kohli, P.; Hassabis, D. Highly Accurate Protein Structure Prediction with AlphaFold. *Nature* **2021**, *596* (7873), 583–589. https://doi.org/10.1038/s41586-021-03819-2.

(21) Huang, B.; Abedi, M.; Ahn, G.; Coventry, B.; Sappington, I.; Tang, C.; Wang, R.; Schlichthaerle, T.; Zhang, J. Z.; Wang, Y.; Goreshnik, I.; Chiu, C. W.; Chazin-Gray, A.; Chan, S.; Gerben, S.; Murray, A.; Wang, S.; O'Neill, J.; Yi, L.; Yeh, R.; Misquith, A.; Wolf, A.; Tomasovic, L. M.; Piraner, D. I.; Duran Gonzalez, M. J.; Bennett, N. R.; Venkatesh, P.; Ahlrichs, M.; Dobbins, C.; Yang, W.; Wang, X.; Sahtoe, D. D.; Vafeados, D.; Mout, R.; Shivaei, S.; Cao, L.; Carter, L.; Stewart, L.; Spangler, J. B.; Roybal, K. T.; Greisen, P. J.; Li, X.; Bernardes, G. J. L.; Bertozzi, C. R.; Baker, D. Designed Endocytosis-Inducing Proteins Degrade Targets and Amplify Signals. *Nature* **2024**, 1–9. https://doi.org/10.1038/s41586-024-07948-2.

(22) Laptev, V. V.; Gerget, O. M.; Markova, N. A. Generative Models Based on VAE and GAN for New Medical Data Synthesis. In *Society 5.0: Cyberspace for Advanced Human-Centered Society*; Kravets, A. G., Bolshakov, A. A., Shcherbakov, M., Eds.; Springer International Publishing: Cham, 2021; pp 217–226. https://doi.org/10.1007/978-3-030-63563-3_17.

(23) Li, Y.; Huang, C.; Ding, L.; Li, Z.; Pan, Y.; Gao, X. Deep Learning in Bioinformatics: Introduction, Application, and Perspective in the Big Data Era. *Methods* **2019**, *166*, 4–21. https://doi.org/10.1016/j.ymeth.2019.04.008.

(24) Notin, P.; Rollins, N.; Gal, Y.; Sander, C.; Marks, D. Machine Learning for Functional Protein Design. *Nat. Biotechnol.* **2024**, *42* (2), 216–228. https://doi.org/10.1038/s41587-024-02127-0.

(25) Moretta, A.; Scieuzo, C.; Petrone, A. M.; Salvia, R.; Manniello, M. D.; Franco, A.; Lucchetti, D.; Vassallo, A.; Vogel, H.; Sgambato, A.; Falabella, P. Antimicrobial Peptides: A New Hope in Biomedical and Pharmaceutical Fields. *Front. Cell. Infect. Microbiol.* **2021**, *11*. https://doi.org/10.3389/fcimb.2021.668632.

(26) Levy, S. B.; Marshall, B. Antibacterial Resistance Worldwide: Causes, Challenges and Responses. *Nat. Med.* **2004**, *10* (12), S122–S129. https://doi.org/10.1038/nm1145.

(27) Ramazi, S.; Mohammadi, N.; Allahverdi, A.; Khalili, E.; Abdolmaleki, P. A Review on Antimicrobial Peptides Databases and the

Computational Tools. *Database* **2022**, *2022*, baac011. https://doi.org/10.1093/database/baac011.

(28) *Advancing Additive Manufacturing through Deep Learning: A Comprehensive Review of Current Progress and Future Challenges*. https://arxiv.org/html/2403.00669v1 (accessed 2024-12-12).

(29) Wang, G.; Li, X.; Wang, Z. APD3: The Antimicrobial Peptide Database as a Tool for Research and Education. *Nucleic Acids Res.* **2016**, *44* (D1), D1087–D1093. https://doi.org/10.1093/nar/gkv1278.

(30) Ashby, M.; Petkova, A.; Gani, J.; Mikut, R.; Hilpert, K. Use of Peptide Libraries for Identification and Optimization of Novel Antimicrobial Peptides. *Curr. Top. Med. Chem.* **2017**, *17* (5), 537–553. https://doi.org/10.2174/1568026616666160713125555.

(31) Wang, J.; Feng, J.; Kang, Y.; Pan, P.; Ge, J.; Wang, Y.; Wang, M.; Wu, Z.; Zhang, X.; Yu, J.; Zhang, X.; Wang, T.; Wen, L.; Yan, G.; Deng, Y.; Shi, H.; Hsieh, C.-Y.; Jiang, Z.; Hou, T. A Foundation Model Approach to Guide Antimicrobial Peptide Design in the Era of Artificial Intelligence Driven Scientific Discovery. arXiv July 17, 2024. https://doi.org/10.48550/arXiv.2407.12296.

(32) Wang, P.; Hu, L.; Liu, G.; Jiang, N.; Chen, X.; Xu, J.; Zheng, W.; Li, L.; Tan, M.; Chen, Z.; Song, H.; Cai, Y.-D.; Chou, K.-C. Prediction of Antimicrobial Peptides Based on Sequence Alignment and Feature Selection Methods. *PLOS ONE* **2011**, *6* (4), e18476. https://doi.org/10.1371/journal.pone.0018476.

(33) Cao, Q.; Ge, C.; Wang, X.; Harvey, P. J.; Zhang, Z.; Ma, Y.; Wang, X.; Jia, X.; Mobli, M.; Craik, D. J.; Jiang, T.; Yang, J.; Wei, Z.; Wang, Y.; Chang, S.; Yu, R. Designing Antimicrobial Peptides Using Deep Learning and Molecular Dynamic Simulations. *Brief. Bioinform.* **2023**, *24* (2), bbad058. https://doi.org/10.1093/bib/bbad058.

(34) Sun, S. Progress in the Identification and Design of Novel Antimicrobial Peptides Against Pathogenic Microorganisms. *Probiotics Antimicrob. Proteins* **2024**. https://doi.org/10.1007/s12602-024-10402-4.

(35) Fjell, C. D.; Hiss, J. A.; Hancock, R. E. W.; Schneider, G. Designing Antimicrobial Peptides: Form Follows Function. *Nat. Rev. Drug Discov.* **2012**, *11* (1), 37–51. https://doi.org/10.1038/nrd3591.

(36) Ma, X.; Wang, Q.; Ren, K.; Xu, T.; Zhang, Z.; Xu, M.; Rao, Z.; Zhang, X. A Review of Antimicrobial Peptides: Structure, Mechanism of Action, and Molecular Optimization Strategies. *Fermentation* **2024**, *10* (11), 540. https://doi.org/10.3390/fermentation10110540.

(37) Jenssen, H.; Hamill, P.; Hancock, R. E. W. Peptide Antimicrobial Agents. *Clin. Microbiol. Rev.* **2006**, *19* (3), 491–511. https://doi.org/10.1128/cmr.00056-05.

(38) Zasloff, M. Antimicrobial Peptides of Multicellular Organisms. *Nature* **2002**, *415* (6870), 389–395. https://doi.org/10.1038/415389a.

(39) Hancock, R. E. W.; Sahl, H.-G. Antimicrobial and Host-Defense Peptides as New Anti-Infective Therapeutic Strategies. *Nat. Biotechnol.* **2006**, *24* (12), 1551–1557. https://doi.org/10.1038/nbt1267.

(40) Yeaman, M. R.; Yount, N. Y. Mechanisms of Antimicrobial Peptide Action and Resistance. *Pharmacol. Rev.* **2003**, *55* (1), 27–55. https://doi.org/10.1124/pr.55.1.2.

(41) Wiesner, J.; Vilcinskas, A. Antimicrobial Peptides: The Ancient Arm of the Human Immune System. *Virulence* **2010**, *1* (5), 440–464. https://doi.org/10.4161/viru.1.5.12983.

(42) Oliva, R.; Chino, M.; Pane, K.; Pistorio, V.; De Santis, A.; Pizzo, E.; D'Errico, G.; Pavone, V.; Lombardi, A.; Del Vecchio, P.; Notomista, E.; Nastri, F.; Petraccone, L. Exploring the Role of Unnatural Amino Acids in Antimicrobial Peptides. *Sci. Rep.* **2018**, *8* (1), 8888. https://doi.org/10.1038/s41598-018-27231-5.

(43) *PR-39, a proline-rich antibacterial peptide that inhibits phagocyte NADPH oxidase activity by binding to Src homology 3 domains of p47 phox. | PNAS*. https://www.pnas.org/doi/abs/10.1073/pnas.93.12.6014 (accessed 2024-12-05).

(44) Hao, G.; Shi, Y.-H.; Tang, Y.-L.; Le, G.-W. The Intracellular Mechanism of Action on Escherichia Coli of BF2-A/C, Two Analogues of the Antimicrobial Peptide Buforin 2. *J. Microbiol.* **2013**, *51* (2), 200–206. https://doi.org/10.1007/s12275-013-2441-1.

(45) Cardoso, M. H.; Meneguetti, B. T.; Costa, B. O.; Buccini, D. F.; Oshiro, K. G. N.; Preza, S. L. E.; Carvalho, C. M. E.; Migliolo, L.; Franco, O. L. Non-Lytic Antibacterial Peptides That Translocate Through Bacterial Membranes to Act on Intracellular Targets. *Int. J. Mol. Sci.* **2019**, *20* (19), 4877. https://doi.org/10.3390/ijms20194877.

(46) Brogden, K. A. Antimicrobial Peptides: Pore Formers or Metabolic Inhibitors in Bacteria? *Nat. Rev. Microbiol.* **2005**, *3* (3), 238–250. https://doi.org/10.1038/nrmicro1098.

(47) Cleveland, J.; Montville, T. J.; Nes, I. F.; Chikindas, M. L. Bacteriocins: Safe, Natural Antimicrobials for Food Preservation. *Int. J. Food Microbiol.* **2001**, *71* (1), 1–20. https://doi.org/10.1016/s0168-1605(01)00560-8.

(48) Montesinos, E. Antimicrobial Peptides and Plant Disease Control. *FEMS Microbiol. Lett.* **2007**, *270* (1), 1–11. https://doi.org/10.1111/j.1574-6968.2007.00683.x.

(49) Defoirdt, T.; Sorgeloos, P.; Bossier, P. Alternatives to Antibiotics for the Control of Bacterial Disease in Aquaculture. *Curr. Opin. Microbiol.* **2011**, *14* (3), 251–258. https://doi.org/10.1016/j.mib.2011.03.004.

(50) Wenzel, M.; Chiriac, A. I.; Otto, A.; Zweytick, D.; May, C.; Schumacher, C.; Gust, R.; Albada, H. B.; Penkova, M.; Krämer, U.; Erdmann, R.; Metzler-Nolte, N.; Straus, S. K.; Bremer, E.; Becher, D.; Brötz-Oesterhelt, H.; Sahl, H.-G.; Bandow, J. E. Small Cationic Antimicrobial Peptides Delocalize Peripheral Membrane Proteins. *Proc. Natl. Acad. Sci.* **2014**, *111* (14), E1409–E1418. https://doi.org/10.1073/pnas.1319900111.

(51) Huan, Y.; Kong, Q.; Mou, H.; Yi, H. Antimicrobial Peptides: Classification, Design, Application and Research Progress in Multiple Fields. *Front. Microbiol.* **2020**, *11*. https://doi.org/10.3389/fmicb.2020.582779.

(52) Chen, T.; Guestrin, C. XGBoost: A Scalable Tree Boosting System. In *Proceedings of the 22nd ACM SIGKDD International Conference on Knowledge Discovery and Data Mining*; KDD '16; Association for Computing Machinery: New York, NY, USA, 2016; pp 785–794. https://doi.org/10.1145/2939672.2939785.

(53) Hubel, D. H.; Wiesel, T. N. Receptive Fields of Single Neurones in the Cat's Striate Cortex. https://doi.org/10.1113/jphysiol.1959.sp006308.

(54) Fukushima, K. Visual Feature Extraction by a Multilayered Network of Analog Threshold Elements. *IEEE Trans. Syst. Sci. Cybern.* **1969**, *5* (4), 322–333. https://doi.org/10.1109/TSSC.1969.300225.

(55) Phung, V. H.; Rhee, E. J. A High-Accuracy Model Average Ensemble of Convolutional Neural Networks for Classification of Cloud Image Patches on Small Datasets. *Appl. Sci.* **2019**, *9* (21), 4500. https://doi.org/10.3390/app9214500.

(56) Wang, S.; Peng, J.; Ma, J.; Xu, J. Protein Secondary Structure Prediction Using Deep Convolutional Neural Fields. *Sci. Rep.* **2016**, *6* (1), 18962. https://doi.org/10.1038/srep18962.

(57) Xu, J.; McPartlon, M.; Li, J. Improved Protein Structure Prediction by Deep Learning Irrespective of Co-Evolution Information. *Nat. Mach. Intell.* **2021**, *3* (7), 601–609. https://doi.org/10.1038/s42256-021-00348-5.

(58) Gligorijević, V.; Renfrew, P. D.; Kosciolek, T.; Leman, J. K.; Berenberg, D.; Vatanen, T.; Chandler, C.; Taylor, B. C.; Fisk, I. M.;

Vlamakis, H.; Xavier, R. J.; Knight, R.; Cho, K.; Bonneau, R. Structure-Based Protein Function Prediction Using Graph Convolutional Networks. *Nat. Commun.* **2021**, *12* (1), 3168. https://doi.org/10.1038/s41467-021-23303-9.

(59) Zhou, W.; Liu, Y.; Li, Y.; Kong, S.; Wang, W.; Ding, B.; Han, J.; Mou, C.; Gao, X.; Liu, J. TriNet: A Tri-Fusion Neural Network for the Prediction of Anticancer and Antimicrobial Peptides. *Patterns* **2023**, *4* (3). https://doi.org/10.1016/j.patter.2023.100702.

(60) Sun, T.-J.; Bu, H.-L.; Yan, X.; Sun, Z.-H.; Zha, M.-S.; Dong, G.-F. LABAMPsGCN: A Framework for Identifying Lactic Acid Bacteria Antimicrobial Peptides Based on Graph Convolutional Neural Network. *Front. Genet.* **2022**, *13*. https://doi.org/10.3389/fgene.2022.1062576.

(61) Witten, J.; Witten, Z. Deep Learning Regression Model for Antimicrobial Peptide Design. bioRxiv July 12, 2019, p 692681. https://doi.org/10.1101/692681.

(62) Yan, J.; Bhadra, P.; Li, A.; Sethiya, P.; Qin, L.; Tai, H. K.; Wong, K. H.; Siu, S. W. I. Deep-AmPEP30: Improve Short Antimicrobial Peptides Prediction with Deep Learning. *Mol. Ther. Nucleic Acids* **2020**, *20*, 882–894. https://doi.org/10.1016/j.omtn.2020.05.006.

(63) Mienye, I. D.; Swart, T. G.; Obaido, G. Recurrent Neural Networks: A Comprehensive Review of Architectures, Variants, and Applications. *Information* **2024**, *15* (9), 517. https://doi.org/10.3390/info15090517.

(64) Sherstinsky, A. Fundamentals of Recurrent Neural Network (RNN) and Long Short-Term Memory (LSTM) Network. *Phys. Nonlinear Phenom.* **2020**, *404*, 132306. https://doi.org/10.1016/j.physd.2019.132306.

(65) Pascanu, R.; Mikolov, T.; Bengio, Y. On the Difficulty of Training Recurrent Neural Networks. arXiv February 16, 2013. https://doi.org/10.48550/arXiv.1211.5063.

(66) Hamid, M.-N.; Friedberg, I. Identifying Antimicrobial Peptides Using Word Embedding with Deep Recurrent Neural Networks. *Bioinformatics* **2019**, *35* (12), 2009–2016. https://doi.org/10.1093/bioinformatics/bty937.

(67) Capecchi, A.; Cai, X.; Personne, H.; Köhler, T.; Delden, C. van; Reymond, J.-L. Machine Learning Designs Non-Hemolytic Antimicrobial Peptides. *Chem. Sci.* **2021**, *12* (26), 9221–9232. https://doi.org/10.1039/D1SC01713F.

(68) Bolatchiev, A.; Baturin, V.; Shchetinin, E.; Bolatchieva, E. Novel Antimicrobial Peptides Designed Using a Recurrent Neural Network

Reduce Mortality in Experimental Sepsis. *Antibiotics* **2022**, *11* (3), 411. https://doi.org/10.3390/antibiotics11030411.

(69) Wang, C.; Garlick, S.; Zloh, M. Deep Learning for Novel Antimicrobial Peptide Design. *Biomolecules* **2021**, *11* (3), 471. https://doi.org/10.3390/biom11030471.

(70) Wang, C.; Garlick, S.; Zloh, M. Deep Learning for Novel Antimicrobial Peptide Design. *Biomolecules* **2021**, *11* (3), 471. https://doi.org/10.3390/biom11030471.

(71) Kingma, D. P.; Welling, M. Auto-Encoding Variational Bayes. arXiv December 10, 2022. https://doi.org/10.48550/arXiv.1312.6114.

(72) Shlens, J. Notes on Kullback-Leibler Divergence and Likelihood. arXiv April 8, 2014. https://doi.org/10.48550/arXiv.1404.2000.

(73) Hou, X.; Shen, L.; Sun, K.; Qiu, G. Deep Feature Consistent Variational Autoencoder: 17th IEEE Winter Conference on Applications of Computer Vision, WACV 2017. *Proc. - 2017 IEEE Winter Conf. Appl. Comput. Vis. WACV 2017* **2017**, 1133–1141. https://doi.org/10.1109/WACV.2017.131.

(74) Bowman, S. R.; Vilnis, L.; Vinyals, O.; Dai, A.; Jozefowicz, R.; Bengio, S. Generating Sentences from a Continuous Space. In *Proceedings of the 20th SIGNLL Conference on Computational Natural Language Learning*; Riezler, S., Goldberg, Y., Eds.; Association for Computational Linguistics: Berlin, Germany, 2016; pp 10–21. https://doi.org/10.18653/v1/K16-1002.

(75) Lopez, R.; Regier, J.; Cole, M. B.; Jordan, M. I.; Yosef, N. Deep Generative Modeling for Single-Cell Transcriptomics. *Nat. Methods* **2018**, *15* (12), 1053–1058. https://doi.org/10.1038/s41592-018-0229-2.

(76) Dean, S. N.; Walper, S. A. Variational Autoencoder for Generation of Antimicrobial Peptides. *ACS Omega* **2020**, *5* (33), 20746–20754. https://doi.org/10.1021/acsomega.0c00442.

(77) Xu, Y.; Zhang, S.; Zhu, F.; Liang, Y. A Deep Learning Model for Anti-Inflammatory Peptides Identification Based on Deep Variational Autoencoder and Contrastive Learning. *Sci. Rep.* **2024**, *14* (1), 18451. https://doi.org/10.1038/s41598-024-69419-y.

(78) Renaud, S.; Mansbach, R. A. Latent Spaces for Antimicrobial Peptide Design. *Digit. Discov.* **2023**, *2* (2), 441–458. https://doi.org/10.1039/D2DD00091A.

(79) Goodfellow, I. J.; Pouget-Abadie, J.; Mirza, M.; Xu, B.; Warde-Farley, D.; Ozair, S.; Courville, A.; Bengio, Y. Generative Adversarial

Networks. arXiv June 10, 2014. https://doi.org/10.48550/arXiv.1406.2661.

(80) Tucs, A.; Tran, D. P.; Yumoto, A.; Ito, Y.; Uzawa, T.; Tsuda, K. Generating Ampicillin-Level Antimicrobial Peptides with Activity-Aware Generative Adversarial Networks. *ACS Omega* **2020**, *5* (36), 22847–22851. https://doi.org/10.1021/acsomega.0c02088.

(81) Lin, T.-T.; Yang, L.-Y.; Lin, C.-Y.; Wang, C.-T.; Lai, C.-W.; Ko, C.-F.; Shih, Y.-H.; Chen, S.-H. Intelligent De Novo Design of Novel Antimicrobial Peptides against Antibiotic-Resistant Bacteria Strains. *Int. J. Mol. Sci.* **2023**, *24* (7), 6788. https://doi.org/10.3390/ijms24076788.

(82) Lin, T.-T.; Yang, L.-Y.; Wang, C.-T.; Lai, G.-W.; Ko, C.-F.; Shih, Y.-H.; Chen, S.-H.; Lin, C.-Y. Discovering Novel Antimicrobial Peptides in Generative Adversarial Network. bioRxiv November 23, 2021, p 2021.11.22.469634. https://doi.org/10.1101/2021.11.22.469634.

(83) Van Oort, C. M.; Ferrell, J. B.; Remington, J. M.; Wshah, S.; Li, J. AMPGAN v2: Machine Learning-Guided Design of Antimicrobial Peptides. *J. Chem. Inf. Model.* **2021**, *61* (5), 2198–2207. https://doi.org/10.1021/acs.jcim.0c01441.

(84) Vaswani, A.; Shazeer, N.; Parmar, N.; Uszkoreit, J.; Jones, L.; Gomez, A. N.; Kaiser, L.; Polosukhin, I. Attention Is All You Need. arXiv August 2, 2023. https://doi.org/10.48550/arXiv.1706.03762.

(85) Vaswani, A.; Shazeer, N.; Parmar, N.; Uszkoreit, J.; Jones, L.; Gomez, A. N.; Kaiser, L.; Polosukhin, I. Attention Is All You Need. arXiv August 2, 2023. http://arxiv.org/abs/1706.03762 (accessed 2024-10-27).

(86) Ferruz, N.; Schmidt, S.; Höcker, B. ProtGPT2 Is a Deep Unsupervised Language Model for Protein Design. *Nat. Commun.* **2022**, *13* (1), 4348. https://doi.org/10.1038/s41467-022-32007-7.

(87) Nijkamp, E.; Ruffolo, J. A.; Weinstein, E. N.; Naik, N.; Madani, A. ProGen2: Exploring the Boundaries of Protein Language Models. *Cell Syst.* **2023**, *14* (11), 968-978.e3. https://doi.org/10.1016/j.cels.2023.10.002.

(88) Elnaggar, A.; Heinzinger, M.; Dallago, C.; Rihawi, G.; Wang, Y.; Jones, L.; Gibbs, T.; Feher, T.; Angerer, C.; Steinegger, M.; Bhowmik, D.; Rost, B. ProtTrans: Towards Cracking the Language of Life's Code Through Self-Supervised Deep Learning and High Performance Computing. arXiv May 4, 2021. https://doi.org/10.48550/arXiv.2007.06225.

(89) Pang, Y.; Yao, L.; Xu, J.; Wang, Z.; Lee, T.-Y. Integrating Transformer and Imbalanced Multi-Label Learning to Identify Antimicrobial Peptides and Their Functional Activities. *Bioinformatics* **2022**, *38* (24), 5368–5374. https://doi.org/10.1093/bioinformatics/btac711.

(90) Salem, M.; Keshavarzi Arshadi, A.; Yuan, J. S. AMPDeep: Hemolytic Activity Prediction of Antimicrobial Peptides Using Transfer Learning. *BMC Bioinformatics* **2022**, *23* (1), 389. https://doi.org/10.1186/s12859-022-04952-z.

(91) Wang, J.; Feng, J.; Kang, Y.; Pan, P.; Ge, J.; Wang, Y.; Wang, M.; Wu, Z.; Zhang, X.; Yu, J.; Zhang, X.; Wang, T.; Wen, L.; Yan, G.; Deng, Y.; Shi, H.; Hsieh, C.-Y.; Jiang, Z.; Hou, T. A Foundation Model Approach to Guide Antimicrobial Peptide Design in the Era of Artificial Intelligence Driven Scientific Discovery. arXiv July 17, 2024. https://doi.org/10.48550/arXiv.2407.12296.

(92) Yu, Y.; Si, X.; Hu, C.; Zhang, J. A Review of Recurrent Neural Networks: LSTM Cells and Network Architectures. *Neural Comput.* **2019**, *31* (7), 1235–1270. https://doi.org/10.1162/neco_a_01199.

(93) Szymczak, P.; Możejko, M.; Grzegorzek, T.; Jurczak, R.; Bauer, M.; Neubauer, D.; Sikora, K.; Michalski, M.; Sroka, J.; Setny, P.; Kamysz, W.; Szczurek, E. Discovering Highly Potent Antimicrobial Peptides with Deep Generative Model HydrAMP. *Nat. Commun.* **2023**, *14* (1), 1453. https://doi.org/10.1038/s41467-023-36994-z.

(94) Zervou, M. A.; Doutsi, E.; Pantazis, Y.; Tsakalides, P. De Novo Antimicrobial Peptide Design with Feedback Generative Adversarial Networks. *Int. J. Mol. Sci.* **2024**, *25* (10), 5506. https://doi.org/10.3390/ijms25105506.

(95) Szymczak, P.; Mo, M.; Michalski, M.; Sroka, J.; Setny, P.; Kamysz, W.; Szczurek, E. HydrAMP: A Deep Generative Model for Antimicrobial Peptide Discovery.

(96) Liu, G.-Y.; Yu, D.; Fan, M.-M.; Zhang, X.; Jin, Z.-Y.; Tang, C.; Liu, X.-F. Antimicrobial Resistance Crisis: Could Artificial Intelligence Be the Solution? *Mil. Med. Res.* **2024**, *11* (1), 7. https://doi.org/10.1186/s40779-024-00510-1.

(97) Li, C.; Sutherland, D.; Hammond, S. A.; Yang, C.; Taho, F.; Bergman, L.; Houston, S.; Warren, R. L.; Wong, T.; Hoang, L. M. N.; Cameron, C. E.; Helbing, C. C.; Birol, I. AMPlify: Attentive Deep Learning Model for Discovery of Novel Antimicrobial Peptides Effective against WHO Priority Pathogens. *BMC Genomics* **2022**, *23* (1), 77. https://doi.org/10.1186/s12864-022-08310-4.

(98) Li, C.; Warren, R. L.; Birol, I. Models and Data of AMPlify: A Deep Learning Tool for Antimicrobial Peptide Prediction. *BMC Res. Notes* **2023**, *16* (1), 11. https://doi.org/10.1186/s13104-023-06279-1.

(99) Zhao, M.; Zhang, Y.; Wang, M.; Ma, L. Z. dsAMP and dsAMPGAN: Deep Learning Networks for Antimicrobial Peptides Recognition and Generation. *Antibiotics* **2024**, *13* (10), 948. https://doi.org/10.3390/antibiotics13100948.

(100) Das, P.; Wadhawan, K.; Chang, O.; Sercu, T.; Santos, C. D.; Riemer, M.; Chenthamarakshan, V.; Padhi, I.; Mojsilovic, A. PepCVAE: Semi-Supervised Targeted Design of Antimicrobial Peptide Sequences. arXiv November 13, 2018. https://doi.org/10.48550/arXiv.1810.07743.

(101) Das, P.; Sercu, T.; Wadhawan, K.; Padhi, I.; Gehrmann, S.; Cipcigan, F.; Chenthamarakshan, V.; Strobelt, H.; dos Santos, C.; Chen, P.-Y.; Yang, Y. Y.; Tan, J. P. K.; Hedrick, J.; Crain, J.; Mojsilovic, A. Accelerated Antimicrobial Discovery via Deep Generative Models and Molecular Dynamics Simulations. *Nat. Biomed. Eng.* **2021**, *5* (6), 613–623. https://doi.org/10.1038/s41551-021-00689-x.

(102) Boone, K.; Wisdom, C.; Camarda, K.; Spencer, P.; Tamerler, C. Combining Genetic Algorithm with Machine Learning Strategies for Designing Potent Antimicrobial Peptides. *BMC Bioinformatics* **2021**, *22* (1), 239. https://doi.org/10.1186/s12859-021-04156-x.

(103) Zhong, G.; Liu, H.; Deng, L. Ensemble Machine Learning and Predicted Properties Promote Antimicrobial Peptide Identification. *Interdiscip. Sci. Comput. Life Sci.* **2024**, *16* (4), 951–965. https://doi.org/10.1007/s12539-024-00640-z.

(104) Jing, W.; Demcoe, A. R.; Vogel, H. J. Conformation of a Bactericidal Domain of Puroindoline a: Structure and Mechanism of Action of a 13-Residue Antimicrobial Peptide. *J. Bacteriol.* **2003**, *185* (16), 4938–4947. https://doi.org/10.1128/jb.185.16.4938-4947.2003.

(105) Chan, D. I.; Prenner, E. J.; Vogel, H. J. Tryptophan- and Arginine-Rich Antimicrobial Peptides: Structures and Mechanisms of Action. *Biochim. Biophys. Acta* **2006**, *1758* (9), 1184–1202. https://doi.org/10.1016/j.bbamem.2006.04.006.

(106) Zhu, Y.; Akhtar, M. U.; Li, B.; Chou, S.; Shao, C.; Li, J.; Shan, A. The Design of Cell-Selective Tryptophan and Arginine-Rich Antimicrobial Peptides by Introducing Hydrophilic Uncharged Residues. *Acta Biomater.* **2022**, *153*, 557–572. https://doi.org/10.1016/j.actbio.2022.09.028.

(107) Clark, S.; Jowitt, T. A.; Harris, L. K.; Knight, C. G.; Dobson, C. B. The Lexicon of Antimicrobial Peptides: A Complete Set of Arginine and Tryptophan Sequences. *Commun. Biol.* **2021**, *4* (1), 1–14. https://doi.org/10.1038/s42003-021-02137-7.

(108) Ekmekci, B.; McAnany, C. E.; Mura, C. An Introduction to Programming for Bioscientists: A Python-Based Primer. *PLOS Comput. Biol.* **2016**, *12* (6), e1004867. https://doi.org/10.1371/journal.pcbi.1004867.

(109) De Sanctis, G.; Spinelli, M.; Vanoni, M.; Sacco, E. K-Ras Activation Induces Differential Sensitivity to Sulfur Amino Acid Limitation and Deprivation and to Oxidative and Anti-Oxidative Stress in Mouse Fibroblasts. *PLoS ONE* **2016**, *11* (9), e0163790. https://doi.org/10.1371/journal.pone.0163790.

(110) Varnava, K. G.; Sarojini, V. Making Solid-Phase Peptide Synthesis Greener: A Review of the Literature. *Chem. – Asian J.* **2019**, *14* (8), 1088–1097. https://doi.org/10.1002/asia.201801807.

(111) Sowińska, M.; Szeliga, M.; Morawiak, M.; Zabłocka, B.; Urbanczyk-Lipkowska, Z. Design, Synthesis and Activity of New N1-Alkyl Tryptophan Functionalized Dendrimeric Peptides against Glioblastoma. *Biomolecules* **2022**, *12* (8), 1116. https://doi.org/10.3390/biom12081116.

(112) Mueller, L. K.; Baumruck, A. C.; Zhdanova, H.; Tietze, A. A. Challenges and Perspectives in Chemical Synthesis of Highly Hydrophobic Peptides. *Front. Bioeng. Biotechnol.* **2020**, *8*. https://doi.org/10.3389/fbioe.2020.00162.

(113) Nguyen, L. T.; Haney, E. F.; Vogel, H. J. The Expanding Scope of Antimicrobial Peptide Structures and Their Modes of Action. *Trends Biotechnol.* **2011**, *29* (9), 464–472. https://doi.org/10.1016/j.tibtech.2011.05.001.

(114) Jiang, Z.; Vasil, A. I.; Hale, J. D.; Hancock, R. E. W.; Vasil, M. L.; Hodges, R. S. Effects of Net Charge and the Number of Positively Charged Residues on the Biological Activity of Amphipathic Alpha-Helical Cationic Antimicrobial Peptides. *Biopolymers* **2008**, *90* (3), 369–383. https://doi.org/10.1002/bip.20911.

(115) Phuong, H. B. T.; Tran, V. A.; Ngoc, K. N.; Huu, V. N.; Thu, H. N.; Van, M. C.; Thi, H. P.; Hong, M. N.; Tran, H. T.; Xuan, H. L. Effect of Substituting Glutamine with Lysine on Structural and Biological Properties of Antimicrobial Peptide Polybia-MP1. *Amino Acids* **2023**, *55* (7), 881–890. https://doi.org/10.1007/s00726-023-03276-3.

(116) Mwangi, J.; Kamau, P. M.; Thuku, R. C.; Lai, R. Design Methods for Antimicrobial Peptides with Improved Performance. *Zool. Res.* **2023**, *44* (6), 1095–1114. https://doi.org/10.24272/j.issn.2095-8137.2023.246.

(117) Fernando, J. C.; Batucan, J. D.; Peran, J. E.; Salvador-Reyes, L. A.; Villaraza, A. J. L. The Wheel of Fortune: Helical Wheel Alanine Scanning of a Spider Venom Antimicrobial Peptide Reveals Residues Involved in Antimicrobial and Cytotoxic Activity. *ChemMedChem* **2024**, *19* (23), e202400488. https://doi.org/10.1002/cmdc.202400488.

(118) Purwin, M.; Bruzgo, I.; Markowska, A.; Midura-Nowaczek, K. Short Peptides Containing L-Lysine and Epsilon-Aminocaproic Acid as Potential Plasmin Inhibitors. *Pharm.* **2009**, *64* (11), 765–767.

(119) Kowalska-Krochmal, B.; Dudek-Wicher, R. The Minimum Inhibitory Concentration of Antibiotics: Methods, Interpretation, Clinical Relevance. *Pathogens* **2021**, *10* (2), 165. https://doi.org/10.3390/pathogens10020165.

(120) Daffé, M.; Marrakchi, H. Unraveling the Structure of the Mycobacterial Envelope. *Microbiol. Spectr.* **2019**, *7* (4), 10.1128/microbiolspec.gpp3-0027–2018. https://doi.org/10.1128/microbiolspec.gpp3-0027-2018.

(121) Ladokhin, A. S.; Jayasinghe, S.; White, S. H. How to Measure and Analyze Tryptophan Fluorescence in Membranes Properly, and Why Bother? *Anal. Biochem.* **2000**, *285* (2), 235–245. https://doi.org/10.1006/abio.2000.4773.

(122) Teixeira, V.; Feio, M. J.; Rivas, L.; De la Torre, B. G.; Andreu, D.; Coutinho, A.; Bastos, M. Influence of Lysine Nε-Trimethylation and Lipid Composition on the Membrane Activity of the Cecropin A-Melittin Hybrid Peptide CA(1−7)M(2−9). *J. Phys. Chem. B* **2010**, *114* (49), 16198–16208. https://doi.org/10.1021/jp106915c.

(123) *Principles of Fluorescence Spectroscopy*; Lakowicz, J. R., Ed.; Springer US: Boston, MA, 2006. https://doi.org/10.1007/978-0-387-46312-4.

(124) Grishina, I. B.; Woody, R. W. Contributions of Tryptophan Side Chains to the Circular Dichroism of Globular Proteins: Exciton Couplets and Coupled Oscillators. *Faraday Discuss.* **1994**, No. 99, 245–262. https://doi.org/10.1039/fd9949900245.

(125) Woody, R. W. Contributions of Tryptophan Side Chains to the Far-Ultraviolet Circular Dichroism of Proteins. *Eur. Biophys. J. EBJ* **1994**, *23* (4), 253–262. https://doi.org/10.1007/BF00213575.

(126) Bozelli, J. C.; Yune, J.; Dang, X.; Narayana, J. L.; Wang, G.; Epand, R. M. Membrane Activity of Two Short Trp-Rich Amphipathic Peptides. *Biochim. Biophys. Acta BBA - Biomembr.* **2020**, *1862* (7), 183280. https://doi.org/10.1016/j.bbamem.2020.183280.

(127) Oliva, R.; Chino, M.; Lombardi, A.; Nastri, F.; Notomista, E.; Petraccone, L.; Del Vecchio, P. Similarities and Differences for Membranotropic Action of Three Unnatural Antimicrobial Peptides. *J. Pept. Sci.* **2020**, *26* (8), e3270. https://doi.org/10.1002/psc.3270.

(128) Rozek, A.; Powers, J.-P. S.; Friedrich, C. L.; Hancock, R. E. W. Structure-Based Design of an Indolicidin Peptide Analogue with Increased Protease Stability,. *Biochemistry* **2003**, *42* (48), 14130–14138. https://doi.org/10.1021/bi035643g.

(129) Nagpal, S.; Gupta, V.; Kaur, K. J.; Salunke, D. M. Structure-Function Analysis of Tritrypticin, an Antibacterial Peptide of Innate Immune Origin *. *J. Biol. Chem.* **1999**, *274* (33), 23296–23304. https://doi.org/10.1074/jbc.274.33.23296.

(130) Ladokhin, A. S.; Selsted, M. E.; White, S. H. CD Spectra of Indolicidin Antimicrobial Peptides Suggest Turns, Not Polyproline Helix. *Biochemistry* **1999**, *38* (38), 12313–12319. https://doi.org/10.1021/bi9907936.

(131) Epand, R. M.; Vogel, H. J. Diversity of Antimicrobial Peptides and Their Mechanisms of Action. *Biochim. Biophys. Acta BBA - Biomembr.* **1999**, *1462* (1), 11–28. https://doi.org/10.1016/S0005-2736(99)00198-4.

(132) Pozo Navas, B.; Lohner, K.; Deutsch, G.; Sevcsik, E.; Riske, K. A.; Dimova, R.; Garidel, P.; Pabst, G. Composition Dependence of Vesicle Morphology and Mixing Properties in a Bacterial Model Membrane System. *Biochim. Biophys. Acta* **2005**, *1716* (1), 40–48. https://doi.org/10.1016/j.bbamem.2005.08.003.

(133) Oliva, R.; Vecchio, P. D.; Grimaldi, A.; Notomista, E.; Cafaro, V.; Pane, K.; Schuabb, V.; Winter, R.; Petraccone, L. Membrane Disintegration by the Antimicrobial Peptide (P)GKY20: Lipid Segregation and Domain Formation. *Phys. Chem. Chem. Phys.* **2019**, *21* (7), 3989–3998. https://doi.org/10.1039/C8CP06280C.

(134) Joanne, P.; Galanth, C.; Goasdoué, N.; Nicolas, P.; Sagan, S.; Lavielle, S.; Chassaing, G.; El Amri, C.; Alves, I. D. Lipid Reorganization Induced by Membrane-Active Peptides Probed Using Differential Scanning Calorimetry. *Biochim. Biophys. Acta* **2009**, *1788* (9), 1772–1781. https://doi.org/10.1016/j.bbamem.2009.05.001.

(135) Epand, R. M. Detecting the Presence of Membrane Domains Using DSC. *Biophys. Chem.* **2007**, *126* (1–3), 197–200. https://doi.org/10.1016/j.bpc.2006.05.008.
(136) McElhaney, R. N. Differential Scanning Calorimetric Studies of Lipid-Protein Interactions in Model Membrane Systems. *Biochim. Biophys. Acta* **1986**, *864* (3–4), 361–421. https://doi.org/10.1016/0304-4157(86)90004-3.
(137) Parasassi, T.; De Stasio, G.; Ravagnan, G.; Rusch, R. M.; Gratton, E. Quantitation of Lipid Phases in Phospholipid Vesicles by the Generalized Polarization of Laurdan Fluorescence. *Biophys. J.* **1991**, *60* (1), 179–189. https://doi.org/10.1016/S0006-3495(91)82041-0.
(138) Gironi, B.; Oliva, R.; Petraccone, L.; Paolantoni, M.; Morresi, A.; Del Vecchio, P.; Sassi, P. Solvation Properties of Raft-like Model Membranes. *Biochim. Biophys. Acta BBA - Biomembr.* **2019**, *1861* (11), 183052. https://doi.org/10.1016/j.bbamem.2019.183052.
(139) Oliva, R.; Vecchio, P. D.; Grimaldi, A.; Notomista, E.; Cafaro, V.; Pane, K.; Schuabb, V.; Winter, R.; Petraccone, L. Membrane Disintegration by the Antimicrobial Peptide (P)GKY20: Lipid Segregation and Domain Formation. *Phys. Chem. Chem. Phys.* **2019**, *21* (7), 3989–3998. https://doi.org/10.1039/C8CP06280C.
(140) Oliva, R.; Chino, M.; Pane, K.; Pistorio, V.; De Santis, A.; Pizzo, E.; D'Errico, G.; Pavone, V.; Lombardi, A.; Del Vecchio, P.; Notomista, E.; Nastri, F.; Petraccone, L. Exploring the Role of Unnatural Amino Acids in Antimicrobial Peptides. *Sci. Rep.* **2018**, *8* (1), 8888. https://doi.org/10.1038/s41598-018-27231-5.
(141) Mahanta, U.; Khandelwal, M.; Deshpande, A. S. Antimicrobial Surfaces: A Review of Synthetic Approaches, Applicability and Outlook. *J. Mater. Sci.* **2021**, *56* (32), 17915–17941. https://doi.org/10.1007/s10853-021-06404-0.
(142) Harnessing the Potential of Antimicrobial Peptides: Current Advances and Future Applications. *J. Bacteriol. Mycol. Open Access* **2024**, *Volume 12* (Issue 1). https://doi.org/10.15406/jbmoa.2024.12.00369.
(143) Xu, S.; Tan, P.; Tang, Q.; Wang, T.; Ding, Y.; Fu, H.; Zhang, Y.; Zhou, C.; Song, M.; Tang, Q.; Sun, Z.; Ma, X. Enhancing the Stability of Antimicrobial Peptides: From Design Strategies to Applications. *Chem. Eng. J.* **2023**, *475*, 145923. https://doi.org/10.1016/j.cej.2023.145923.
(144) *Antimicrobial peptides (AMPs): A promising class of antimicrobial compounds | Journal of Applied Microbiology | Oxford Academic*.

https://academic.oup.com/jambio/article/132/3/1573/6988795?login=true#no-access-message#no-access-message (accessed 2024-12-12).

(145) Alves, D.; Olívia Pereira, M. Mini-Review: Antimicrobial Peptides and Enzymes as Promising Candidates to Functionalize Biomaterial Surfaces. *Biofouling* **2014**, *30* (4), 483–499. https://doi.org/10.1080/08927014.2014.889120.

(146) Browne, K.; Chakraborty, S.; Chen, R.; Willcox, M. D.; Black, D. S.; Walsh, W. R.; Kumar, N. A New Era of Antibiotics: The Clinical Potential of Antimicrobial Peptides. *Int. J. Mol. Sci.* **2020**, *21* (19), 7047. https://doi.org/10.3390/ijms21197047.

(147) Nicolas, M.; Beito, B.; Oliveira, M.; Tudela Martins, M.; Gallas, B.; Salmain, M.; Boujday, S.; Humblot, V. Strategies for Antimicrobial Peptides Immobilization on Surfaces to Prevent Biofilm Growth on Biomedical Devices. *Antibiotics* **2022**, *11* (1), 13. https://doi.org/10.3390/antibiotics11010013.

(148) Nasseri, S.; Sharifi, M. Therapeutic Potential of Antimicrobial Peptides for Wound Healing. *Int. J. Pept. Res. Ther.* **2022**, *28* (1), 38. https://doi.org/10.1007/s10989-021-10350-5.

(149) Negut, I.; Bita, B.; Groza, A. Polymeric Coatings and Antimicrobial Peptides as Efficient Systems for Treating Implantable Medical Devices Associated-Infections. *Polymers* **2022**, *14* (8), 1611. https://doi.org/10.3390/polym14081611.

(150) Costa, F.; Carvalho, I. F.; Montelaro, R. C.; Gomes, P.; Martins, M. C. L. Covalent Immobilization of Antimicrobial Peptides (AMPs) onto Biomaterial Surfaces. *Acta Biomater.* **2011**, *7* (4), 1431–1440. https://doi.org/10.1016/j.actbio.2010.11.005.

(151) Vodnar, D. C.; Pop, O. L.; Dulf, F. V.; Socaciu, C. Antimicrobial Efficiency of Edible Films in Food Industry. *Not. Bot. Horti Agrobot. Cluj-Napoca* **2015**, *43* (2), 302–312. https://doi.org/10.15835/nbha43210048.

(152) Álvarez, K.; Alvarez, V. A.; Gutiérrez, T. J. Biopolymer Composite Materials with Antimicrobial Effects Applied to the Food Industry. In *Functional Biopolymers*; Thakur, V. K., Thakur, M. K., Eds.; Springer International Publishing: Cham, 2018; pp 57–96. https://doi.org/10.1007/978-3-319-66417-0_3.

(153) Liu, Y.; Sameen, D. E.; Ahmed, S.; Dai, J.; Qin, W. Antimicrobial Peptides and Their Application in Food Packaging. *Trends Food Sci. Technol.* **2021**, *112*, 471–483. https://doi.org/10.1016/j.tifs.2021.04.019.

(154) Ongey, E. L.; Pflugmacher, S.; Neubauer, P. Bioinspired Designs, Molecular Premise and Tools for Evaluating the Ecological Importance of Antimicrobial Peptides. *Pharmaceuticals* **2018**, *11* (3), 68. https://doi.org/10.3390/ph11030068.
(155) Cherenack, K.; van Pieterson, L. Smart Textiles: Challenges and Opportunities. *J. Appl. Phys.* **2012**, *112* (9), 091301. https://doi.org/10.1063/1.4742728.
(156) Goddard, J. M.; Hotchkiss, J. H. Polymer Surface Modification for the Attachment of Bioactive Compounds. *Prog. Polym. Sci.* **2007**, *32* (7), 698–725. https://doi.org/10.1016/j.progpolymsci.2007.04.002.
(157) Avinash, D.; Bisht, A.; Kumar, M.; Thakur, S.; Patel, P.; Kurmi, B. D. Empowering Antimicrobial Peptides: Harnessing Nanotechnology and Engineering Strategies to Combat Microbial Resistance. *Pept. Sci. n/a* (n/a), e24376. https://doi.org/10.1002/pep2.24376.
(158) Kumar, P.; Kizhakkedathu, J. N.; Straus, S. K. Antimicrobial Peptides: Diversity, Mechanism of Action and Strategies to Improve the Activity and Biocompatibility In Vivo. *Biomolecules* **2018**, *8* (1), 4. https://doi.org/10.3390/biom8010004.
(159) Singh, A.; Sharma, J. J.; Mohanta, B.; Sood, A.; Han, S. S.; Sharma, A. Synthetic and Biopolymers-Based Antimicrobial Hybrid Hydrogels: A Focused Review. *J. Biomater. Sci. Polym. Ed.* **2024**, *35* (5), 675–716. https://doi.org/10.1080/09205063.2023.2278814.
(160) Asokan-Sheeja, H.; Awad, K.; Xu, J.; Le, M.; Nguyen, J. N.; Nguyen, N.; Nguyen, T. P.; Nguyen, K. T.; Hong, Y.; Varanasi, V. G.; Liu, X.; Dong, H. In Situ Synthesis and Self-Assembly of Peptide-PEG Conjugates: A Facile Method for the Construction of Fibrous Hydrogels. *Biomacromolecules* **2024**, *25* (5), 2814–2822. https://doi.org/10.1021/acs.biomac.3c01450.
(161) Blomstrand, E.; Rajasekharan, A. K.; Atefyekta, S.; Andersson, M. Cross-Linked Lyotropic Liquid Crystal Particles Functionalized with Antimicrobial Peptides. *Int. J. Pharm.* **2022**, *627*, 122215. https://doi.org/10.1016/j.ijpharm.2022.122215.
(162) Shiba, K. Programmable Bio-Surfaces for Biomedical Applications. In *Peptides and Peptide-based Biomaterials and their Biomedical Applications*; Sunna, A., Care, A., Bergquist, P. L., Eds.; Springer International Publishing: Cham, 2017; pp 1–20. https://doi.org/10.1007/978-3-319-66095-0_1.
(163) Qi, S.; Kiratzis, I.; Adoni, P.; Tuekprakhon, A.; Hill, H. J.; Stamataki, Z.; Nabi, A.; Waugh, D.; Rodriguez, J. R.; Clarke, S. M.; Fryer, P. J.; Zhang, Z. J. Porous Cellulose Thin Films as Sustainable and Effective

Antimicrobial Surface Coatings. *ACS Appl. Mater. Interfaces* **2023**, *15* (17), 20638–20648. https://doi.org/10.1021/acsami.2c23251.

(164) Akshaya, S.; Rowlo, P. K.; Dukle, A.; Nathanael, A. J. Antibacterial Coatings for Titanium Implants: Recent Trends and Future Perspectives. *Antibiotics* **2022**, *11* (12), 1719. https://doi.org/10.3390/antibiotics11121719.

(165) Corrales-Ureña, Y. R.; Souza-Schiaber, Z.; Lisboa-Filho, P. N.; Marquenet, F.; Noeske, P.-L. M.; Gätjen, L.; Rischka, K. Functionalization of Hydrophobic Surfaces with Antimicrobial Peptides Immobilized on a Bio-Interfactant Layer. *RSC Adv.* **2020**, *10* (1), 376. https://doi.org/10.1039/c9ra07380a.

(166) *Bottom-up strategies for the synthesis of peptide-based polymers - ScienceDirect*. https://www.sciencedirect.com/science/article/pii/S007967002100024 1 (accessed 2024-10-31).

(167) Soyhan, I.; Polat, T.; Mozioglu, E.; Ildenız, T. A. O.; Elmas, M. A.; Cebeci, S.; Unubol, N.; Gok, O. Effective Immobilization of Novel Antimicrobial Peptides via Conjugation onto Activated Silicon Catheter Surfaces. *Pharmaceutics* **2024**, *16* (8), 1045. https://doi.org/10.3390/pharmaceutics16081045.

(168) Boden, A.; Dart, A.; Liao, T.-Y.; Zhu, D. M.; Bhave, M.; Cipolla, L.; Kingshott, P. Enhancing the Activity of Surface Immobilized Antimicrobial Peptides Using Thiol-Mediated Tethering to Poly(Ethylene Glycol). *Macromol. Biosci.* **2023**, *23* (9), e2200411. https://doi.org/10.1002/mabi.202200411.

(169) Loschonsky, S.; Couet, J.; Biesalski, M. Synthesis of Peptide/Polymer Conjugates by Solution ATRP of Butylacrylate Using an Initiator-Modified Cyclic D-Alt-L-Peptide. *Macromol. Rapid Commun.* **2008**, *29* (4), 309–315. https://doi.org/10.1002/marc.200700700.

(170) Mei, Y.; Beers, K. L.; Byrd, H. C. M.; VanderHart, D. L.; Washburn, N. R. Solid-Phase ATRP Synthesis of Peptide−Polymer Hybrids. *J. Am. Chem. Soc.* **2004**, *126* (11), 3472–3476. https://doi.org/10.1021/ja039583d.

(171) Jebors, S.; Pinese, C.; Montheil, T.; Bethry, A.; Verquin, S.; Plais, L.; Moulin, M.; Dupont, C.; Garric, X.; Mehdi, A.; Martinez, J.; Subra, G. Turning Peptides into Bioactive Nylons. *Eur. Polym. J.* **2020**, *135*, 109886. https://doi.org/10.1016/j.eurpolymj.2020.109886.

(172) Zhang, F.; Fan, J.; Wang, S. Interfacial Polymerization: From Chemistry to Functional Materials. *Angew. Chem. Int. Ed.* **2020**, *59* (49), 21840–21856. https://doi.org/10.1002/anie.201916473.

(173) Foster, J. C.; Varlas, S.; Couturaud, B.; Coe, Z.; O'Reilly, R. K. Getting into Shape: Reflections on a New Generation of Cylindrical Nanostructures' Self-Assembly Using Polymer Building Blocks. *J. Am. Chem. Soc.* **2019**, *141* (7), 2742–2753. https://doi.org/10.1021/jacs.8b08648.

(174) Johana Bolívar-Monsalve, E.; Moisés Alvarez, M.; Hosseini, S.; Alejandra Espinosa-Hernandez, M.; Fernando Ceballos-González, C.; Sanchez-Dominguez, M.; Ryon Shin, S.; Cecen, B.; Hassan, S.; Maio, E. D.; Santiago, G. T. Engineering Bioactive Synthetic Polymers for Biomedical Applications: A Review with Emphasis on Tissue Engineering and Controlled Release. *Mater. Adv.* **2021**, *2* (14), 4447–4478. https://doi.org/10.1039/D1MA00092F.

(175) P. Silva, A. R.; S. Guimarães, M.; Rabelo, J.; Herrera Belén, L.; José Perecin, C.; G Farías, J.; M. Santos, J. H. P.; O. Rangel-Yagui, C. Recent Advances in the Design of Antimicrobial Peptide Conjugates. *J. Mater. Chem. B* **2022**, *10* (19), 3587–3600. https://doi.org/10.1039/D1TB02757C.

(176) Glinel, K.; Thebault, P.; Humblot, V.; Pradier, C. M.; Jouenne, T. Antibacterial Surfaces Developed from Bio-Inspired Approaches. *Acta Biomater.* **2012**, *8* (5), 1670–1684. https://doi.org/10.1016/j.actbio.2012.01.011.

(177) Wang, Y.; Wei, G. Recent Trends in Polymer Membranes: Fabrication Technique, Characterization, Functionalization, and Applications in Environmental Science (Part I). *Polymers* **2024**, *16* (20), 2889. https://doi.org/10.3390/polym16202889.

(178) Moulahcene, L.; Skiba, M.; Bounoure, F.; Benamor, M.; Milon, N.; Hallouard, F.; Lahiani-Skiba, M. New Polymer Inclusion Membrane Containing β-Cyclodextrin Polymer: Application for Pharmaceutical Pollutant Removal from Waste Water. *Int. J. Environ. Res. Public. Health* **2019**, *16* (3), 414. https://doi.org/10.3390/ijerph16030414.

(179) Karki, S.; Hazarika, G.; Yadav, D.; Ingole, P. G. Polymeric Membranes for Industrial Applications: Recent Progress, Challenges and Perspectives. *Desalination* **2024**, *573*, 117200. https://doi.org/10.1016/j.desal.2023.117200.

(180) Antibacterial Membranes for Purifying Water. *Nat. India* **2014**. https://doi.org/10.1038/nindia.2014.128.

(181) Regina Corrales-Ureña, Y.; Souza-Schiaber, Z.; Noronha Lisboa-Filho, P.; Marquenet, F.; Noeske, P.-L. M.; Gätjen, L.; Rischka, K. Functionalization of Hydrophobic Surfaces with Antimicrobial

Peptides Immobilized on a Bio-Interfactant Layer. *RSC Adv.* **2020**, *10* (1), 376–386. https://doi.org/10.1039/C9RA07380A.

(182) Li, Y.; Zhu, J.; Cheng, H.; Li, G.; Cho, H.; Jiang, M.; Gao, Q.; Zhang, X. Developments of Advanced Electrospinning Techniques: A Critical Review. *Adv. Mater. Technol.* **2021**, *6* (11), 2100410. https://doi.org/10.1002/admt.202100410.

(183) Duraikkannu, S. L.; Castro-Muñoz, R.; Figoli, A. A Review on Phase-Inversion Technique-Based Polymer Microsphere Fabrication. *Colloid Interface Sci. Commun.* **2021**, *40*, 100329. https://doi.org/10.1016/j.colcom.2020.100329.

(184) Jaafar, J.; Nasir, A. M. Grand Challenge in Membrane Fabrication: Membrane Science and Technology. *Front. Membr. Sci. Technol.* **2022**, *1*. https://doi.org/10.3389/frmst.2022.883913.

(185) Greiner, A.; Wendorff, J. H. Electrospinning: A Fascinating Method for the Preparation of Ultrathin Fibers. *Angew. Chem. Int. Ed.* **2007**, *46* (30), 5670–5703. https://doi.org/10.1002/anie.200604646.

(186) Ahmed, F. E.; Lalia, B. S.; Hashaikeh, R. A Review on Electrospinning for Membrane Fabrication: Challenges and Applications. *Desalination* **2015**, *356*, 15–30. https://doi.org/10.1016/j.desal.2014.09.033.

(187) Chen, J.; Wei, M.; Meng, M. Advanced Development of Molecularly Imprinted Membranes for Selective Separation. *Molecules* **2023**, *28* (15), 5764. https://doi.org/10.3390/molecules28155764.

(188) STRATHMANN, H. Production of Microporous Media by Phase Inversion Processes. In *Materials Science of Synthetic Membranes*; ACS Symposium Series; American Chemical Society, 1985; Vol. 269, pp 165–195. https://doi.org/10.1021/bk-1985-0269.ch008.

(189) Winnacker, M. Polyamides and Their Functionalization: Recent Concepts for Their Applications as Biomaterials. *Biomater. Sci.* **2017**, *5* (7), 1230–1235. https://doi.org/10.1039/C7BM00160F.

(190) Jones, N. A.; Atkins, E. D. T.; Hill, M. J.; Cooper, S. J.; Franco, L. Chain-Folded Lamellar Crystals of Aliphatic Polyamides. Comparisons between Nylons 4 4, 6 4, 8 4, 10 4, and 12 4. *Macromolecules* **1996**, *29* (18), 6011–6018. https://doi.org/10.1021/ma9603490.

(191) Bunn, C. W.; Garner, E. V.; Bragg, W. L. The Crystal Structures of Two Polyamides ('Nylons'). *Proc. R. Soc. Lond. Ser. Math. Phys. Sci.* **1997**, *189* (1016), 39–68. https://doi.org/10.1098/rspa.1947.0028.

(192) Murthy, N. S.; Curran, S. A.; Aharoni, S. M.; Minor, H. Premelting Crystalline Relaxations and Phase Transitions in Nylon 6 and 6,6.

Macromolecules **1991**, *24* (11), 3215–3220. https://doi.org/10.1021/ma00011a027.

(193) Papadopoulou, E. L.; Pignatelli, F.; Marras, S.; Marini, L.; Davis, A.; Athanassiou, A.; Bayer, I. S. Nylon 6,6/Graphene Nanoplatelet Composite Films Obtained from a New Solvent. *RSC Adv.* **2016**, *6* (8), 6823–6831. https://doi.org/10.1039/C5RA23647A.

(194) Burke, J. J.; Orofino, T. A. Nylon 66 Polymers. I. Molecular Weight and Compositional Distribution. *J. Polym. Sci. Part -2 Polym. Phys.* **1969**, *7* (1), 1–25. https://doi.org/10.1002/pol.1969.160070101.

(195) Jebors, S.; Pinese, C.; Montheil, T.; Bethry, A.; Verquin, S.; Plais, L.; Moulin, M.; Dupont, C.; Garric, X.; Mehdi, A.; Martinez, J.; Subra, G. Turning Peptides into Bioactive Nylons. *Eur. Polym. J.* **2020**, *135*, 109886. https://doi.org/10.1016/j.eurpolymj.2020.109886.

(196) (PDF) "Grafting Through" Polymerization Involving Surface-Bound Monomers. *ResearchGate* **2024**. https://doi.org/10.1002/pola.27907.

(197) Macchione, M.; Biglione, C.; Strumia, M. Design, Synthesis and Architectures of Hybrid Nanomaterials for Therapy and Diagnosis Applications. *Polymers* **2018**, *10*, 527. https://doi.org/10.3390/polym10050527.

(198) Kim, J.; Choi, Y.; Park, J.; Lee, H.-Y.; Choi, J. Peptides Conjugation on Biomaterials: Chemical Conjugation Approaches and Their Promoted Multifunction for Biomedical Applications. *Biotechnol. Bioprocess Eng.* **2024**, *29* (3), 427–439. https://doi.org/10.1007/s12257-024-00095-5.

(199) Bellotto, O.; Semeraro, S.; Bandiera, A.; Tramer, F.; Pavan, N.; Marchesan, S. Polymer Conjugates of Antimicrobial Peptides (AMPs) with d-Amino Acids (d-Aa): State of the Art and Future Opportunities. *Pharmaceutics* **2022**, *14* (2), 446. https://doi.org/10.3390/pharmaceutics14020446.

(200) (PDF) Intrinsic Fluorescence Spectra of Tryptophan, Tyrosine and Phenyloalanine. In *ResearchGate*. https://doi.org/10.2991/icadme-15.2015.46.

(201) Granicka, L. H.; Piątkiewicz, W. Membrane Systems for Biomedical Engineering. *Membranes* **2022**, *13* (1), 41. https://doi.org/10.3390/membranes13010041.

(202) *Polymers and Solvents Used in Membrane Fabrication: A Review Focusing on Sustainable Membrane Development*. https://www.mdpi.com/2077-0375/11/5/309 (accessed 2024-11-22).

(203) Guillen, G. R.; Pan, Y.; Li, M.; Hoek, E. M. V. Preparation and Characterization of Membranes Formed by Nonsolvent Induced Phase

Separation: A Review. *Ind. Eng. Chem. Res.* **2011**, *50* (7), 3798–3817. https://doi.org/10.1021/ie101928r.

(204) Diwan, T.; Abudi, Z. N.; Al-Furaiji, M. H.; Nijmeijer, A. A Competitive Study Using Electrospinning and Phase Inversion to Prepare Polymeric Membranes for Oil Removal. *Membranes* **2023**, *13* (5), 474. https://doi.org/10.3390/membranes13050474.

(205) Gharaei, R.; Tronci, G.; Davies, R. P.; Goswami, P.; Russell, S. J. An Investigation into the Nano-/Micro-Architecture of Electrospun Poly (ε-Caprolactone) and Self-Assembling Peptide Fibers. *MRS Adv.* **2016**, *1* (11), 711–716. https://doi.org/10.1557/adv.2016.35.

(206) Bergamasco, S.; Fiaschini, N.; Hein, L. A.; Brecciaroli, M.; Vitali, R.; Romagnoli, M.; Rinaldi, A. Electrospun PCL Filtration Membranes Enhanced with an Electrosprayed Lignin Coating to Control Wettability and Anti-Bacterial Properties. *Polymers* **2024**, *16* (5), 674. https://doi.org/10.3390/polym16050674.

(207) Omer, S.; Forgách, L.; Zelkó, R.; Sebe, I. Scale-up of Electrospinning: Market Overview of Products and Devices for Pharmaceutical and Biomedical Purposes. *Pharmaceutics* **2021**, *13* (2), 286. https://doi.org/10.3390/pharmaceutics13020286.

La borsa di dottorato è stata cofinanziata con risorse del

Programma Operativo Nazionale Ricerca e Innovazione 2014-2020, risorse FSE REACT-EU

Azione IV.4 “Dottorati e contratti di ricerca su tematiche dell’innovazione” e Azione IV.5 “Dottorati su tematiche Green”

The doctoral scholarship was co-funded through resources from the

Programma Operativo Nazionale Ricerca e Innovazione 2014-2020, resources FSE REACT-EU

Azione IV.4 “Dottorati e contratti di ricerca su tematiche dell’innovazione” e Azione IV.5 “Dottorati su tematiche Green”